AD

USAAMRDL TECHNICAL REPORT 71-72

EVALUATION OF AN ADVANCED INSTRUMENTATION SYSTEM FOR HELICOPTER ROTORS

By

Gerald A. Shockey
Thomas H. Bowden

February 1972

EUSTIS DIRECTORATE
U. S. ARMY AIR MOBILITY RESEARCH AND DEVELOPMENT LABORATORY
FORT EUSTIS, VIRGINIA

CONTRACT DAAJ02-70-C-0036
BELL HELICOPTER COMPANY
FORT WORTH, TEXAS

99

DISCLAIMERS

The findings in this report are not to be construed as an official Department of the Army position unless so designated by other authorized documents.

When Government drawings, specifications, or other data are used for any purpose other than in connection with a definitely related Government procurement operation, the United States Government thereby incurs no responsibility nor any obligation whatsoever; and the fact that the Government may have formulated, furnished, or in any way supplied the said drawings, specifications, or other data is not to be regarded by implication or otherwise as in any manner licensing the holder or any other person or corporation, or conveying any rights or permission, to manufacture, use, or sell any patented invention that may in any way be related thereto.

Trade names cited in this report do not constitute an official endorsement or approval of the use of such commercial hardware or software.

DISPOSITION INSTRUCTIONS

Destroy this report when no longer needed. Do not return it to the originator.

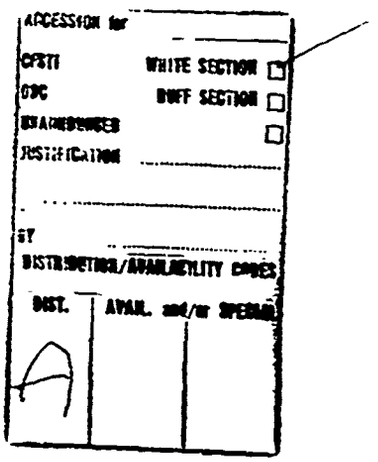

14 KEY WORDS	LINK A		LINK B		LINK C	
	ROLE	WT	ROLE	WT	ROLE	WT
Helicopter instrumentation						
reduction of slip rings required						
time division multiplexing						
pulse amplitude modulation (PAM) switch						
tail rotor aerodynamic data during hover						

Unclassified

Security Classification

DOCUMENT CONTROL DATA - R & D

(Security classification of title, body of abstract and indexing annotation must be entered when the overall report is classified)

1. ORIGINATING ACTIVITY (Corporate author)	2a. REPORT SECURITY CLASSIFICATION
Bell Helicopter Company Fort Worth, Texas	Unclassified 2b. GROUP

3. REPORT TITLE

EVALUATION OF AN ADVANCED INSTRUMENTATION SYSTEM FOR HELICOPTER ROTORS

4. DESCRIPTIVE NOTES (Type of report and inclusive dates)

Final

5. AUTHOR(S) (First name, middle initial, last name)

Gerald A. Shockey
Thomas H. Bowden

6. REPORT DATE	7a. TOTAL NO. OF PAGES	7b. NO. OF REFS
February 1972	98	10

8a. CONTRACT OR GRANT NO.	9a. ORIGINATOR'S REPORT NUMBER(S)
DAAJ02-70-C-0036 b. PROJECT NO. 1F162204A13903 c. d.	USAAMRDL Technical Rpt. 71-72 9b. OTHER REPORT NO(S) (Any other numbers that may be assigned this report) BHC Rpt. 299-099-497

10. DISTRIBUTION STATEMENT

Approved for public release; distribution unlimited.

11. SUPPLEMENTARY NOTES	12. SPONSORING MILITARY ACTIVITY
	Eustis Directorate U.S.Army Air Mobility R&D Laboratory Fort Eustis, Virginia

13. ABSTRACT

A test was conducted on the Bell Helicopter High Accuracy Rotor Test Stand to evaluate a time division multiplexing system for a rotor environment. The test model was a standard UH-1 tail rotor with a 0.1-inch-thick glove wrapped around the surface for the installation of transducers. The objective of this program was to develop and test a method of obtaining numerous channels of transducer information from a rotating system using a small number of slip rings. The system multiplexed the signal in the rotating system and demultiplexed the signal in the stationary system. Aerodynamic data were measured to evaluate the instrumentation system. Comparisons were made between multiplexed and unmultiplexed signals and between measured data and theory. The comparisons show that the multiplexing system does transmit data without degradation of the results.

DD FORM 1 NOV 68 1473 REPLACES DD FORM 1473, 1 JAN 64, WHICH IS OBSOLETE FOR ARMY USE.

Unclassified

Security Classification

DEPARTMENT OF THE ARMY
U. S. ARMY AIR MOBILITY RESEARCH & DEVELOPMENT LABORATORY
EUSTIS DIRECTORATE
FORT EUSTIS, VIRGINIA 23604

This report has been reviewed by the Eustis Directorate, U. S. Army Air Mobility Research and Development Laboratory and is considered to be technically sound. This program was initiated to extend the application of a time-multiplex data acquisition system to the helicopter rotor environment in order to reduce the presently required number of slip rings per channel of data in transferring data from a rotating to a stationary environment.

The program was conducted under the technical management of Patrick A. Cancro of the Aeromechanics Division of this Directorate.

Task 1F162204A13903
Contract DAAJ02-70-C-0036
USAAMRDL Technical Report 71-72
February 1972

EVALUATION OF AN ADVANCED INSTRUMENTATION SYSTEM FOR HELICOPTER ROTORS

Final Report

Bell Helicopter Company Report 299-099-497

By

Gerald A. Shockey
Thomas H. Bowden

Prepared by

Bell Helicopter Company
Fort Worth, Texas

for

EUSTIS DIRECTORATE
U. S. ARMY AIR MOBILITY
RESEARCH AND DEVELOPMENT LABORATORY
FORT EUSTIS, VIRGINIA

SUMMARY

A test was conducted on the Bell Helicopter High Accuracy Rotor Test Stand to evaluate a time division multiplexing system for a rotor environment. The test model was a standard UH-1 tail rotor with a 0.1-inch-thick glove wrapped around the surface for the installation of transducers. The objective of this program was to develop and test a method of obtaining numerous channels of transducer information from a rotating system using a small number of slip rings. The system multiplexed the signal in the rotating system and demultiplexed the signal in the stationary system. Aerodynamic data were measured to evaluate the instrumentation system. Comparisons were made between multiplexed and unmultiplexed signals and between measured data and theory. The comparisons show that the multiplexing system does transmit data without degradation of the results.

FOREWORD

The investigation described herein was conducted at the Bell Helicopter Company High Accuracy Rotor Test Stand (HARTS) under U. S. Army Contract DAAJ02-70-C-0036 (Task 1F162204A13903). The program was sponsored by the Eustis Directorate, U. S. Army Air Mobility Research and Development Laboratory, Fort Eustis, Virginia; and was administered by Mr. Patrick Cancro. The contributions of C. E. Smith and Aaron Whitener of Bell Helicopter Company are appreciated by the authors. The analytical techniques used in this report and the advanced instrumentation were developed as part of the Bell Helicopter Company Independent Research and Development Program and prior government-sponsored programs.

TAP .E OF CONTENTS

Page

APPENDIXES

LIST OF ILLUSTRATIONS

LIST OF ILLUSTRATIONS - Continued

LIST OF ILLUSTRATIONS - Continued

LIST OF SYMBOLS

a_{1_s}	first component of longitudinal flapping with respect to the shaft; constant coefficient of the first cosine term in the Fourier Series expressing flapping with respect to a plane normal to the shaft axis, deg
b_{1_s}	first component of lateral flapping with respect to the shaft; constant coefficient of the first sine term in the Fourier Series expressing flapping with respect to a plane normal to the shaft axis, deg
c	blade chord, in.
C_c	airfoil chord force coefficient, $C_c = \oint C_p \, d(y/c)$
C_m	airfoil pitching moment coefficient about the quarter chord, $C_m = \oint C_p(.25-x/c) \, d(x/c) + \oint C_p(y/c) \, d(y/c)$
C_n	airfoil normal force coefficient, $C_n = \oint C_p \, d(x/c)$
C_p	absolute pressure coefficient, $C_p = \frac{P_{measured} - P_{free\text{-}stream\ static}}{dynamic\ pressure}$
r	distance along the rotor radius, in.
x/c	nondimensional distance along the chord
y/c	nondimensional distance perpendicular to the chord
α	local angle of attack, deg
β	flapping angle at any azimuth position referred to the plane normal to the shaft axis, positive up, deg

θ	blade pitch, angle at any azimuth position referred to the shaft axis, deg
σ'	air density ratio, ratio of the measured density to density at sea-level standard conditions

INTRODUCTION

The development of transducers has advanced to the point that detailed measurements of a helicopter rotor environment can be obtained. Combinations of accelerometers, pressure transducers, hot wire anemometers, and strain gages have been used to measure the aerodynamic and dynamic characteristics of a rotor at one radius station. Future objectives of rotor testing include detailed measurements along the span as well as the chord continuously around the azimuth. Transmitting this amount of data from the rotating system to the data acquisition system using a standard slip-ring assembly is not feasible due to the size of the slip-ring assembly needed to accommodate the channels of data envisioned. This program was an investigation of the feasibility of using a time-division multiplexing system to alleviate this problem. This system reduced the required number of slip rings from 68 to 9 for 32 channels of data. Time multiplexed data acquisition systems have been used successfully in several applications including airborne systems such as fixed-wing aircraft and missiles. This test was to extend the application of such a system to the helicopter rotor environment, which adds centrifugal force effects to the envelope of operating conditions. The test conditions, therefore, were main rotor rpm and main rotor g-forces.

INSTRUMENTATION SYSTEM

The data acquisition system was a standard magnetic tape instrumentation system used to measure rotor data with the addition of a multiplexer and demultiplexer ahead of and behind the slip ring. The instrumentation system included the following components:

Transducers

- Absolute pressure (piezoresistive)
- Differential pressure (piezoresistive)
- Accelerometers (piezoresistive)
- Hot wire anemometer
- Strain gages

Pulse Amplitude Modulation (PAM) Switch

- Multiplexer
- Demultiplexer
- Clock

Signal Conditioning

- ILD-082 (Bell)
- PR-100 (Astronics)
- SC-100 (Astronics)
- Hot wire SC(Bell)

Power Supplies

Voltage Controlled Oscillators

Mixer

Tape Deck

Figure 1 is a block diagram of the instrumentation system. The difference between this system and the data acquisition system normally used is the PAM multiplexer. The PAM is a solid-state, nonreturn-to-zero, four-pole, 16-position, low-level switch. This system used two 16-channel printed circuit boards so that 32 channels of data were passed, two channels at a time. One-half of the PAM is the master and the other is the slave, with the positions being interchangeable. The signals were multiplexed just ahead of the slip ring, then demultiplexed just after the slip ring. Both halves of the switch are controlled by a clock. The clock sets the rate at which the switch operates. The clock also keeps each half in synchronization with the other. At the end of each

16-channel sweep, the clock sends an enable pulse to each module; then, starting with channels 1 and 17, it continues to cycle through channels 16 and 32. This cycling is continued as long as power is supplied to the clock. The clock also provides power to the switches. Within the demultiplexing side of the switch, the two input signals are broken up into the original 32 signals and routed out on separate output leads that take them into the signal conditioners. Figure 2 is a photograph showing the multiplexer, clock, SC-100's, and demultiplexer installed in the test stand.

The PAM is a step and hold time division multiplexer so that each signal is recorded 1/16 of the time with this system. The switching rate can be varied up to 160,000 Hz. Experimenting with the switching rate resulted in the selection of a switching frequency of 60,000 Hz as the optimum rate with respect to noise. This gave an output signal rate of 3740 samples/sec. The direct channels were continuous output signals. The data were then digitized for each five degrees azimuth.

The transducers were wired into the system in three ways: multiplexed only, direct only, and parallel (one transducer wired in parallel, one side being multiplexed and the other wired direct through the slip ring) as shown in Figure 1. Several types of transducers were used in the evaluation of the system. Most of the transducers were of the piezoresistive type. All the pressures, absolute and differential, and the accelerometers were piezoresistive. The strain gages were standard foil make. The hot wire anemometer was a constant-current continuous wire type with 10 sensors.

The different types of transducers made it necessary to use several kinds of signal conditioners. The PK-100 and SC-100 amplifiers which are high input impedance signal conditioners were used with piezoresistive pressure transducers, piezoresistive accelerometers, and strain gage transducers. The ILD-082, which is a low input impedance amplifier, received only strain gage transducers. A special signal conditioner was built for the hot wire anemometer.

It was necessary to completely isolate the signal conditioning racks to keep the regulators from interfering with each other; therefore, four power supplies were used. Three power supplies were used to furnish 28 VDC to the standard signal conditioners, and one was used to furnish ±15 VDC to the hot wire signal conditioners.

After the signal conditioning was completed, the high-level signals were passed to Voltage Controlled Oscillators (VCO's) and then into a mixer. The VCO's also acted as high-frequency

filters which helped to reduce the signal noise. After being mixed, the signals were placed on 1-inch-wide 14-track magnetic tape.

ROTOR AND ROTOR INSTRUMENTATION

The test model was a modified full-scale UH-1 tail rotor assembly. Basic characteristics of this rotor are given below.

Airfoil Designation	NACA 0015
Chord	8.41 in.
Radius	51 in.
Twist	0 deg

The modified rotor was enclosed in a 0.10-inch-thick glove similar to that described in Reference 1. The glove, which extended from the doubler to the blade tip, provided a means by which instrumentation could be mounted on the rotor while still maintaining a smooth aerodynamic surface. Figure 3 shows instrumentation embedded in the gloved rotor. With the addition of the 0.10-inch-thick glove, the coordinates of the blade airfoil section were:

x/c	y/c	x/c	y/c
0	0	.485	.069
.014	.029	.539	.064
.027	.038	.593	.058
.050	.049	.646	.052
.083	.060	.700	.045
.116	.067	.754	.039
.160	.073	.808	.032
.215	.077	.862	.026
.269	.079	.915	.019
.323	.078	.962	.013
.377	.076	1.000	.009
.431	.073		

The basic airfoil chord was extended from 8.41 to 9.30 inches to fair the trailing edge of the airfoil to a reasonable thickness. To minimize the mutual interference of the various pieces of instrumentation, the absolute pressure transducers were installed on one blade, and the leading-edge hot wire anemometer and boundary layer buttons were installed on the other.

ABSOLUTE PRESSURE TRANSDUCERS

Nine absolute pressure transducers were mounted on the upper and lower airfoil surfaces to measure static pressure. The chord and span locations of transducers are given in Figure 4.

The pressure gages were subminiature pressure transducers of 0-20 psia range. The installation is shown in Figure 3. The transducers were attached to a 3-inch-thick contoured aluminum plate. Staggering of the transducers near the leading and trailing edges was necessary because of space limitations.

BOUNDARY LAYER BUTTONS

The Boundary Layer Button (BLB) is a pressure measuring device developed to measure flow magnitude and direction on a rotating surface. The BLB cap consisted of two total pressure tubes and a static port. Each of the total pressure tubes is connected to the top of a diaphragm of a subminiature differential pressure transducer. The backsides of the diaphragms of the two transducers are connected to a common static port. Therefore, the output of each transducer is converted to dynamic pressure. Using the dynamic pressure, the velocity magnitude can be calculated. Each BLB cap is calibrated for flow direction for an included angle of 32 degrees.

Four BLB's were installed at the 0.75 radius station: two on each surface at the 0.30 and 0.85 chord stations (Figure 5). The tube height of the BLB's was 0.0625 inch above the airfoil surface.

LEADING-EDGE HOT WIRE ANEMOMETER

The hot wire anemometer is a constant-current device using ten sensors to measure the stagnation point location along the airfoil profile. A sketch of the hot wire installation is given in Figure 6.

All channels of the system are set to a no-wind common voltage, and the relative velocity is recorded for all channels. The stagnation point is determined by locating the sensor which has the maximum voltage. The angle of attack is determined from the stagnation point location (velocity null). The location of the velocity null is determined from the known locations of the hot wire segments, and the angles of attack corresponding to these stagnation point locations are determined by using theoretical values of angle of attack versus distance along the airfoil contour to the stagnation point (References 2 and 3). Therefore, the accuracy of measuring the angle of attack depends on the spacing between the sensors

with respect to the chord. For the spacing used, the accuracy is within one degree of angle of attack. Two-dimensional test results with this instrument are published in Reference 4.

ACCELEROMETERS AND STRAIN GAGES

Two miniature, piezoresistive accelerometers were mounted on the upper surface of the blade. The inboard one was located at 15 percent chord and radius station 13.1, which was on a doubler. The outboard accelerometer was at 25 percent chord and radius station 40.7. The accelerometer installation is shown in Figure 5. They were oriented to measure flapwise accelerations. Three foil-type strain gages were installed around the 75 percent radius station (Figure 5) to measure beam bending.

TEST FACILITY

The test was conducted on the Bell High Accuracy Rotor Test Stand (HARTS). The stand is powered by two constant-speed AC motors which can deliver a combined total of 1000 horsepower to the rotor. Speed control is accomplished by means of an eddy-current coupling and a speed change gearbox. The rotational speed can be varied to 3000 rpm. Rotors are mounted in the vertical plane with the center of rotation 15 feet above the ground. The model installation on the test stand is shown in Figure 7.

TEST CONDITIONS AND PROCEDURE

The test conditions are given in the table on page 15. Aerodynamic data were taken at one radius station (75 percent radius) at two rotational speeds. The blade azimuth and wind direction are defined in Figure 8. The data obtained were:

Angle of attack

Chordwise pressure distributions

Local velocity magnitude and direction

Flapwise bending moments

Flapwise accelerations

In addition, the tail rotor test stand balance data were recorded and are presented in Figures 9 and 10, along with theory. The accuracy of the balance for the forces measured during this test was ±10 pounds thrust and ±1.4 horsepower at 866 rpm and ±0.5 horsepower at 324 rpm.

There were two basic test cases. The rotational speeds of 324 rpm and 866 rpm were used to simulate main rotor rpm and main rotor g-forces, respectively. For each rotational speed, data were recorded for every 2 degrees of blade pitch within the range of 0 to 20 degrees.

MULTIPLEX RESULTS

Evaluation of the multiplex system's performance was accomplished by comparisons between multiplexed data and data recorded directly through slip rings. Because the system is intended to transmit aerodynamic data, such as pressure distributions, etc., transducers were used which have been proven in previous aerodynamic tests (Reference 1). The aerodynamic results were compared with theory and previous experimental data as a secondary evaluation of the multiplexing system and are discussed in Appendix II.

The data were recorded as follows:

Direct only through the slip ring

Multiplexed only ahead of the slip ring and demultiplexed on the stationary side

Parallel - direct and multiplexed simultaneously

It was the intent of this program to have at least one of each type of transducer, as listed on page 2, recorded in parallel. Then the paralleled signals would be compared to each other with the direct side of the paralleled signals taken as reference. The multiplexed-only and direct-only signals were to be used for secondary comparisons.

Of the 32 multiplex data channels available, 25 were used. Of these, 16 were absolute pressure transducers, 6 were differential pressure transducers, 1 was an accelerometer, and 2 were strain gages.

ABSOLUTE PRESSURE TRANSDUCERS

One absolute pressure transducer was parallel recorded, one was direct only, and 15 were multiplexed only. The paralleled pressures are shown for every 4 degrees of blade pitch for 866 rpm (Figure 11). The pressure transducer whose output was paralleled was located at $x/c = .55$ of the lower surface. The agreement between the paralleled signals is good. The differences are caused by noise which existed in the direct side of the paralleled signal. The pressure distributions (refer to Appendix II) show that the multiplexed-only pressures exhibit the expected trends, are of the correct order of magnitude, and agree very well with the direct-only pressure located at $x/c = .80$ of the lower surface.

DIFFERENTIAL PRESSURE TRANSDUCERS

Two differential pressure transducers, which made up one boundary layer button, were recorded in parallel; the other four transducers were multiplexed only. The paralleled pressures are shown for every 4 degrees of blade pitch at 866 rpm (Figure 12). The agreement between the paralleled signals is excellent. The multiplexed-only signals agree well with the paralleled signals and show the expected aerodynamic trends (refer to Appendix II).

ACCELEROMETERS

The outboard accelerometer was connected in parallel; however, the direct side of the paralleled signal was lost. The inboard accelerometer was recorded direct only. Since the direct side of the paralleled accelerometer went out, no direct comparisons can be made, but order-of-magnitude comparisons of the inboard (direct only) and outboard (multiplexed side of the paralleled signal) accelerations can be made. The accelerometer results versus azimuth for every 4 degrees of blade pitch at 866 rpm are shown in Figure 13. The mean value of the accelerometer measurements is the flapwise component of centrifugal force due to coning. The multiplexed outboard accelerometer measurements are of the same order of magnitude, and larger than the inboard accelerations, as expected. Therefore, it appears that the multiplexed accelerometer performed as well as the direct-only accelerometer; however, no other conclusions can be made because of the lack of data.

STRAIN GAGES

One strain gage was recorded in parallel, one was multiplexed only, and four were recorded direct only. The parallel flapwise bending moments versus azimuth for every 4 degrees of blade pitch at 866 rpm are shown in Figure 14. Due to electrical noise and poor resolution, the agreement is generally poor. The resolution was such that the measured values were less than five percent of full scale, thus resulting in unreliable values. Also, all strain gages used had a one-per-rev noise whose amplitude was of the same order of magnitude as the measurements themselves. In addition, the two multiplexed strain gage signals (one multiplexed only, one multiplexed side of the parallel signal) had 60-cycle noise. The 60-cycle noise in the multiplexed signals can be caused by any stray induction; however, one possible cause is a nonoptimum switching rate of the multiplexer system. The switching rate was set to that rate which minimized noise in the pressure transducer signals. There is no assurance that this rate also minimizes noise in other types of instrumentation.

The mean flapwise bending moments versus blade pitch for blade station 37.8 are shown in Figure 15. These data show that once the oscillatory noise is neglected, the agreement of the paralleled signals is much improved and the multiplexed-only strain gage data agree well with the paralleled signals. Figure 16a puts the strain gage data even more into perspective by presenting time history traces as the tail rotor underwent a manual sweep of blade pitch. Paralleled strain gage time history traces at a constant blade pitch of 12 degrees are shown in Figure 16b. The agreement of the paralleled traces is excellent and in all cases the paralleled signals coincide; however, as discussed, the measured values are less than five percent of full scale. Thus, strain gage signals can be multiplexed effectively, and the differences between the paralleled signals for the reduced strain gage data are caused by the poor resolution of the strain gages.

HOT WIRE ANEMOMETER

For this test the hot wire anemometer was wired direct only. The hot wire anemometer signals could not be wired in parallel because of the internal wiring in the signal conditioning box. When a channel is wired both ways, the input to the amplifier is shorted. However, the hot wire anemometer signal can be wired either multiplexed only or direct only.

Subsequent testing of the gloved rotor used in this program was performed with parallel wiring of the hot wire anemometer signals. The results are given in Appendix I.

MULTIPLEX SYSTEM EVALUATION

The multiplexing system functioned successfully in the rotating environment, and its overall performance was satisfactory. However, the following items required special attention.

POWER SUPPLY SEPARATION

To keep the voltage regulators from interfering with each other, all the signal conditioning racks had to be completely isolated from each other.

SWITCHING NOISE

The multiplexed signals had a noise on them of the same frequency as the switching rate. This problem is common for switching systems. The switching rate which caused the least amount of noise on the absolute pressure transducers was found experimentally to be 60,000 Hz. This rate was used with all the sensors. There is a possibility that a different switching rate would have reduced the noise level on the strain gage data; however, since most of the sensors were piezoresistive, the best rate for them was used.

OVERVOLTAGES

A short circuit generated voltages beyond the normal range causing some of the field effect transistors to break down. Therefore, a blocking diode was installed to protect the system against overvoltages.

AUTHORITY ON BRIDGE BALANCE SIGNAL CONDITIONERS

The authority on the signal conditioners had to be changed to fully balance the piezoresistive pressure transducers. This was done by changing resistance from 10 K ohms to 1 K ohms. This problem was due to the bridge imbalance of the transducers, not the multiplex system.

ZERO SHIFT

Almost all of the pressure transducers experienced a zero shift due to hysteresis and/or temperature change. The zero shift was in the transducers and was totally unrelated to the multiplexing system. The standard deviation of the zero shift was approximately 0.1 psia for the absolute pressure transducers and 0.03 psid for the differential pressure transducers. An attempt was made to account for the zero shift in the transducers; however, only the gross zero shift from the change of pretest and post-test reference zeros was known, and the

exact time, length, and amount of each zero shift for each transducer remained unknown.

Accounting for the zero shift reduced the possible error to approximately .2 to .3 percent of full scale. Although this appears to be very low, a significant error still can be incurred for large-range pressure transducers (e.g., 0 to 20 psia) at low dynamic pressures where low pressures are being read.

CROSSTALK

Crosstalk existed between some of the channels. But, because crosstalk between channels in a low-level multiplex system is normally not measurable (Reference 5), the source of the problem is probably ahead of the switch. Shielded-twisted leads from the sensor to the switch may reduce the crosstalk, but they were not used in this experiment.

As noted above, there were some problems encountered with this system; however, solutions to all of the problems in the multiplex system were found, and the multiplex system achieved the objective of operating in a rotating environment.

CONCLUSIONS

The test proved that the time-division multiplexing system will operate in a rotor environment. The system will transmit a wide variety of signals and a large number of channels through a space-limited slip-ring assembly.

The comparisons between the paralleled data from the absolute and differential pressure transducers and the leading-edge hot wire anemometer (Appendix I) show very good agreement. In many cases, the data coincide exactly. The aerodynamic information obtained through the multiplexer also agrees well with theory. Signals from the strain gages and accelerometers that went through the switches appear to be good; however, there were not enough data to make a conclusive decision about it.

The multiplex system is obviously more sensitive and complicated than a direct system; therefore, more engineering is necessary in the design phase to match the components with the type of signal expected.

The areas of special attention in designing a multiplexing system are:

- Each power supply must be isolated to keep the signal conditioner regulators from contending with each other.
- The switching rates for each type of signal need to be optimized with respect to noise.
- Protection must be provided against overvoltages.

Because of the sensitivity of the system, some problems were encountered; however, solutions to all of the problems relating to the multiplex system were found.

This evaluation has shown that a time-division multiplexer is capable of serving in a data acquisition system to obtain accurate, detailed rotor data. Therefore, either a multiplexer of the type tested (PAM) or one of the other types available should be included in designing an instrumentation system to measure numerous channels of data through a slip ring.

TEST CONDITIONS									
Run	Ctr. No.	RPM	θ (deg)	Flapping a_{1_s}	Flapping b_{1_s}	Wind Vel. (mph)	Wind Dir. (deg)	Baro. Pres. (in. Hg)	OAT (°F)
33A	3	866	0	-.04	-.15	4	90	30.2	64
	5	866	2	.06	-.32	3	90	30.2	64
	6	866	4	.04	-.29	2	100	30.19	64
	7	866	6	-.13	-.16	2	100	30.19	64
	8	866	8	.06	-.10	2	110	30.19	64
	9	866	10	-.01	-.07	2	90	30.19	64
	10	866	12	-.24	-.52	4	100	30.19	64
	11	866	14	-.42	-.52	3	110	30.19	64
	13	866	16	-.24	-.43	3	90	30.19	64
	14	866	18	-.40	-.42	4	80	30.19	64
	15	866	20	-.53	-1.02	2	70	30.19	64
	16	866	10	-.15	-.76	4	80	30.19	64
	17	866	0	.01	-.09	4	90	30.19	64
	18	324	0	0	-.04	3	100	30.18	65
	19	324	2	-.15	-.06	1	90	30.18	65
	20	324	4	.05	-.06	0	-	30.18	65
	21	324	6	-.07	-.06	0	-	30.18	66
	22	324	8	-.18	.01	0	-	30.18	66
	23	324	10	0	-.05	0	-	30.18	66
	24	324	12	-.26	-.74	1	100	30.18	66
	26	324	14	-.80	-.19	4	70	30.18	66
	27	324	16	-.25	-.54	1	60	30.18	66
	28	324	18	-1.11	-1.45	3	100	30.18	66
	29	324	20	-1.75	-1.43	4	60	30.18	65
	30	324	10	-.32	-1.83	4	60	30.18	65
	31	324	0	-.16	-.32	4	90	30.18	64

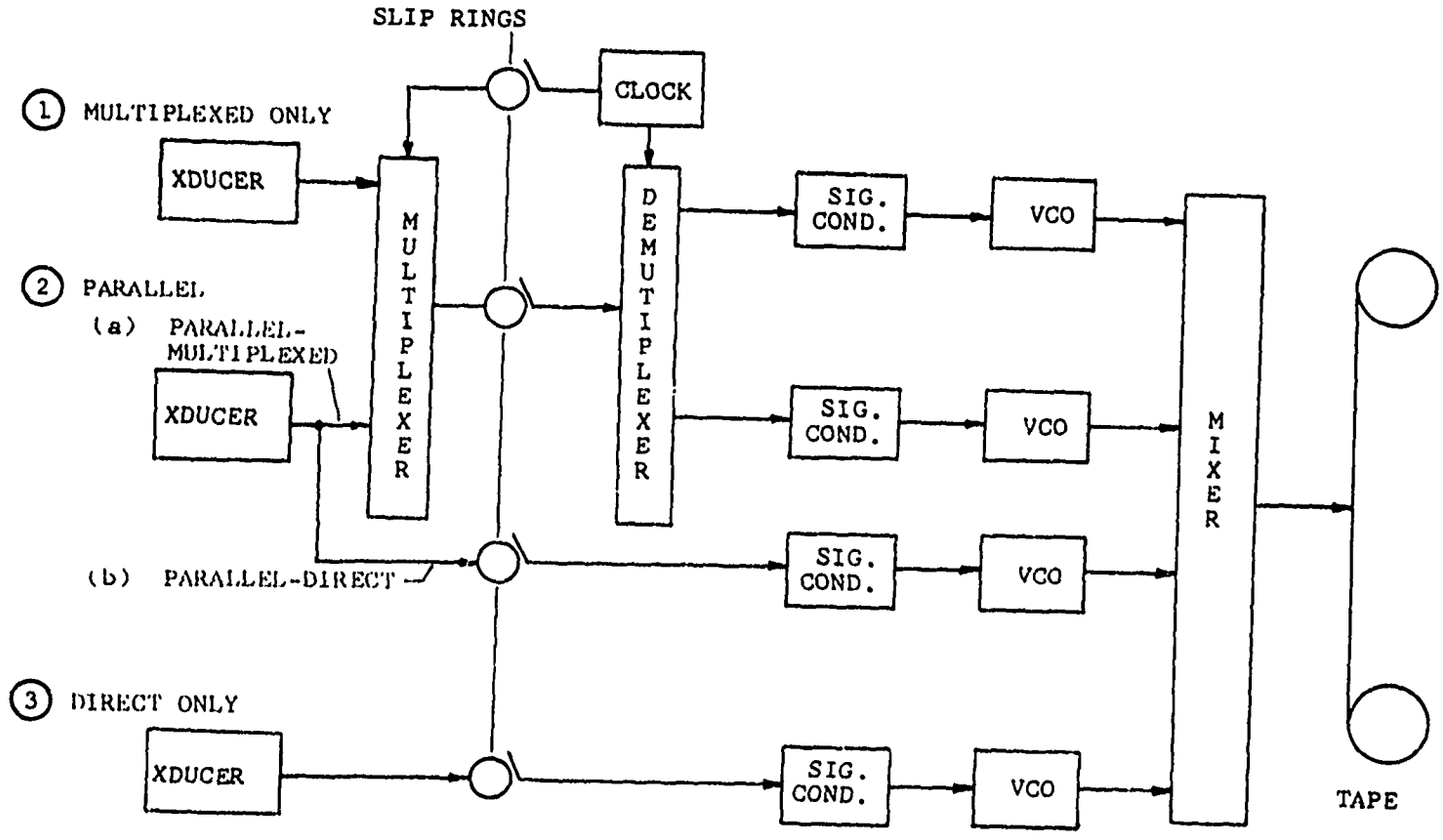

Figure 1. Block Diagram of the Instrumentation System.

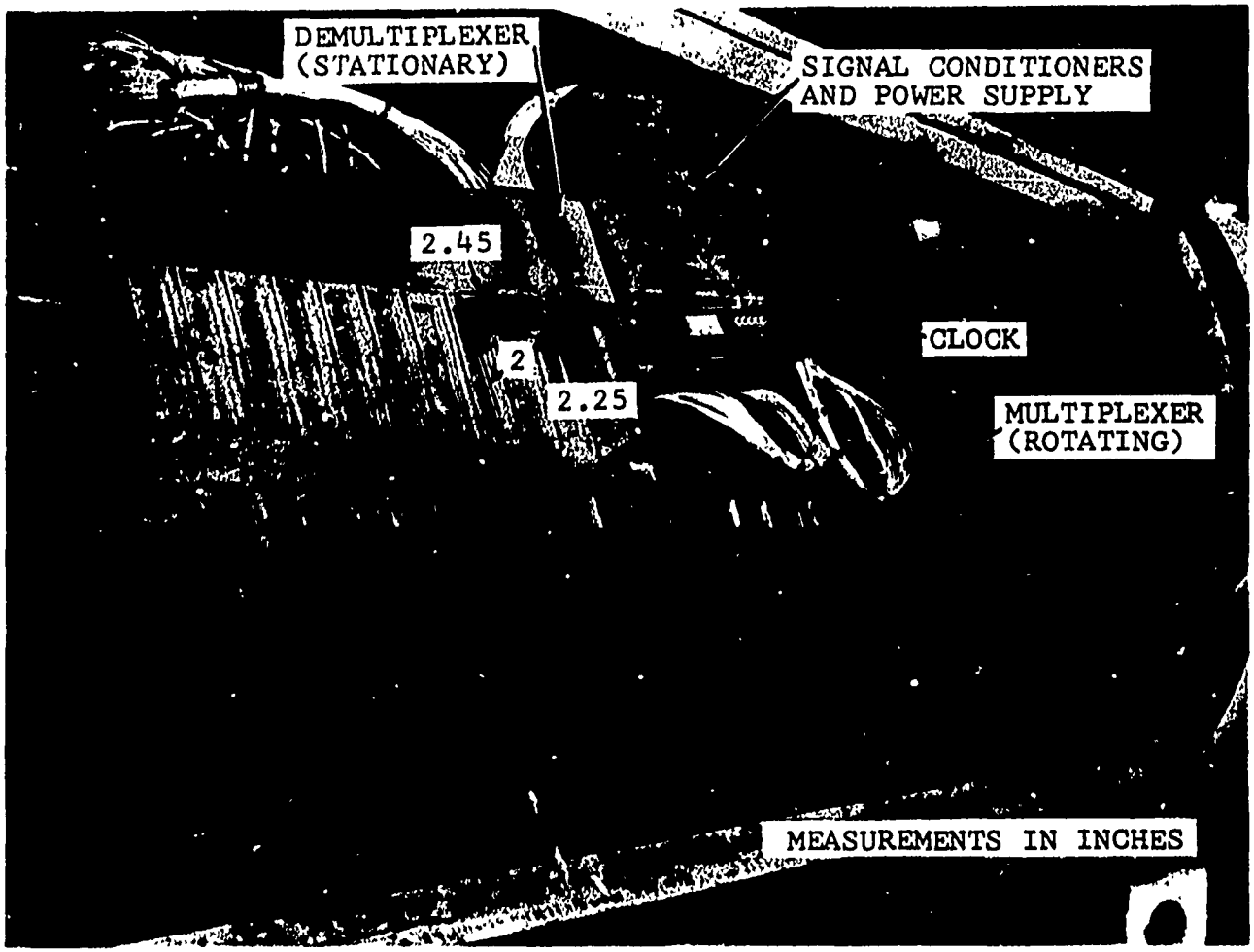

Figure 2. Installation of the Multiplex System.

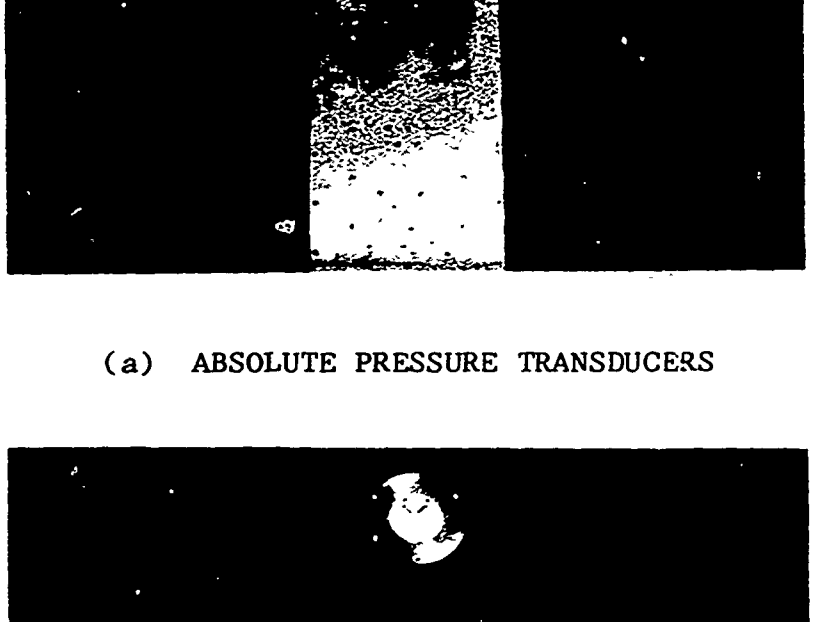

(a) ABSOLUTE PRESSURE TRANSDUCERS

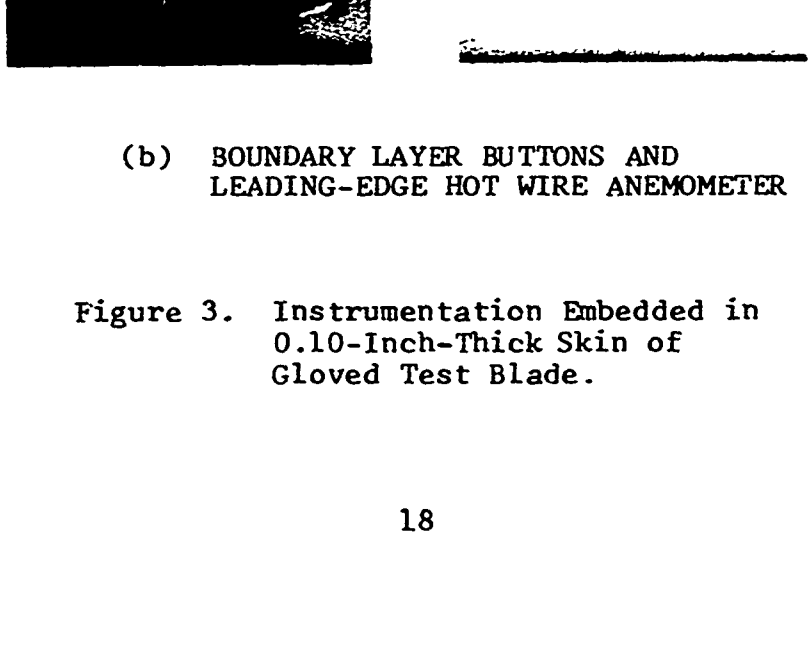

(b) BOUNDARY LAYER BUTTONS AND
LEADING-EDGE HOT WIRE ANEMOMETER

Figure 3. Instrumentation Embedded in 0.10-Inch-Thick Skin of Gloved Test Blade.

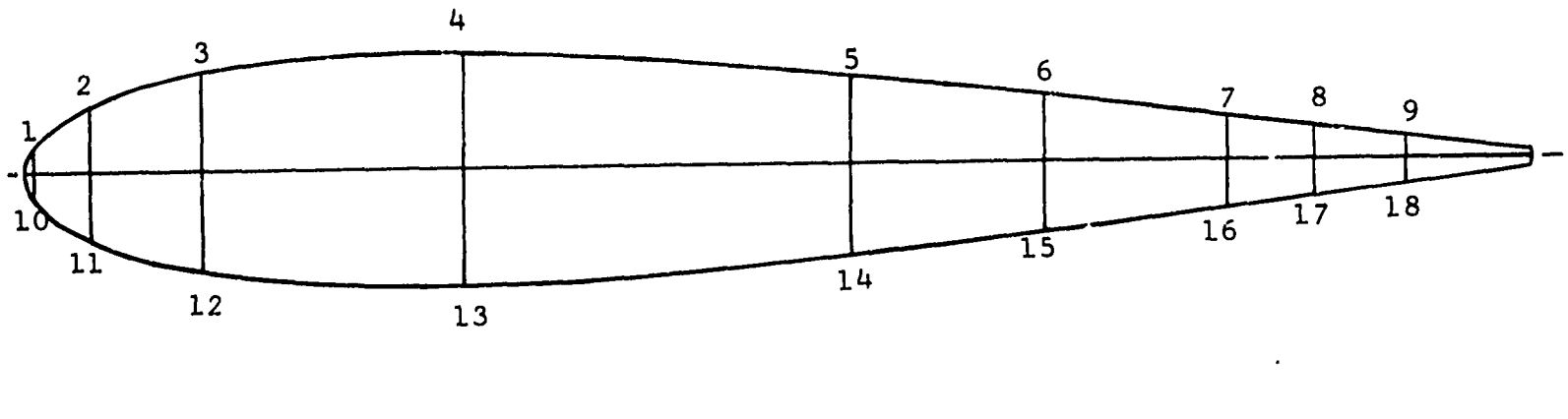

UPPER SURFACE				LOWER SURFACE			
TRANSDUCER NUMBER	x/c	y/c	$r_{(IN.)}$	TRANSDUCER NUMBER	x/c	y/c	$r_{(IN.)}$
1	.01	.02	38.71	10	.01	-.02	37.79
2	.05	.05	37.75	11	.05	-.05	38.75
3	.13	.07	38.53	12	.13	-.07	37.97
4	.30	.08	38.25	13	.30	-.08	38.25
5	.55	.06	38.25	14	.55	-.06	38.25
6	.68	.05	38.25	15	.68	-.05	38.25
7	.80	.03	37.84	16	.80	-.03	38.66
8	.86	.03	38.72	17	.86	-.03	37.78
9	.91	.02	37.82	18	.91	-.02	38.68

Figure 4. Absolute Pressure Transducer Locations.

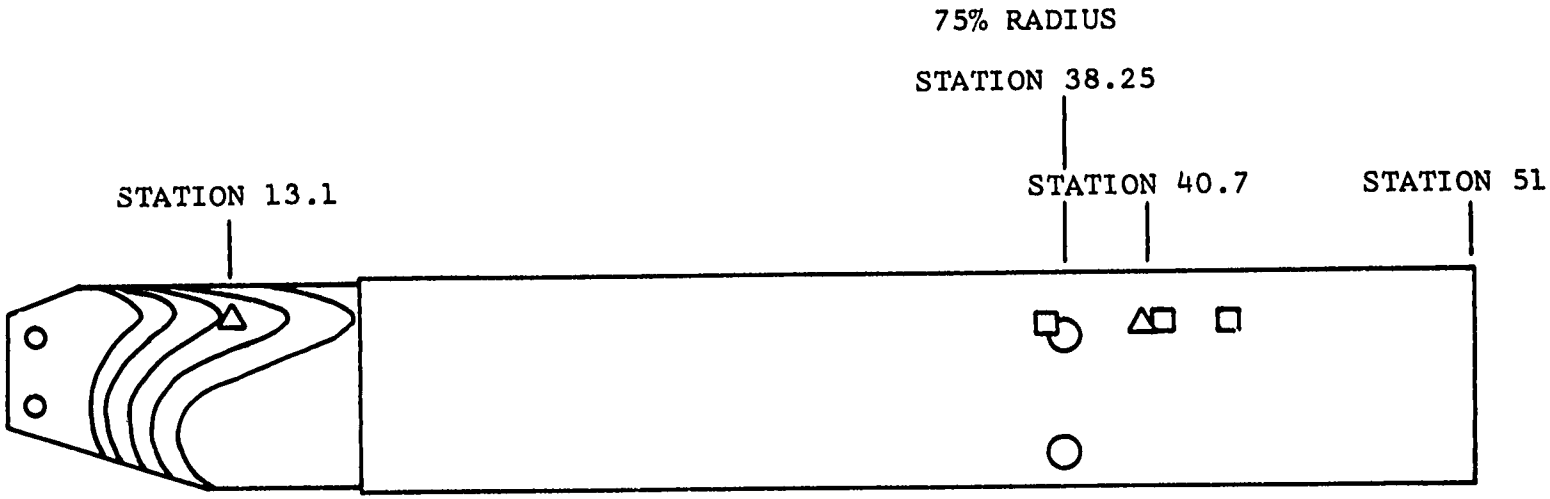

△ ACCELEROMETERS

STA.	x/c
13.1	.15
40.7	.25

○ BOUNDARY LAYER BUTTONS

STA.	x/c
38.25	.30
38.25	.85

□ STRAIN GAGES

STA.	x/c
37.8	.24
41.3	.24
43.2	.24

Figure 5. Accelerometer, Boundary Layer Button, and Strain Gage Locations.

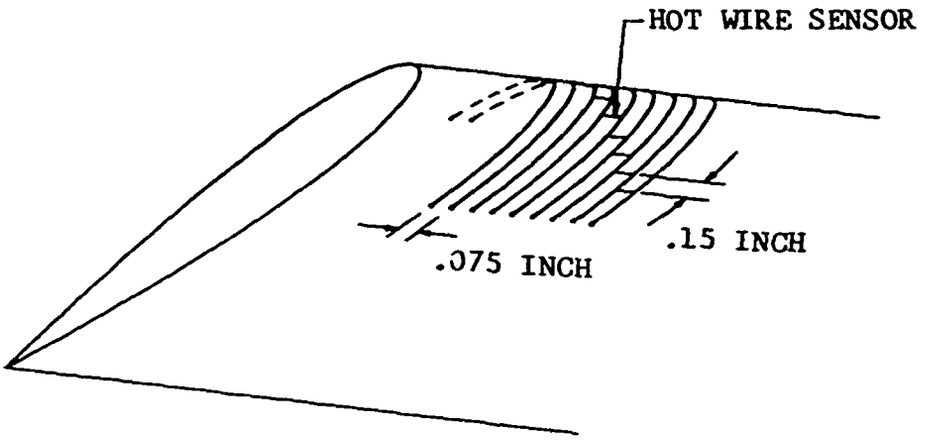

SKETCH OF HOT WIRE ANEMOMETER INSTALLATION

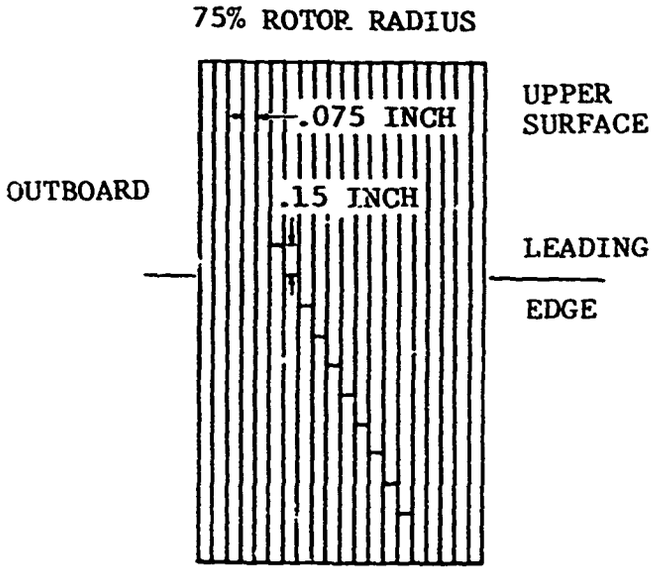

LOCATION OF HOT WIRE SENSORS

Figure 6. Installation and Location of Leading-Edge Hot Wire Anemometer.

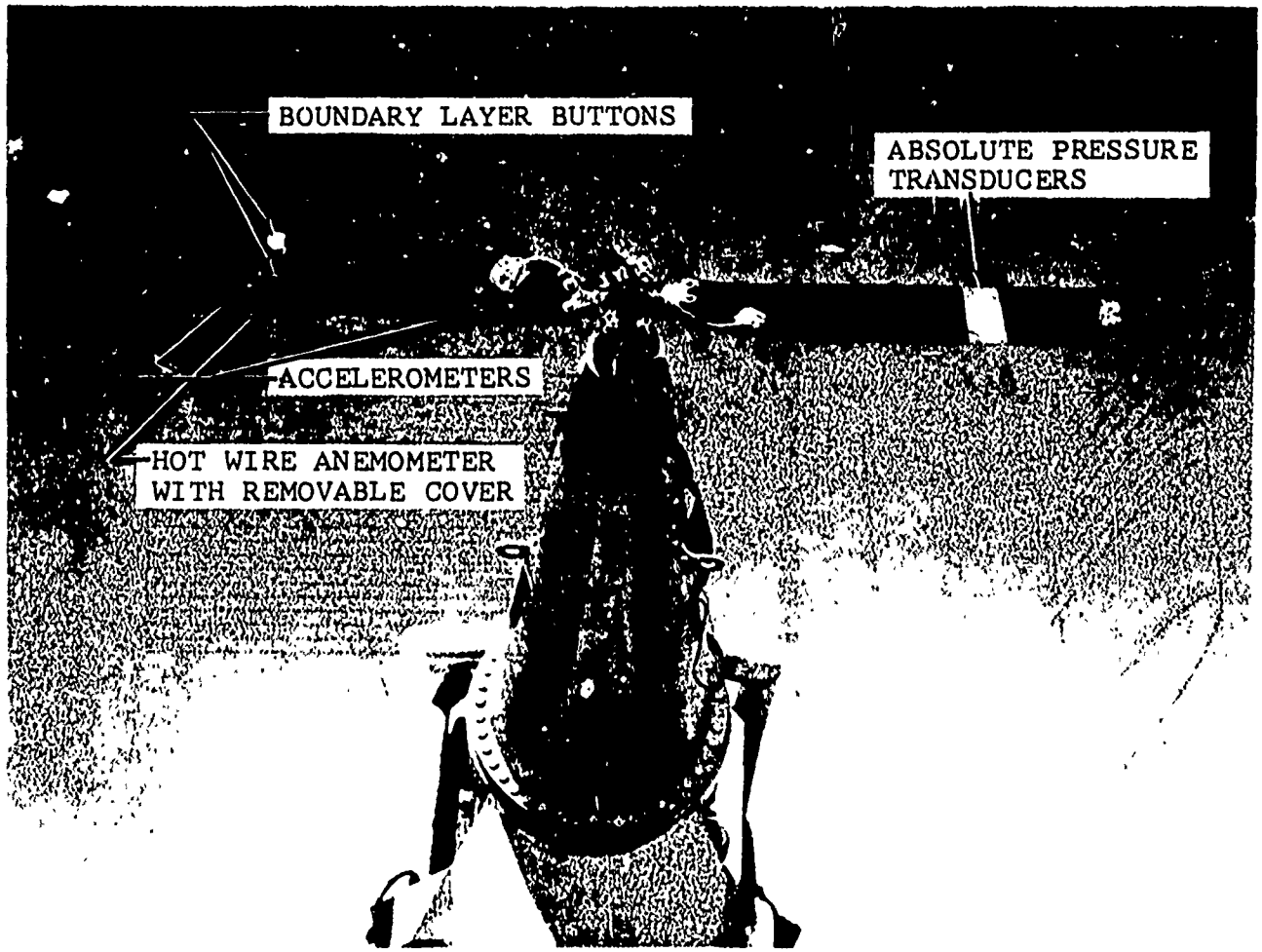

Figure 7. Installation of the Rotor on the Test Stand.

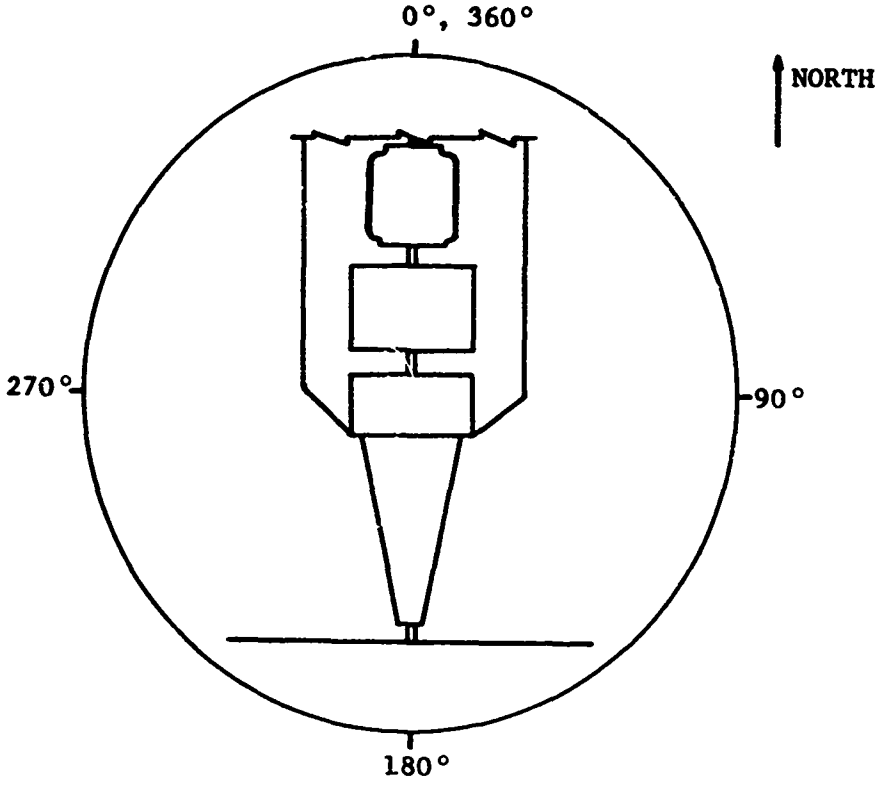

(a) WIND DIRECTION (LOOKING DOWN)

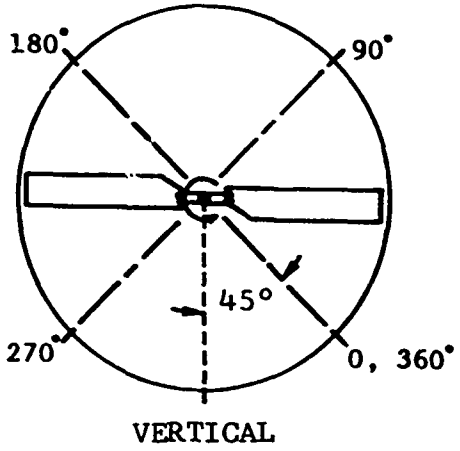

(b) AZIMUTH POSITION (LOOKING AFT)

Figure 8. Sketch Defining Wind Direction and Azimuth Position.

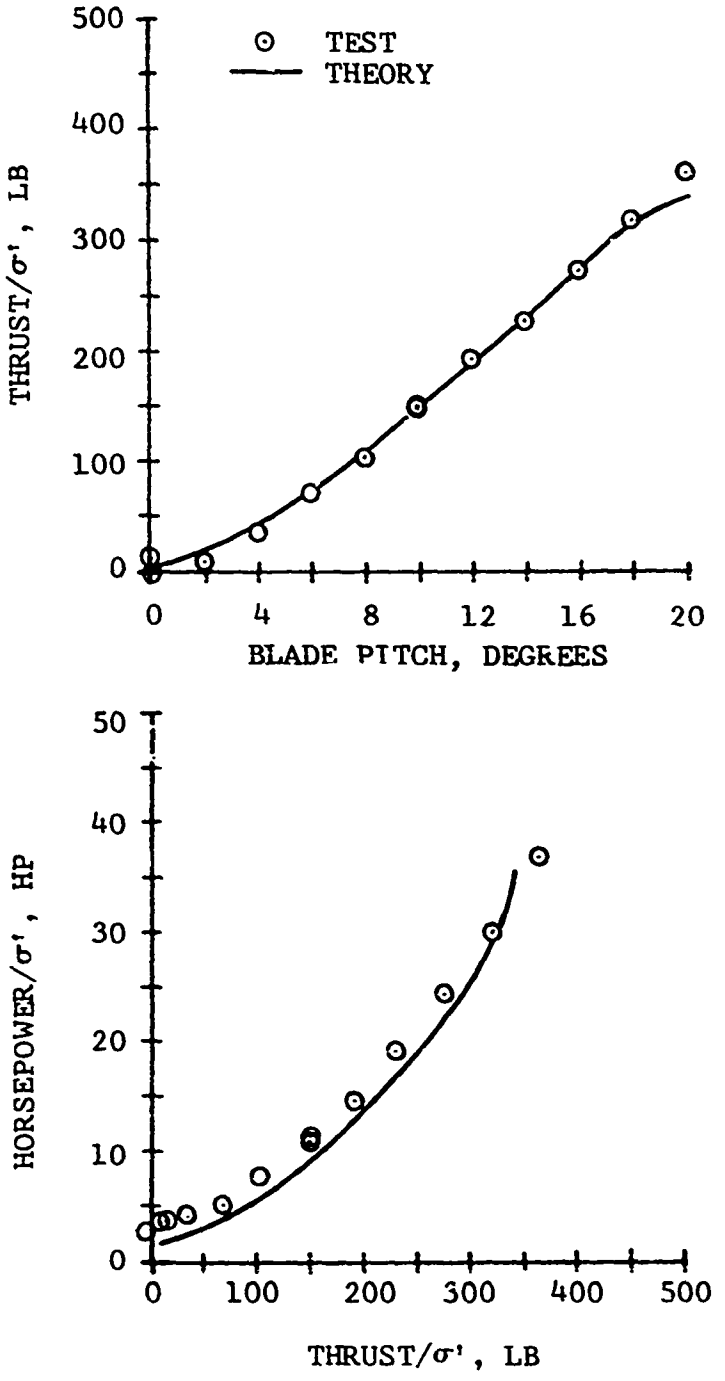

Figure 9. Tail Rotor Test Stand Balance Data at 866 RPM.

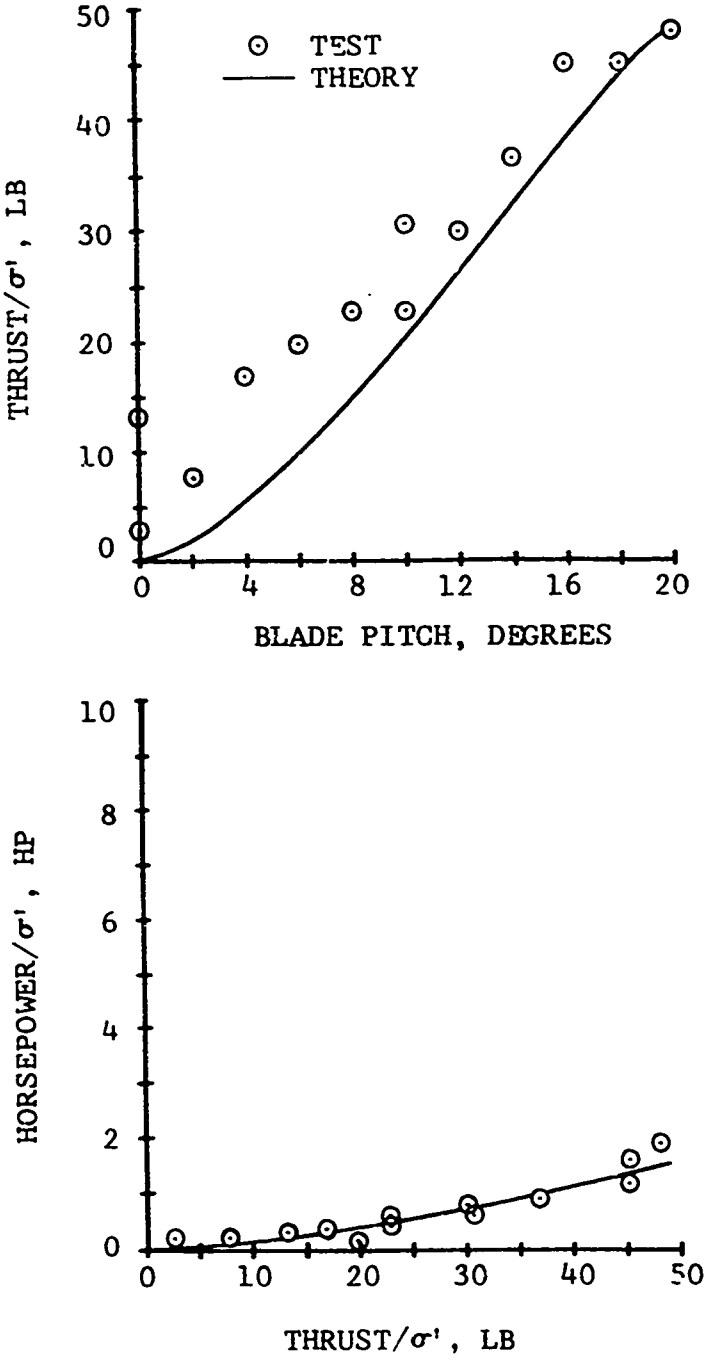

Figure 10. Tail Rotor Test Stand Balance Data at 324 RPM.

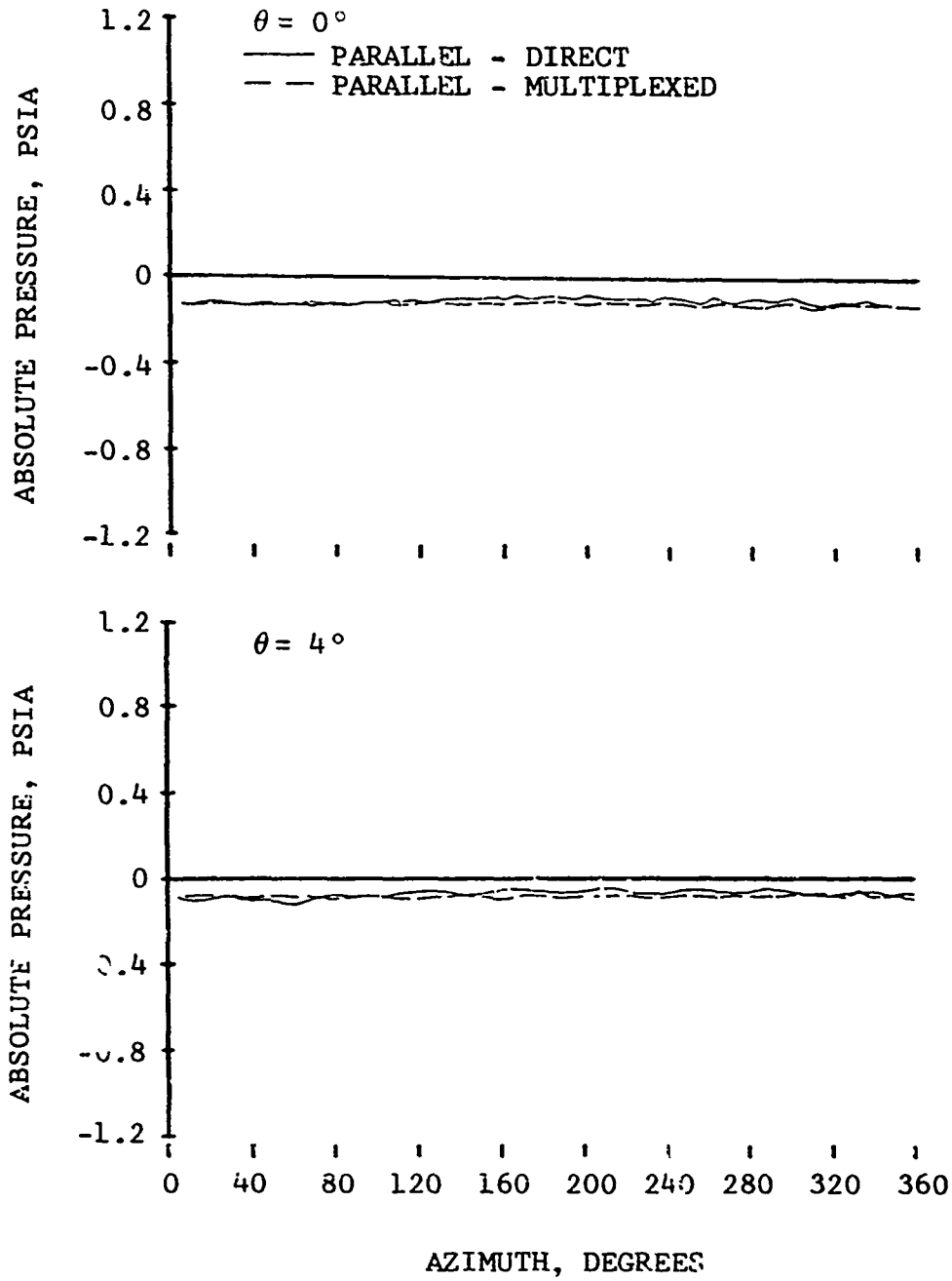

Figure 11. Comparisons of Paralleled Data From an Absolute Pressure Transducer Located at x/c = .55 of the Lower Airfoil Surface at 866 RPM for Various Blade Pitch Angles.

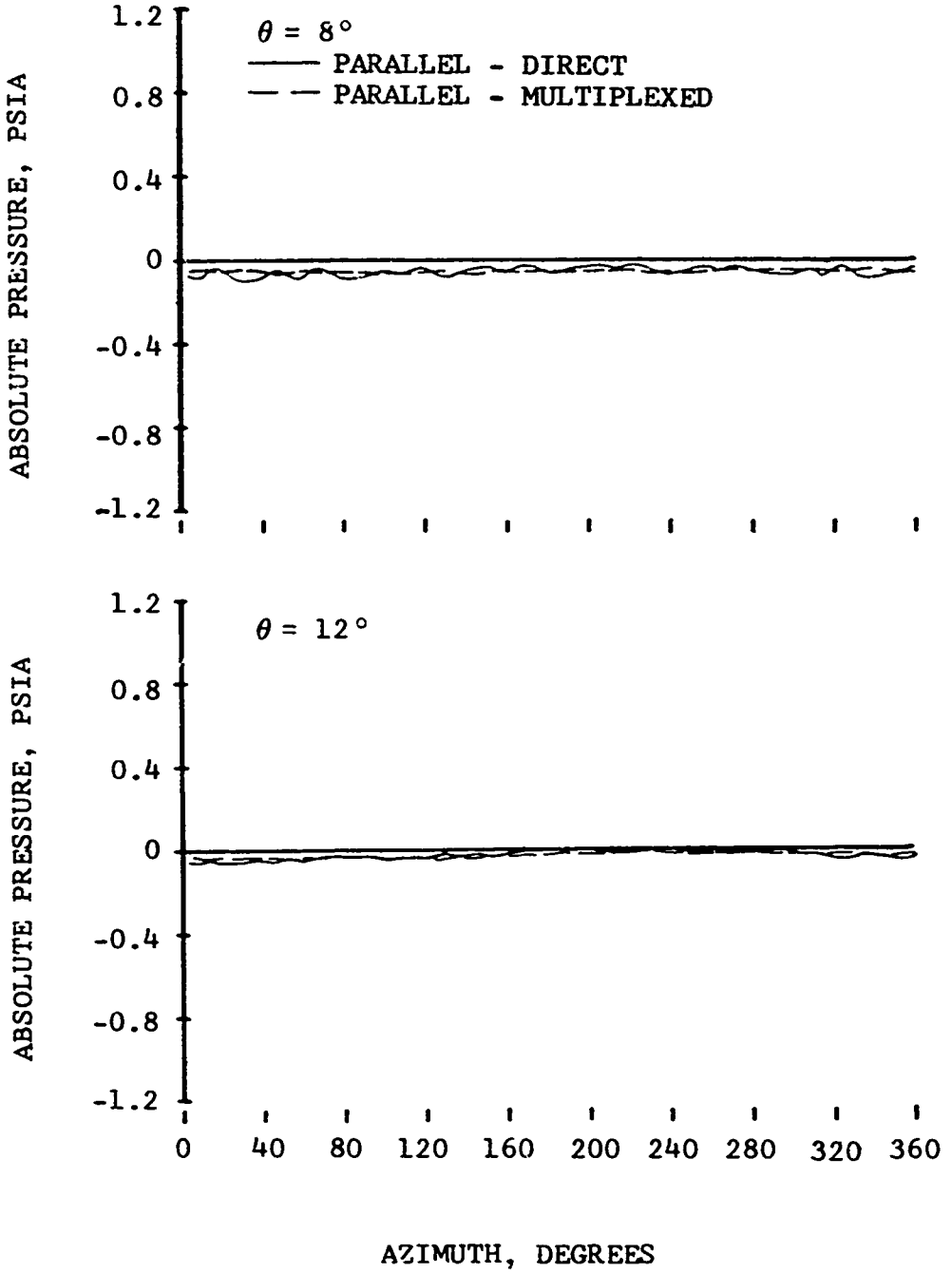

Figure 11. Continued.

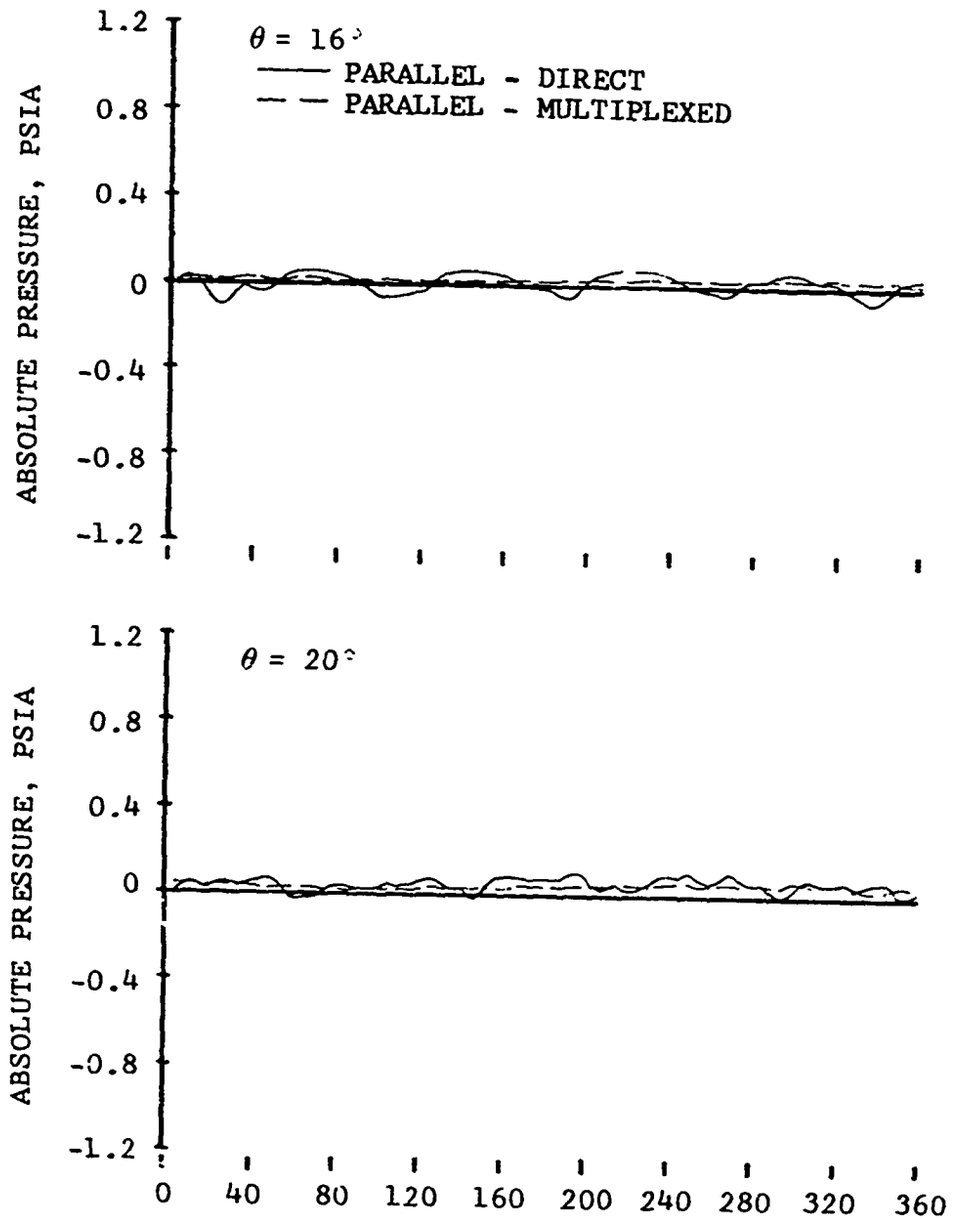

Figure 11. Concluded.

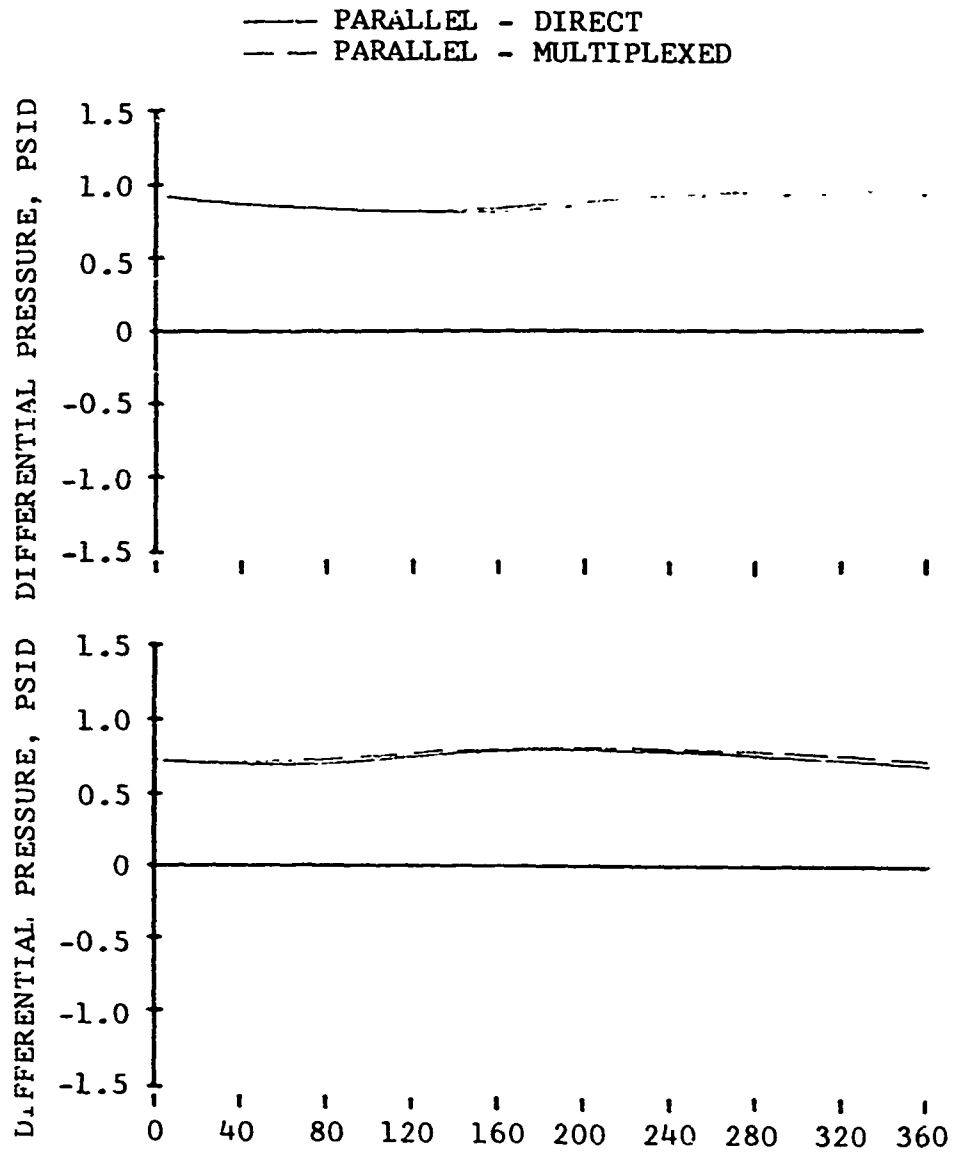

(a) $\theta = 0°$

Figure 12. Comparisons of Paralleled Data From Two Differential Pressure Transducers (One Boundary Layer Button) Located at x/c = .3 of the Upper Surface at 866 RPM for Various Blade Pitch Angles.

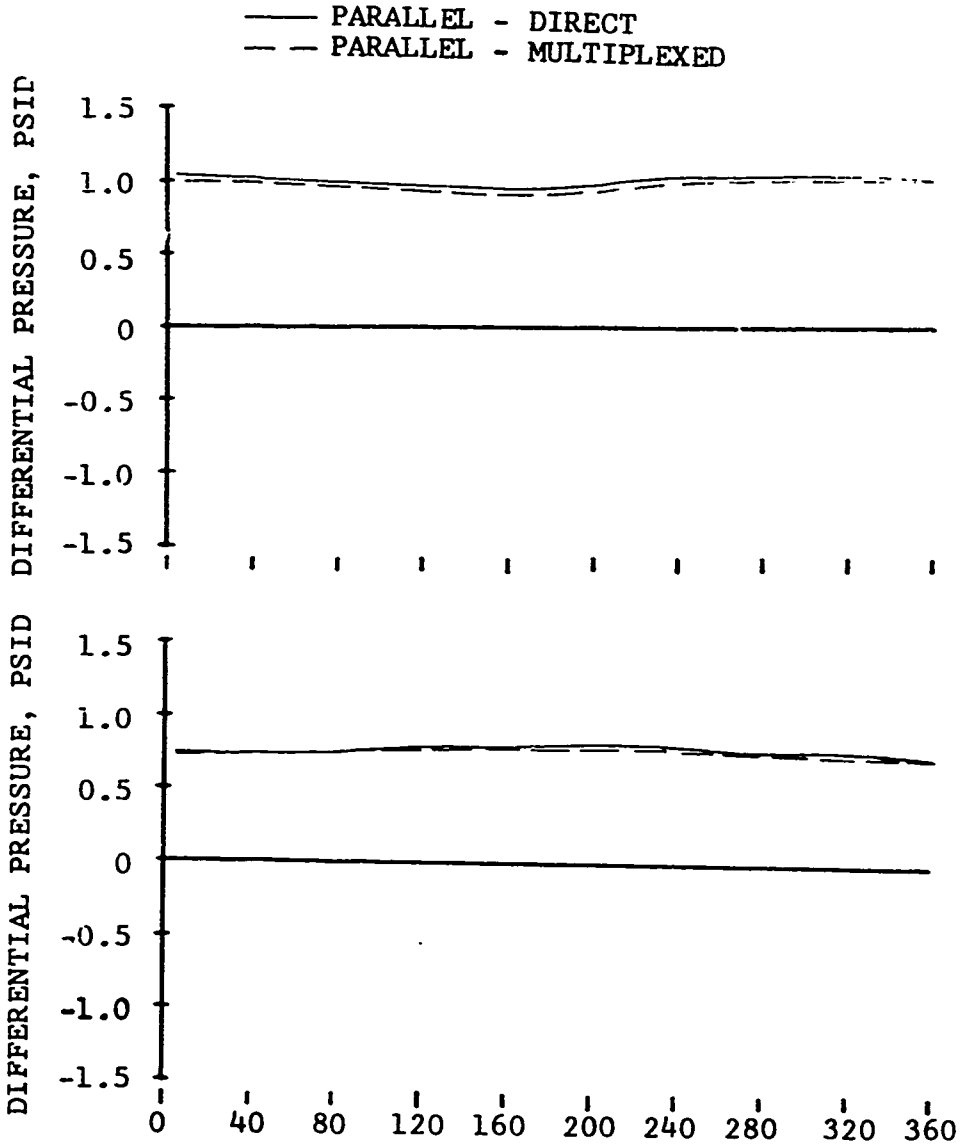

(b) $\theta = 4°$

Figure 12. Continued.

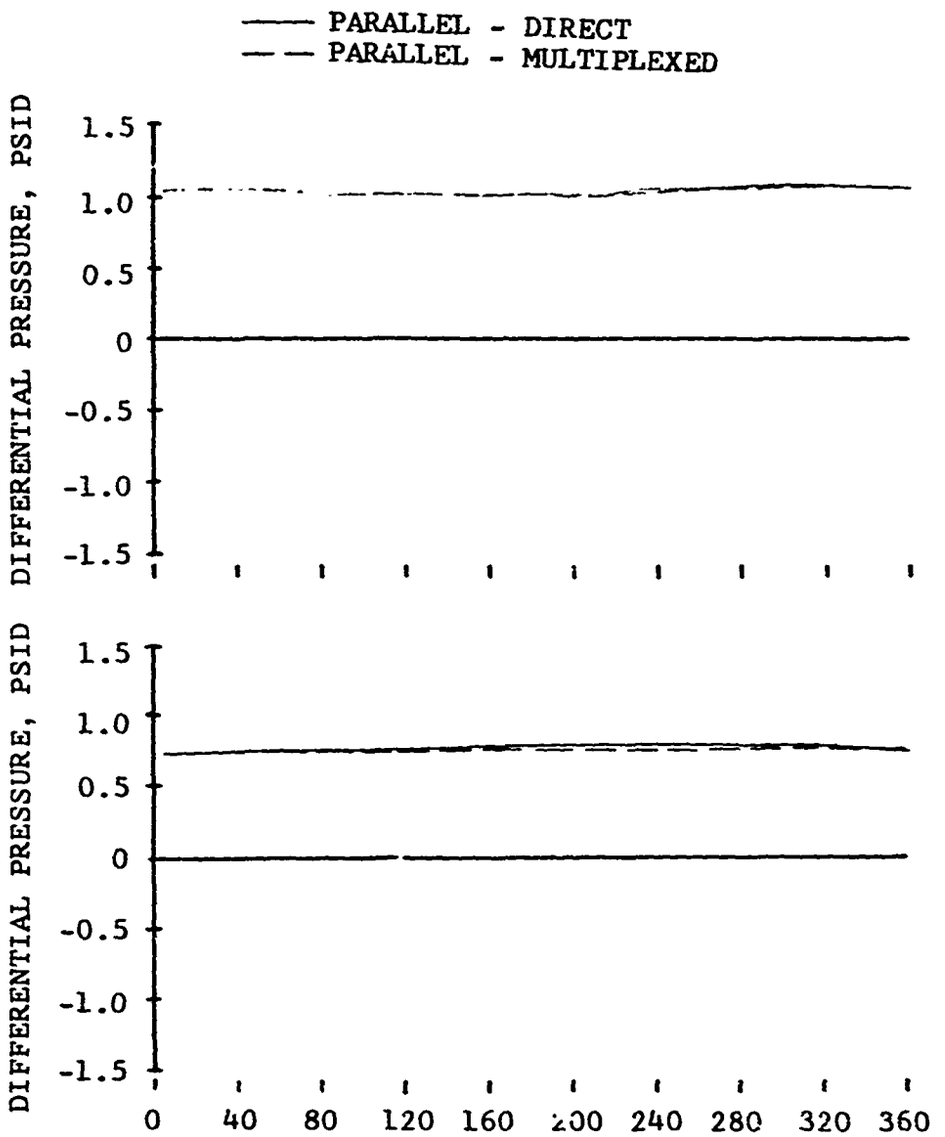

(c) $\theta = 8°$

Figure 12. Continued.

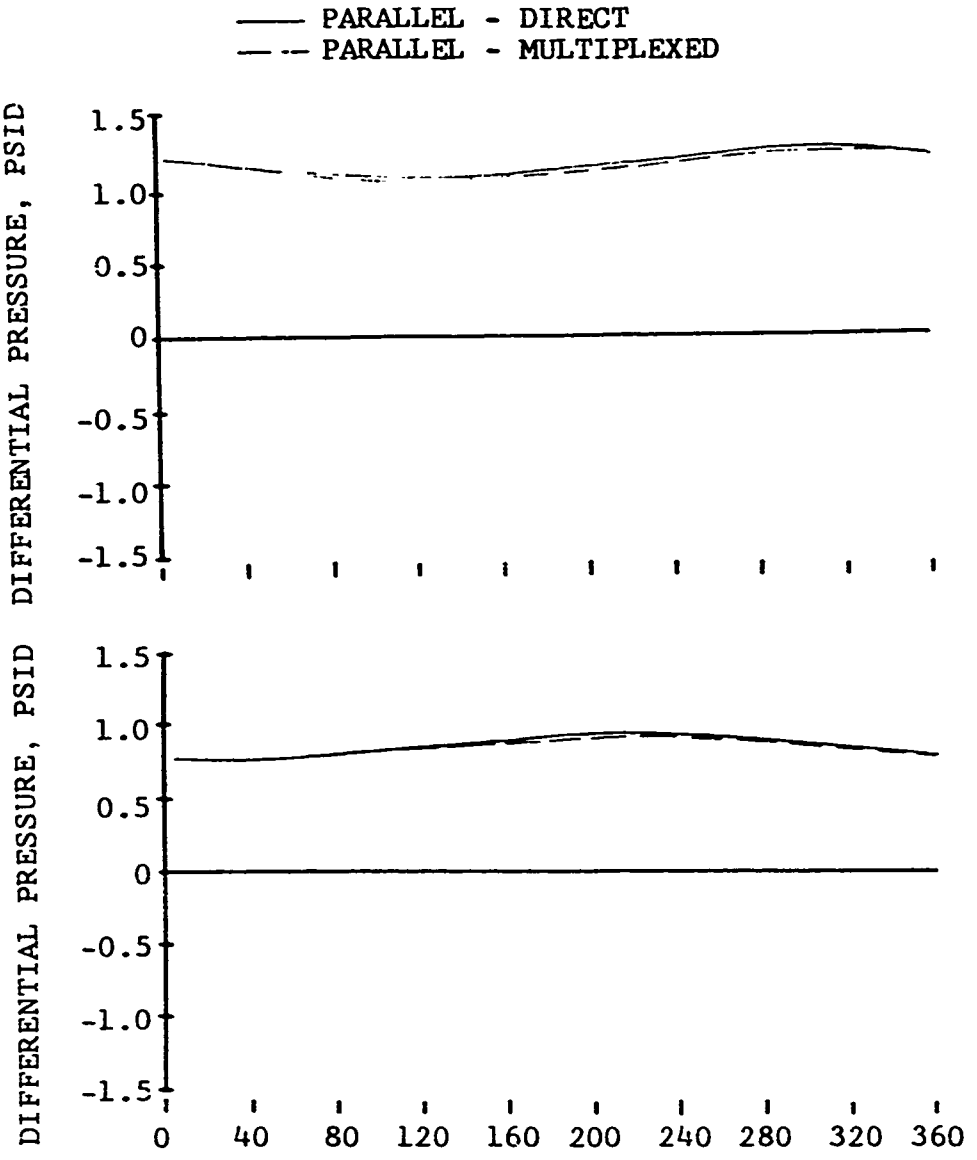

(d) $\theta = 12°$

Figure 12. Continued.

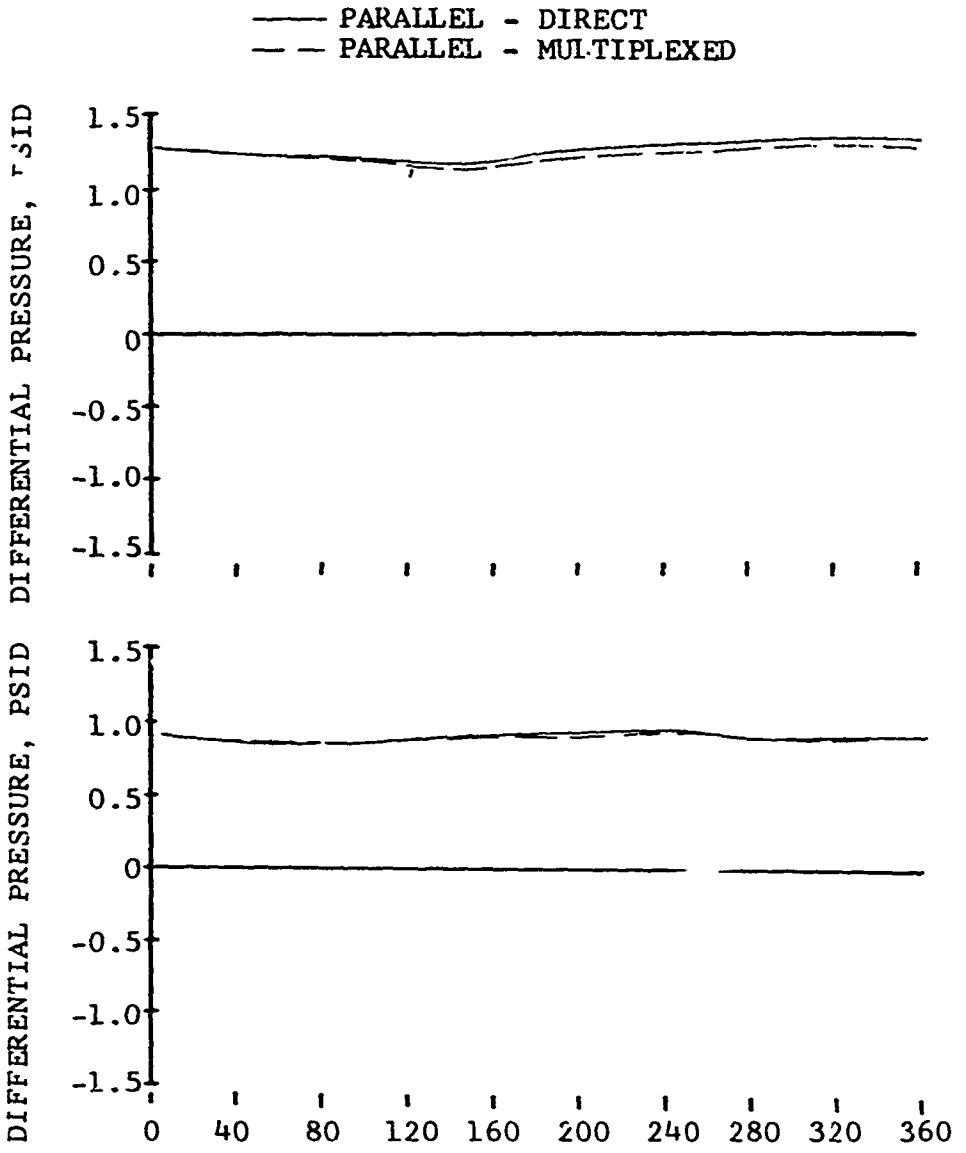

(e) $\theta = 16°$

Figure 12. Continued.

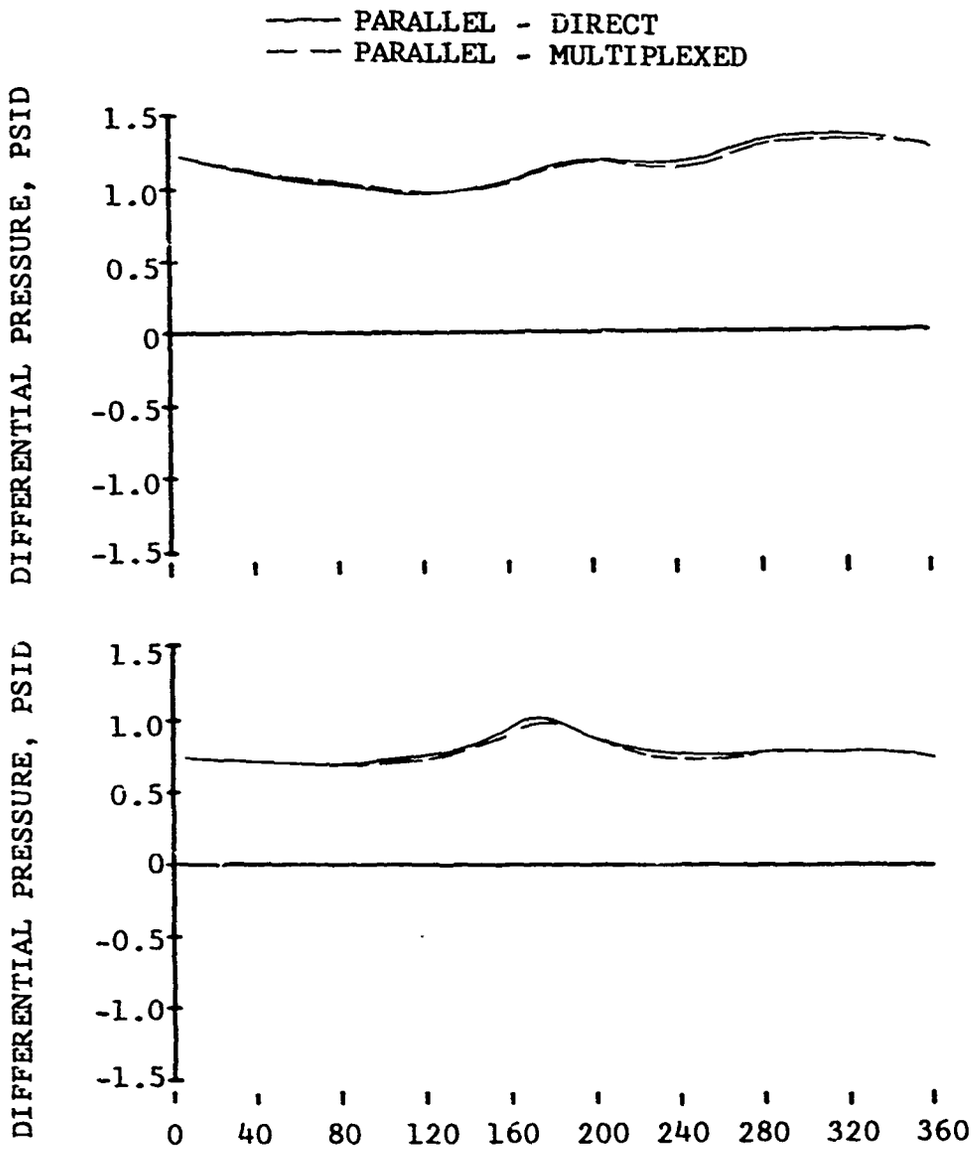

(f) θ = 20°

Figure 12. Concluded.

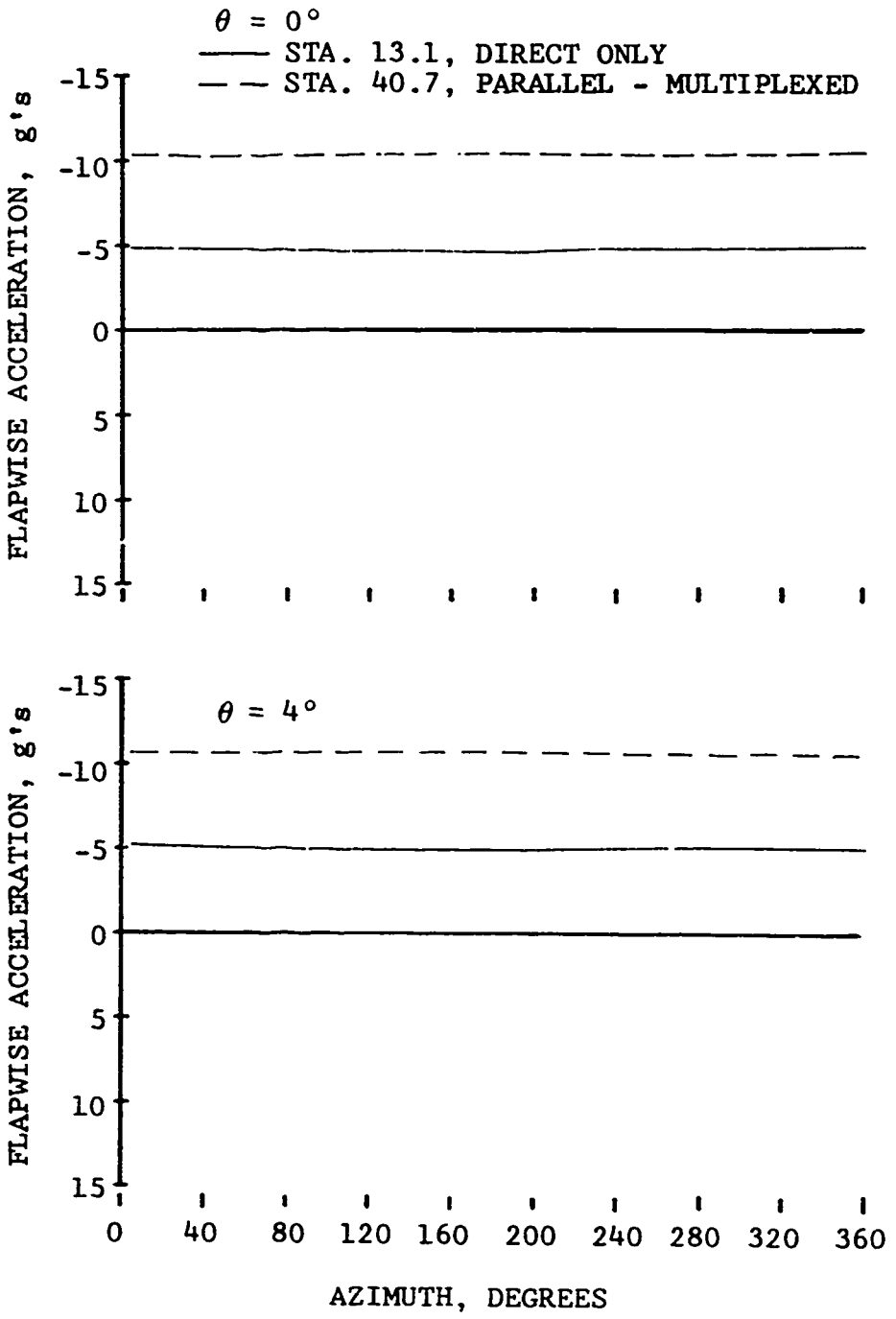

Figure 13. Inboard and Outboard Flapwise Accelerations Versus Azimuth at 866 RPM for Various Blade Pitch Angles.

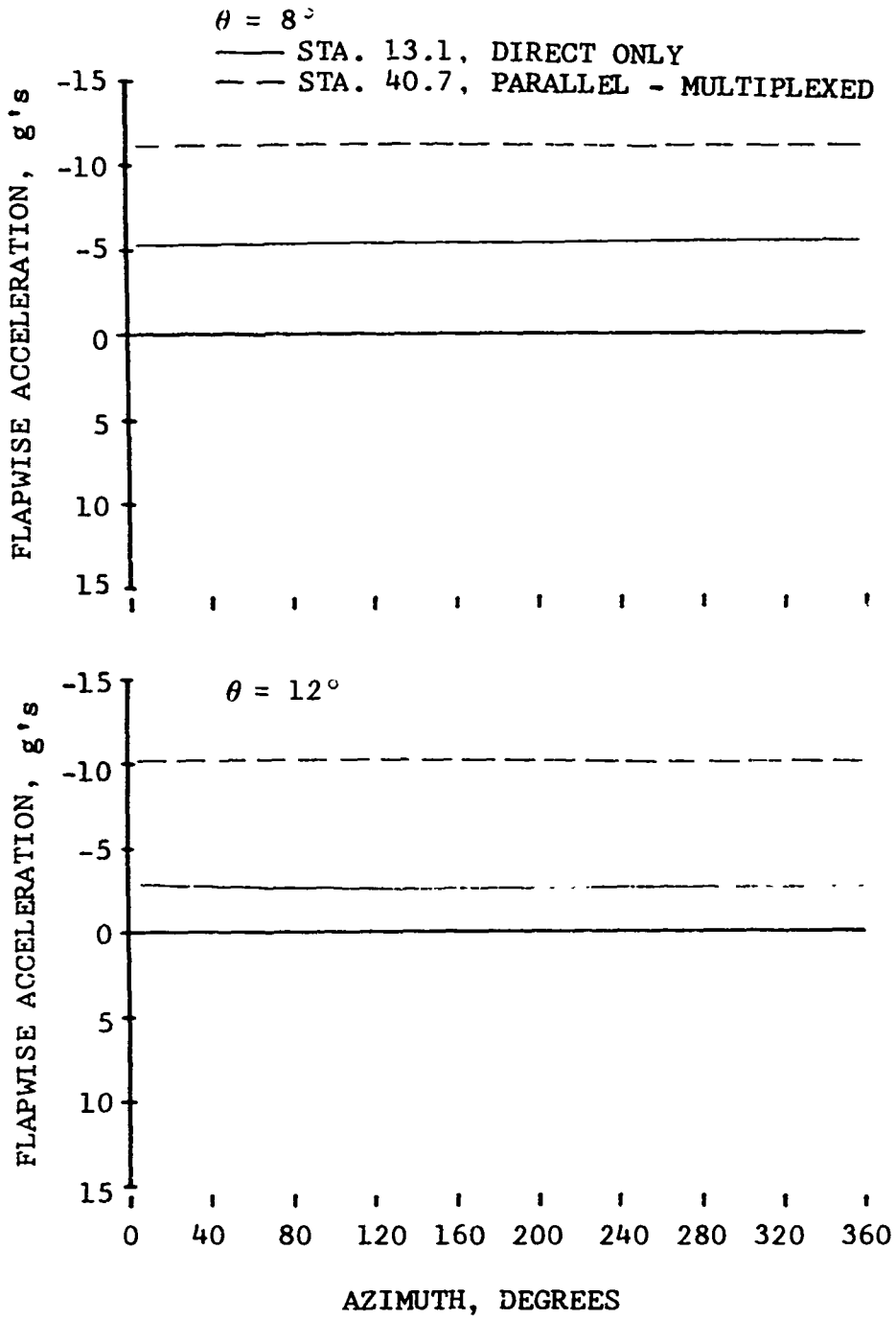

Figure 13. Continued.

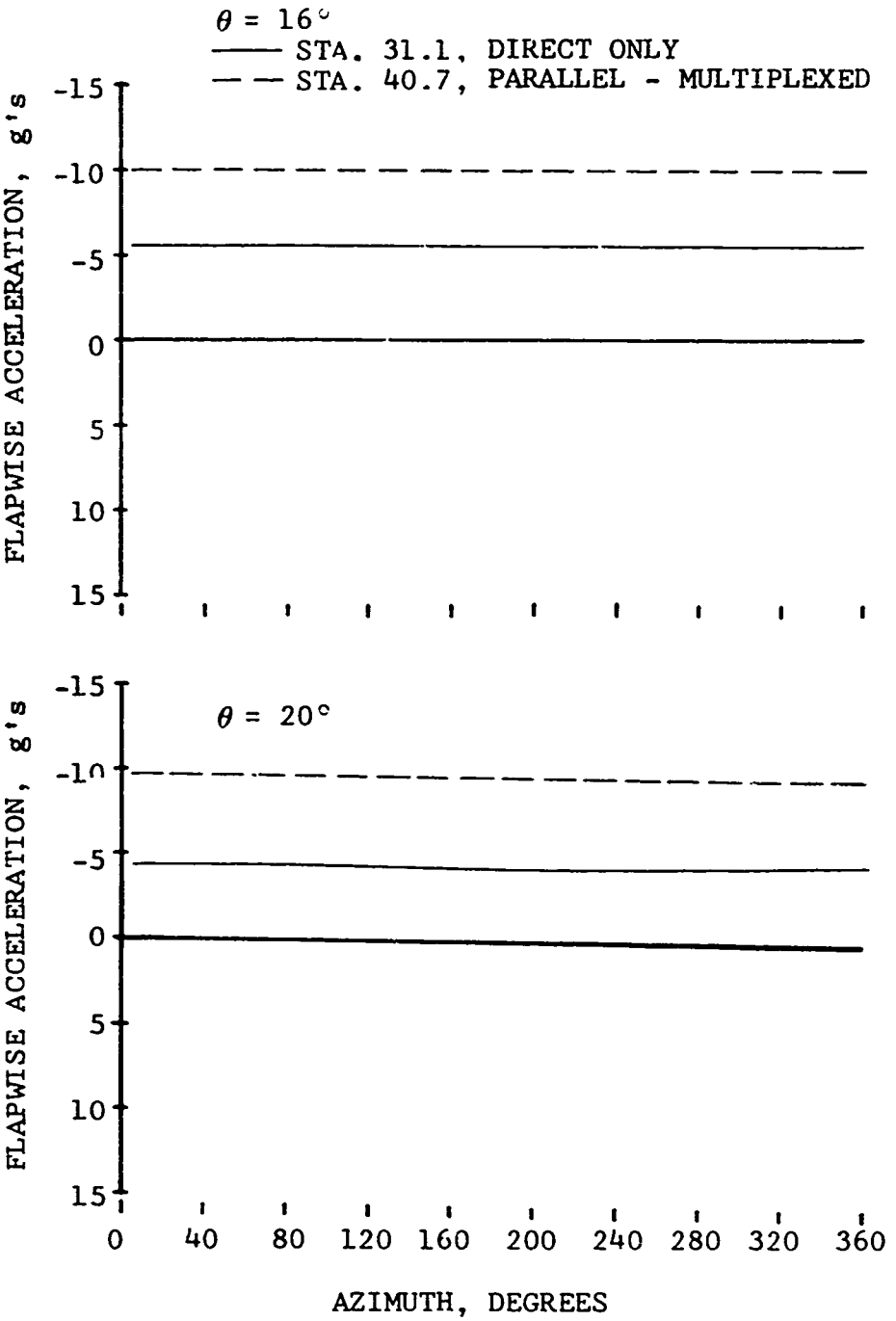

Figure 13. Concluded.

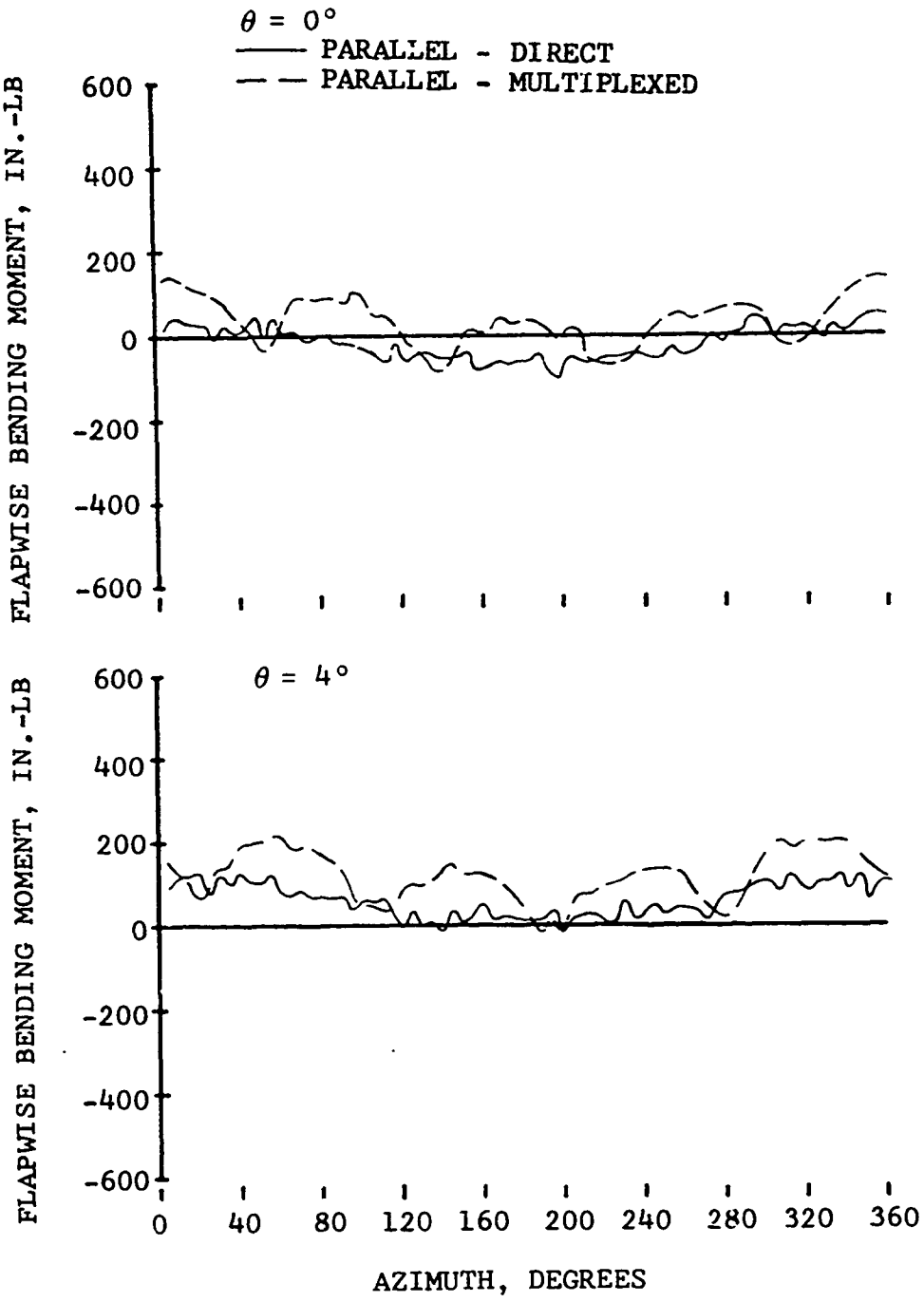

Figure 14. Comparisons of Paralleled Data From a Strain Gage Located at Radial Station 37.8 at 866 RPM for Various Blade Pitch Angles.

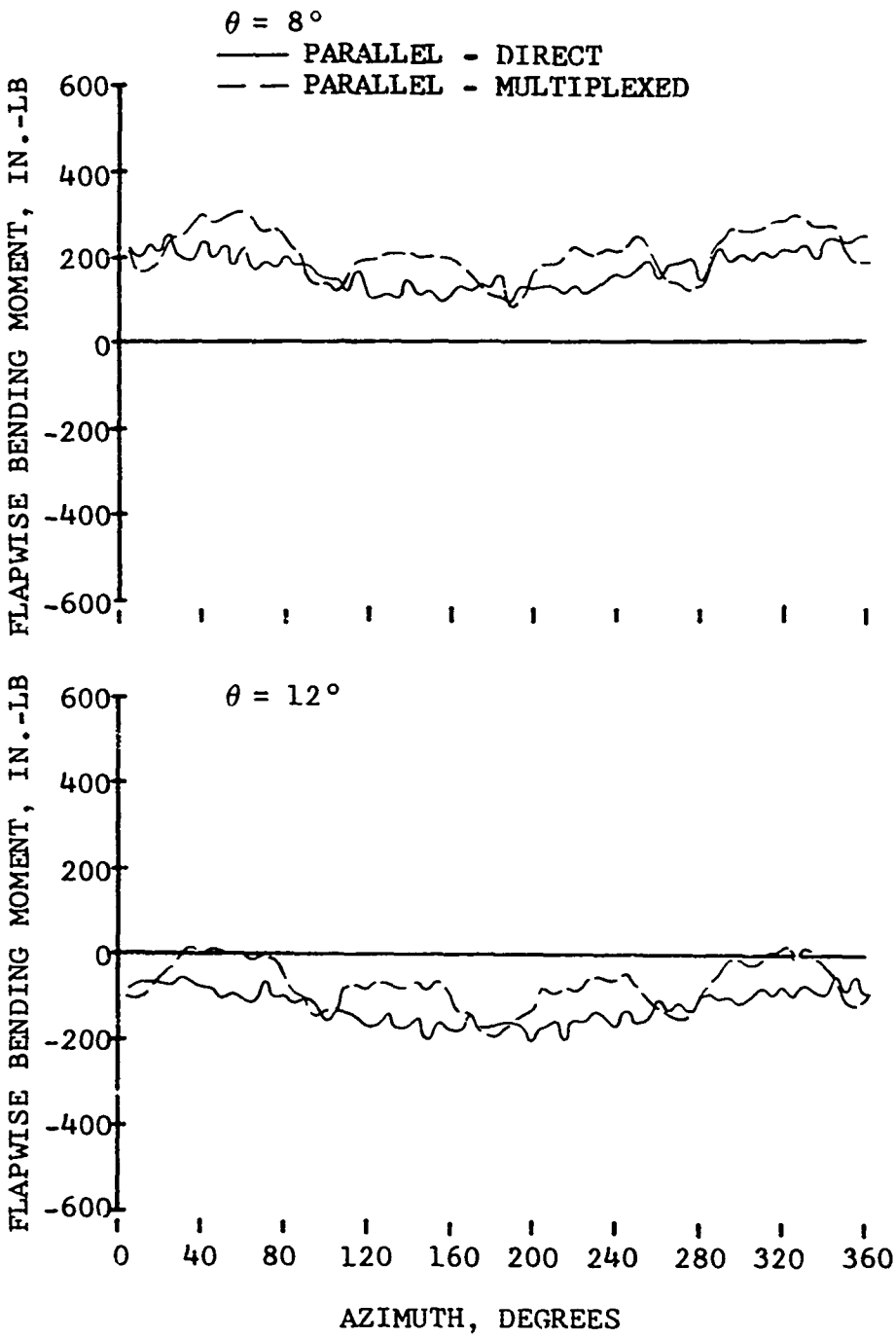

Figure 14. Continued.

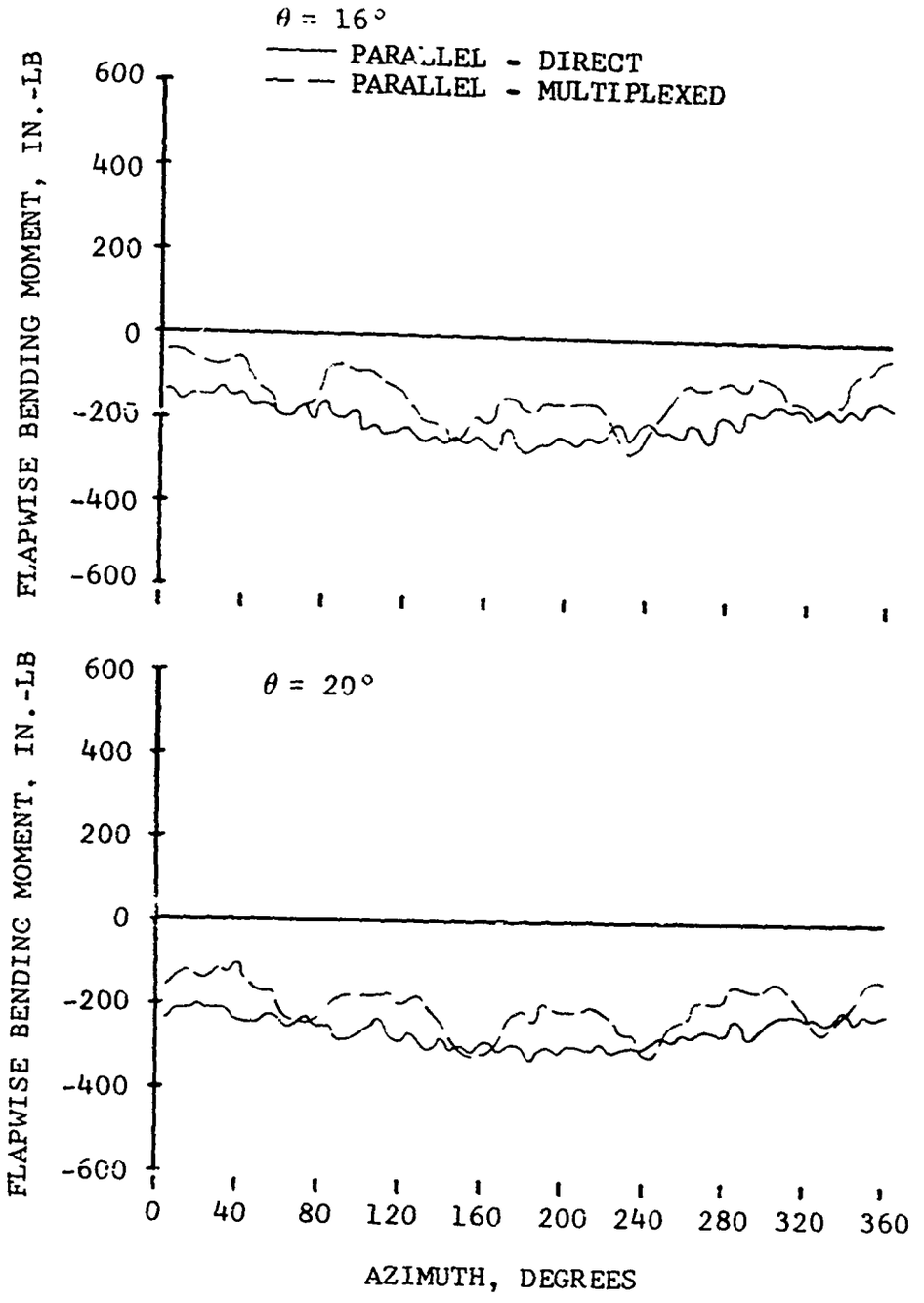

Figure 14. Concluded.

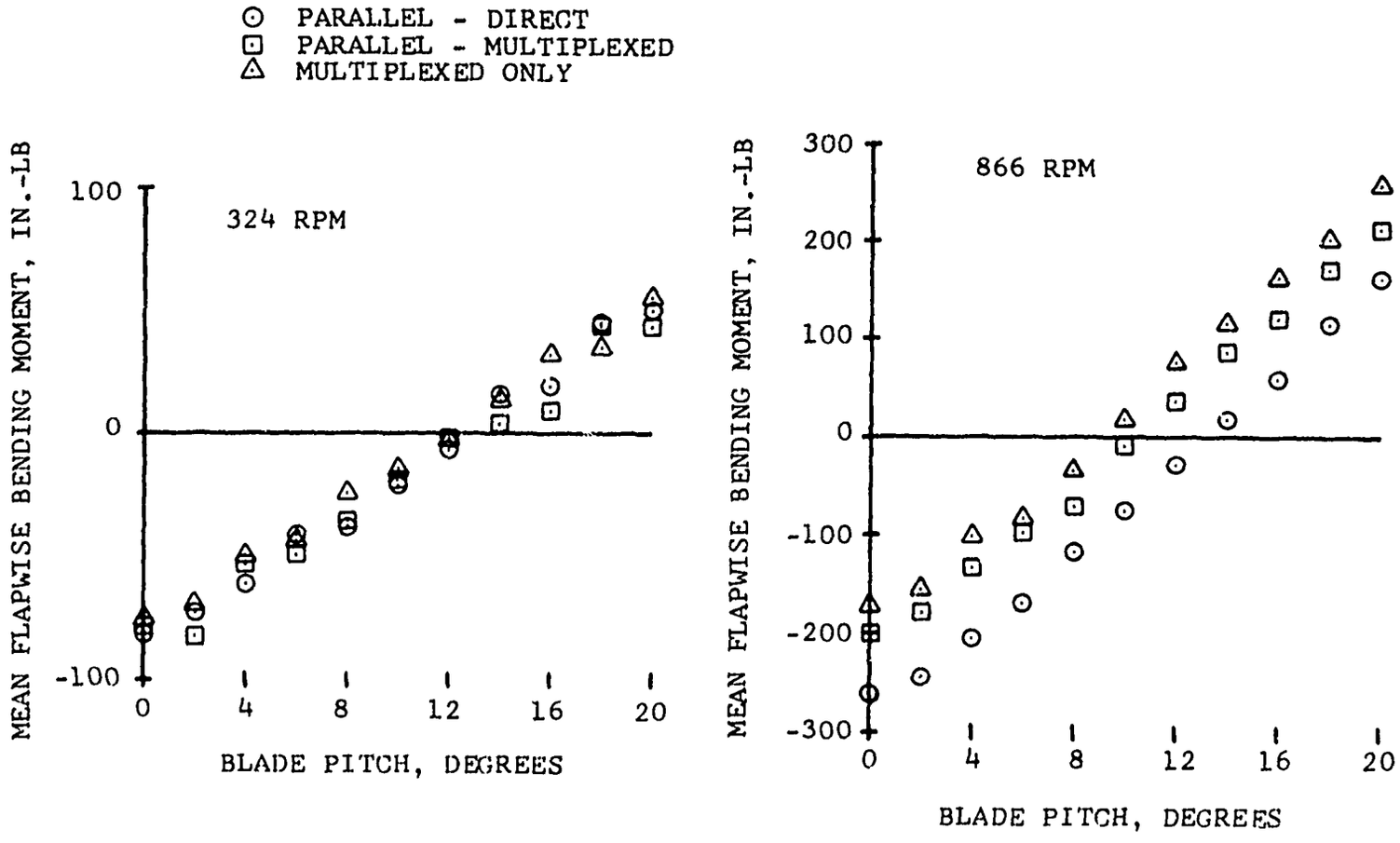

Figure 15. Comparisons of Paralleled Mean Flapwise Bending Moments at Radial Station 37.8.

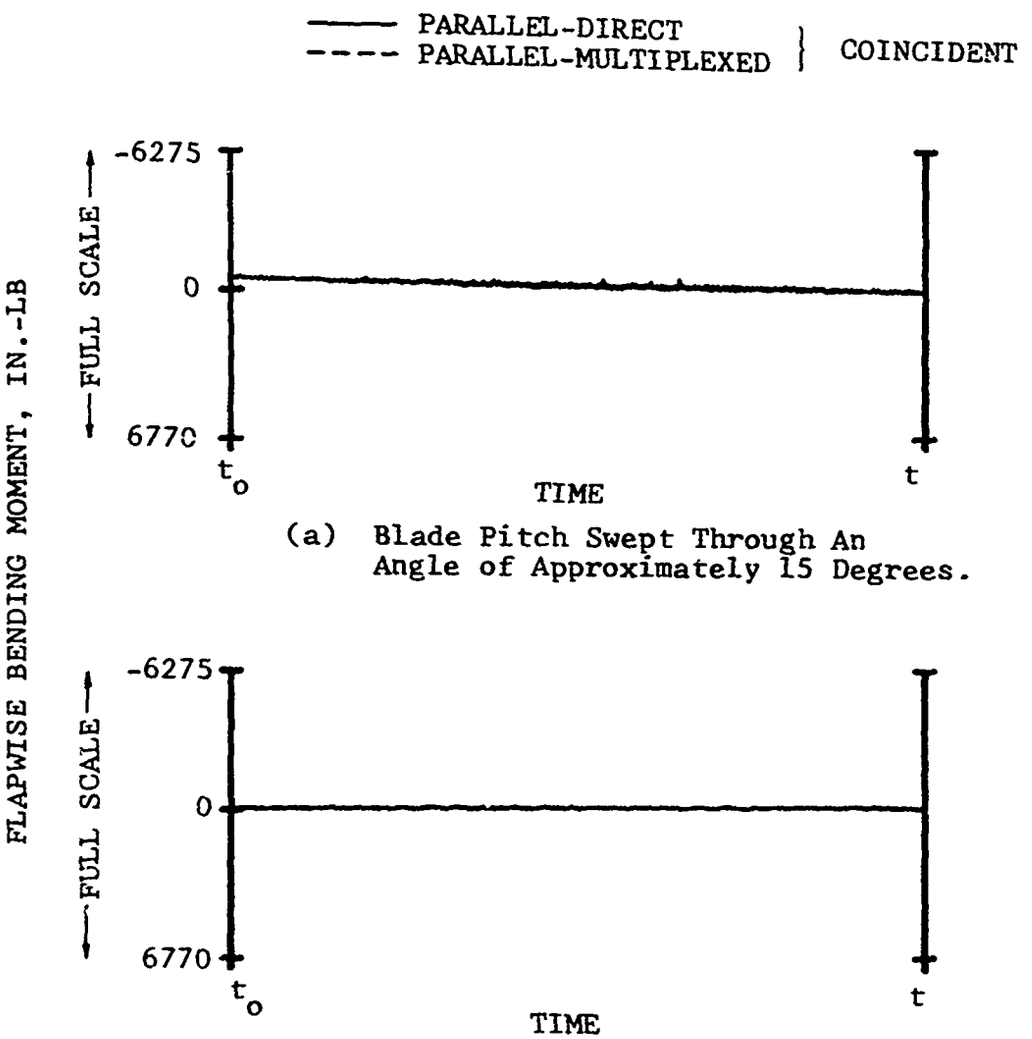

Figure 16. Time-History Comparisons of Paralleled Flapwise Bending Moments at Radial Station 37.8 at 866 RPM.

LITERATURE CITED

1. Bowden, T. H., and Shockey, G. A., A WIND-TUNNEL INVESTIGATION OF THE AERODYNAMIC ENVIRONMENT OF A FULL-SCALE HELICOPTER ROTOR IN FORWARD FLIGHT, Bell Helicopter Company; USAAVLABS Technical Report 70-35, U. S. Army Aviation Materiel Laboratories, Fort Eustis, Va., July 1970, AD 875444.

2. Durand, W. F., AERODYNAMIC THEORY, Vol. I, Division B, New York, Dover Publications, 1963, pp. 175-178.

3. Rauscher, Manfred, INTRODUCTION TO AERONAUTICAL DYNAMICS, New York, John Wiley & Sons, 1953, pp. 324-330.

4. Burpo, F. B., and Tanner, W. H., TWO DIMENSIONAL TESTS OF ADVANCED INSTRUMENTATION FOR ROTORS, Bell Helicopter Company Report 606-099-001, December 1968.

5. Technical Staff of Base Ten Systems, Inc., DESIGNERS HANDBOOK - MULTIPLEXERS AND ENCODERS FOR AIRBORNE DATA ACQUISITION, Base Ten Systems, Inc., August 1969.

6. Livingston, C. L., ROTOR AERODYNAMIC CHARACTERISTICS PROGRAM F35, Bell Helicopter Company Report 599-004-900, June 1967.

7. Hughes, C. W., Jr., TWO-DIMENSIONAL PRESSURE DISTRIBUTION PROGRAM, Bell Helicopter Company Report 599-102-901, January 1970.

8. Yoder, David C., LOW-LEVEL MULTIPLEXING FOR DATA-ACQUISITION SYSTEMS, EEE; The Magazine of Circuit Design Engineering, Vol. 18, No. 7, July 1970, pp. 67-72.

9. Elphick, Michael, MULTIPLEXER ICS, EEE; The Magazine of Circuit Design Engineering, Vol. 17, No. 7, July 1969, pp. 38-51.

10. Mahan, R. E., LOW-LEVEL MULTIPLEXING, Instruments and Control Systems, Vol. 42, No. 10, October 1969, pp. 133-136.

APPENDIX I

MULTIPLEXED HOT WIRE ANEMOMETER RESULTS

A modified instrumentation system was used which enabled parallel wiring of the hot wire anemometer signals. Time history traces of two paralleled hot wire anemometer signals are shown in Figure 17. The agreement is excellent, and in most cases the paralleled signals coincide. The angles of attack from the hot wire anemometer data are plotted in Figure 18 versus blade pitch. The paralleled angles of attack agree well with the largest difference in angle of attack being 0.6 degree. This difference corresponds to a difference in measured stagnation point location of only 0.03 inch. The major errors in hot wire angle-of-attack measurements are incurred during data reduction; translation of voltages (Figure 17) to a stagnation point location, and finally to a local angle of attack (Figure 18). This is shown by the closer agreement of the paralleled signals in Figure 17 as compared to Figure 18.

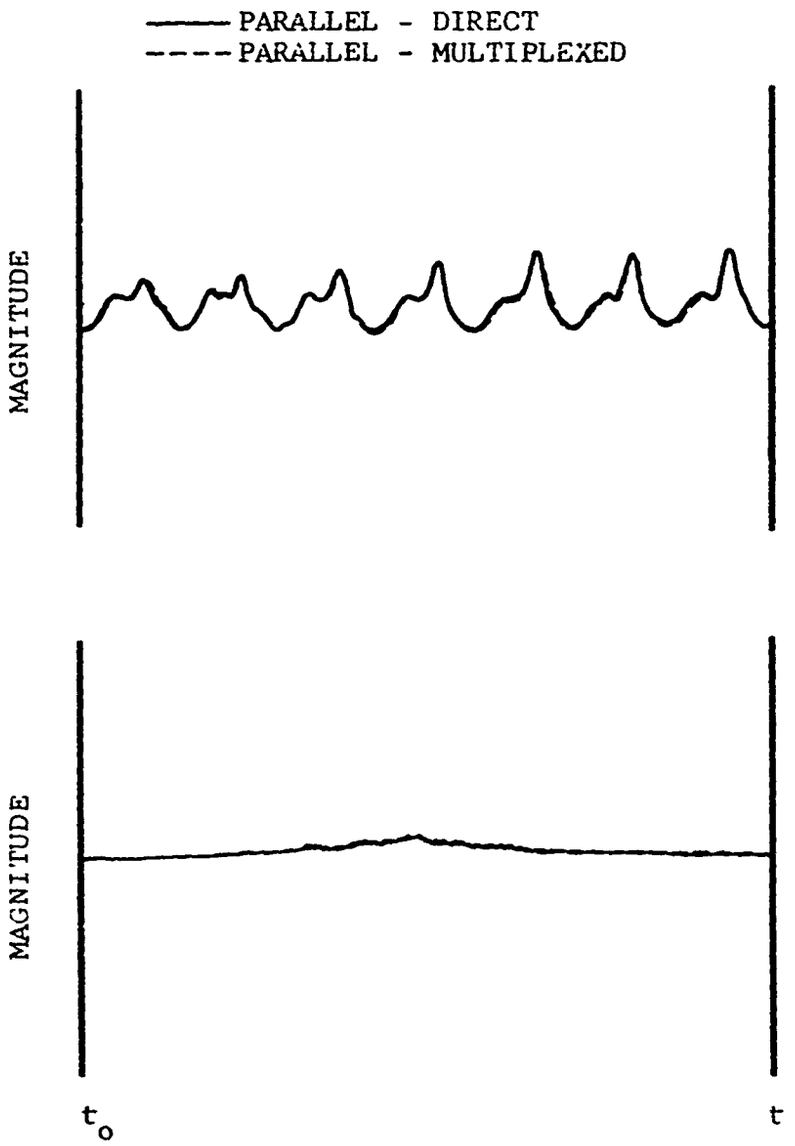

Figure 17. Comparisons of Paralleled Leading-Edge Hot Wire Anemometer Data at 866 RPM.

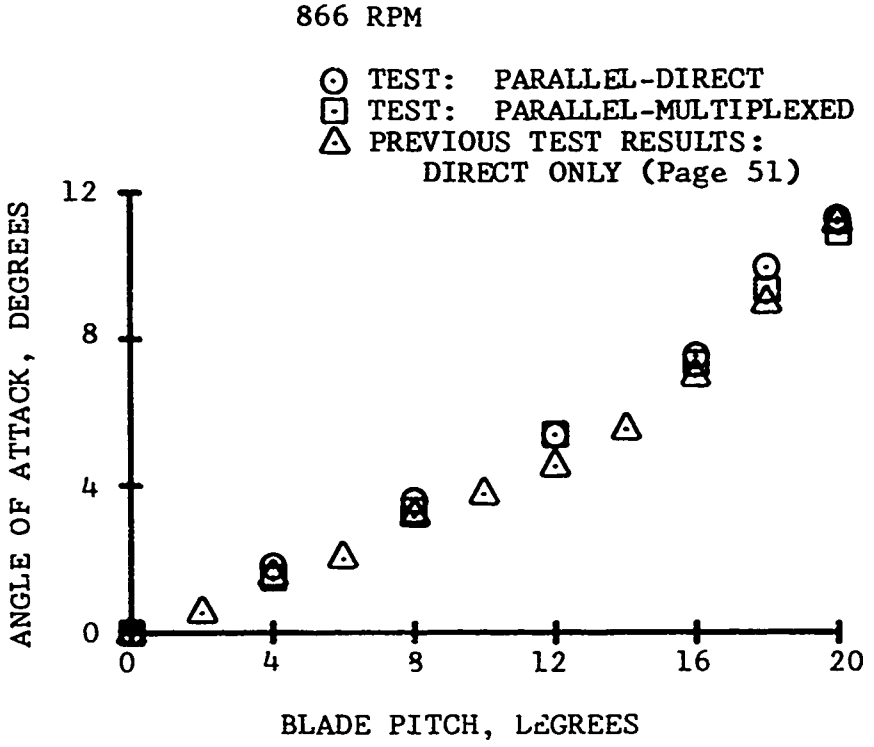

Figure 18. Comparisons of Paralleled Leading-Edge Hot Wire Anemometer Angle-of-Attack Measurements at 866 RPM.

APPENDIX II

AERODYNAMIC TEST RESULTS

The aerodynamic data are presented to give further comparisons between the direct data and the multiplexed data, and for future reference.

The aerodynamic data presented are compared to theoretical calculations from two aerodynamic computer programs. Theoretical rotor forces and angle-of-attack distributions were obtained from an aerodynamic hover computer program (Reference 4). The angles of attack from this program were used as inputs to a two-dimensional potential flow pressure distribution program (Reference 5) which gave theoretical pressure distributions and integrated airfoil section forces.

ANGLE OF ATTACK

Figure 19 shows the angles of attack determined from the leading-edge hot wire measurements versus blade pitch compared to theory. The agreement between experiment and theory is good. Some error may have been incurred because of the resolution. Within the range of $0° \leqslant \alpha \leqslant 8°$, there could be as much as a 4-degree change in angle of attack between adjacent wire segments. Since, in both this test and past efforts (References 1 and 4), the agreement of measured angles of attack with theory has been shown to be good, theory will be used in the future to determine spacing between adjacent wires. Uneven wire spacing will be used so that the number of angles of attack per wire is held constant.

PRESSURE DISTRIBUTIONS

The average pressure values were plotted (Figures 20 and 21), since the pressure distributions were generally repeatable around the azimuth as would be expected in hover. Included to illustrate the repeatability of the pressure distributions and the agreement of the paralleled pressure transducer signals are plots for every 30 degrees azimuth for 12 degrees of blade pitch (Figures 22 and 23). The paralleled pressure coefficients at $x/c = .55$ of the lower surface agree very well, and are often indistinguishable, in both the average plots and the pressure distributions around the azimuth. The differences are caused by electrical noise which existed in the direct side of the paralleled signal.

Pressure coefficients at the leading and trailing edges of the airfoil are necessary for the data reduction, computer program integration routines which calculate the airfoil forces. The difficulty of physically placing pressure transducers at

these locations precludes obtaining experimental data there. To provide the pressure coefficients, the two adjacent upper and two adjacent lower pressure coefficients are extrapolated to give two values at both the leading and trailing edges. These two values, then, are averaged to provide the necessary leading and trailing edge pressure coefficients.

Two-dimensional potential flow theory is included on the average pressure distribution plots (Figures 20 and 21). The agreement between experiment and theory is very good. The pressure coefficients measured at the trailing edge of the airfoil and those given by theory are more negative than would occur on a standard NACA symmetrical airfoil. This is caused by deviations from the standard NACA contour at the airfoil trailing edge.

The possible error in a given transducer signal is about 0.3 percent of full scale. As a result, the smaller-output signals at 324 rpm may contain a larger percentage of error than the 866-rpm test condition. The maximum error in each pressure coefficient at 324 rpm, taking into account the zero shift discussed in the Multiplex Results section, was calculated to be approximately .5, while the maximum error at 866 rpm was calculated to be approximately .05. These errors and their results become more apparent in the integrated force coefficients for 12 degrees of blade pitch at 866 and 324 rpm, respectively (Figures 24 and 25).

INTEGRATED FORCE COEFFICIENTS

Figures 24 and 25 illustrate the repeatability around the azimuth of the integrated force coefficients. The repeatability with respect to azimuth position of the normal and chord force coefficients for both 866 and 324 rpm was generally poor. Averages of the integrated force coefficients around the azimuth are plotted versus angle of attack as determined from the hot wire anemometer measurements (Figure 26). Theory is included on these figures. The potential flow theory predicts pitching moment coefficients of zero for the range of angles of attack encountered. The experimental and theoretical normal force coefficients agree well. The agreement between the experimental and theoretical chord force and pitching moment coefficients is fair. The discrepancies between experimental and theoretical chord force coefficients at low values of angle of attack are primarily due to the lack of pressure measurements close to the leading edge. This is illustrated by Figure 27, which shows that the C_p versus y/c loops, which give positive chord forces, are drastically reduced. The leading-edge pressure coefficient was extrapolated from pressure coefficients which are too far from the y/c value of zero (leading edge) and, therefore, give values

far lower than the expected stagnation point value of +1. As the blade pitch angle increases, the agreement between experiment and theory improves as expected since as the angles of attack increase, the stagnation point moves rearward along the lower airfoil surface. Thus, the stagnation point is physically closer to a pressure transducer, and the measured pressure coefficient there is closer to the stagnation point value of +1. The large and often erratic pitching moment coefficients are a result of insufficient accuracy. Additional pressure transducers were placed close to the trailing edge of the airfoil (x/c = 0.68 and 0.86) in the hope that good pitching moment data could be obtained. The data at 866 rpm show a consistent trend with angle of attack (Figure 26), but the actual magnitudes are suspect. This is because of significant errors which can be incurred on integrated pitching moments by small errors in the measured chordwise pressures. The following and combinations thereof are possible solutions to obtaining accurate pitching moment data:

- Obviously by adding more pressure transducers, especially at the leading and trailing edges of the airfoil
- Better integration techniques, such as first curve fitting the pressure distributions
- Minimizing errors in the chordwise pressure measurements

BOUNDARY LAYER BUTTONS

The boundary layer button is an instrument for measuring the magnitude and direction of the local velocity on a rotor blade. Boundary layer buttons were installed at 30 and 85 percent chord on the upper and lower surfaces at the 75 percent radius station. However, the boundary layer button at 85 percent chord of the lower surface had a transducer failure, and the signal was lost. The radial flow angles at 75 percent radius for every 4 degrees of blade pitch at 866 rpm are shown in Figure 28. The agreement of the paralleled data in all cases is excellent. The radial flow angle at x/c = .3 of the upper surface remains fairly constant, becoming slightly more negative as blade pitch is increased. The radial flow angles at x/c = 0.3 of the lower surface at low collective angles are about the same as the angles measured on the upper surface. As blade pitch is increased, the lower surface angles become markedly more negative due to the increased inflow and wake contraction. The radial flow angles at x/c = 0.85 of the

upper surface at low blade pitch values are about the same as those measured at x/c = 0.3. As the blade pitch angles increase, the angles become more positive as the thickened and later separated boundary layer is centrifuged outward. The radial flow angles for every 4 degrees of blade pitch at 324 rpm are shown in Figure 29. These angles are erratic and very suspect because of the susceptibility to large errors in pressure transducer measurements at 324 rpm, as discussed in the Pressure Distribution section (p. 47).

Local velocity measurements from the boundary layer buttons at 866 rpm for 0, 10, and 20 degrees blade pitch are shown in Figure 30. The paralleled data are again in excellent agreement.

STRAIN GAGE AND ACCELEROMETER

The average mean flapwise bending moments and accelerations versus blade pitch for both 324 and 866 rpm are shown in Figures 31 and 32, respectively. No analysis of these data were attempted other than for comparisons of direct versus multiplexed signals (refer to Multiplex Results section).

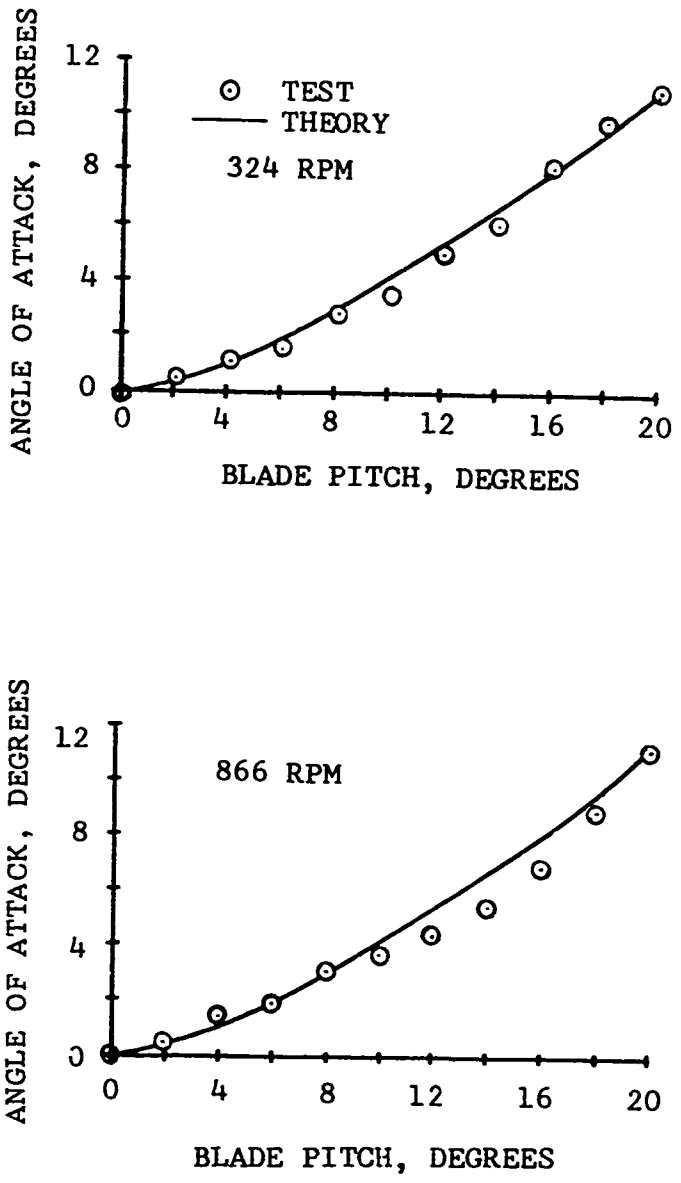

Figure 19. Local Angle of Attack Versus Blade Pitch.

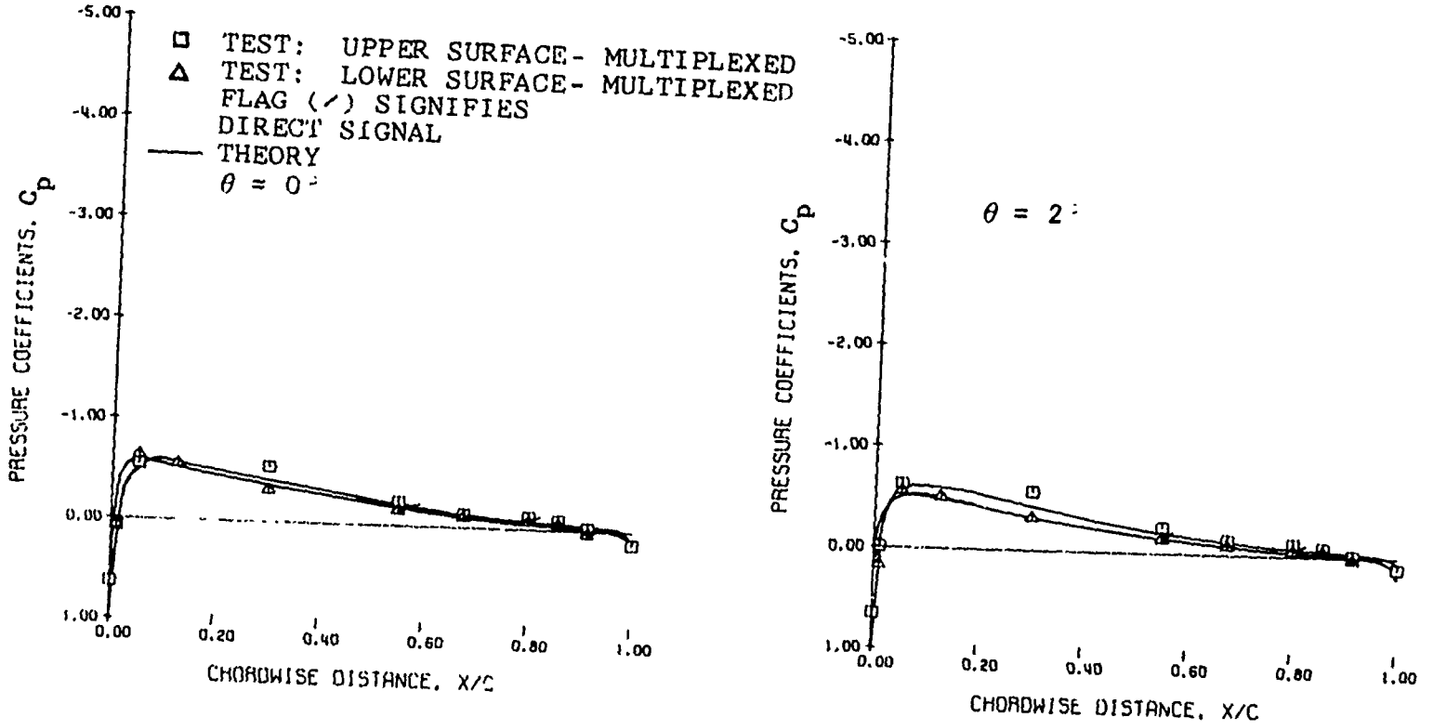

Figure 20. Average Chordwise Pressure Distributions Taken at 866 RPM for Various Blade Pitch Angles.

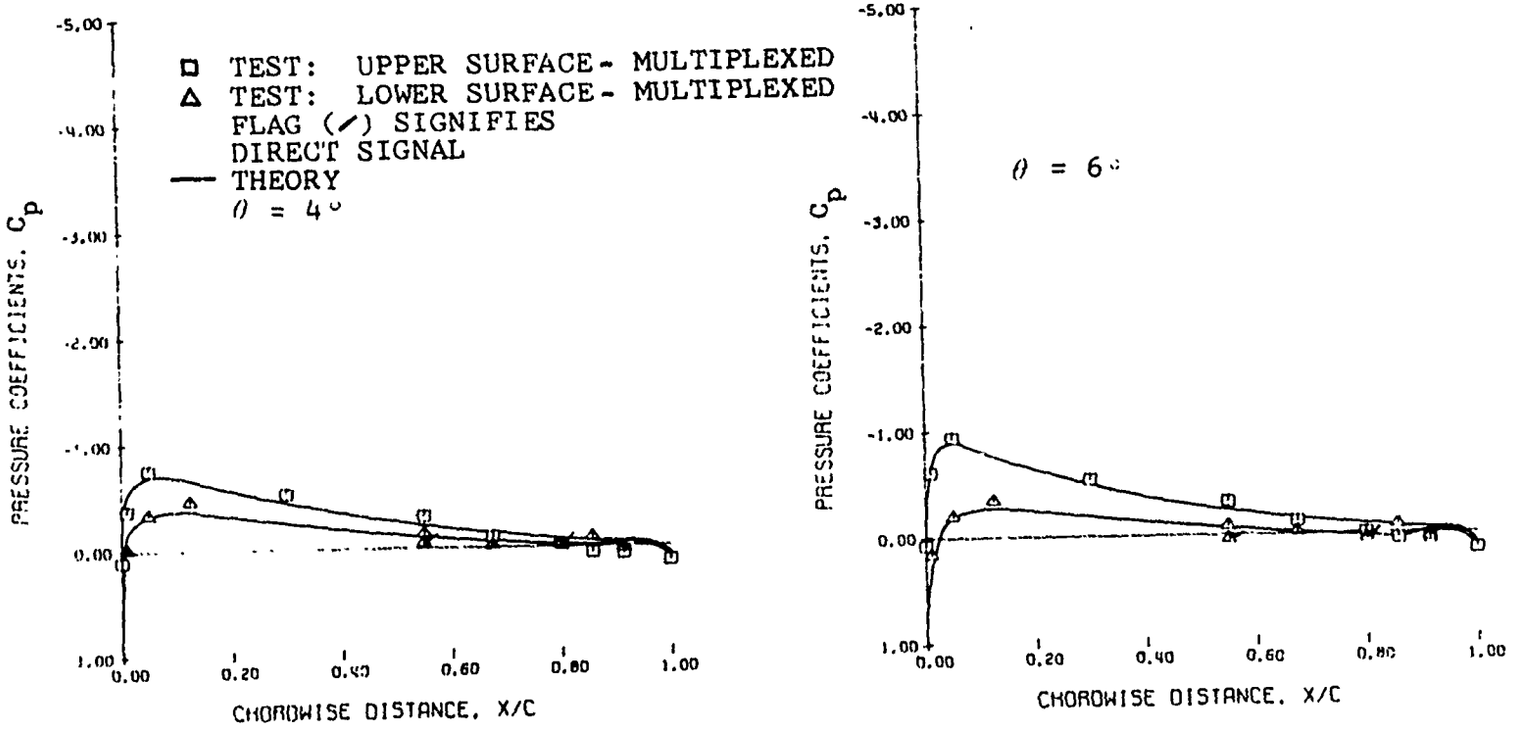

Figure 20. Continued.

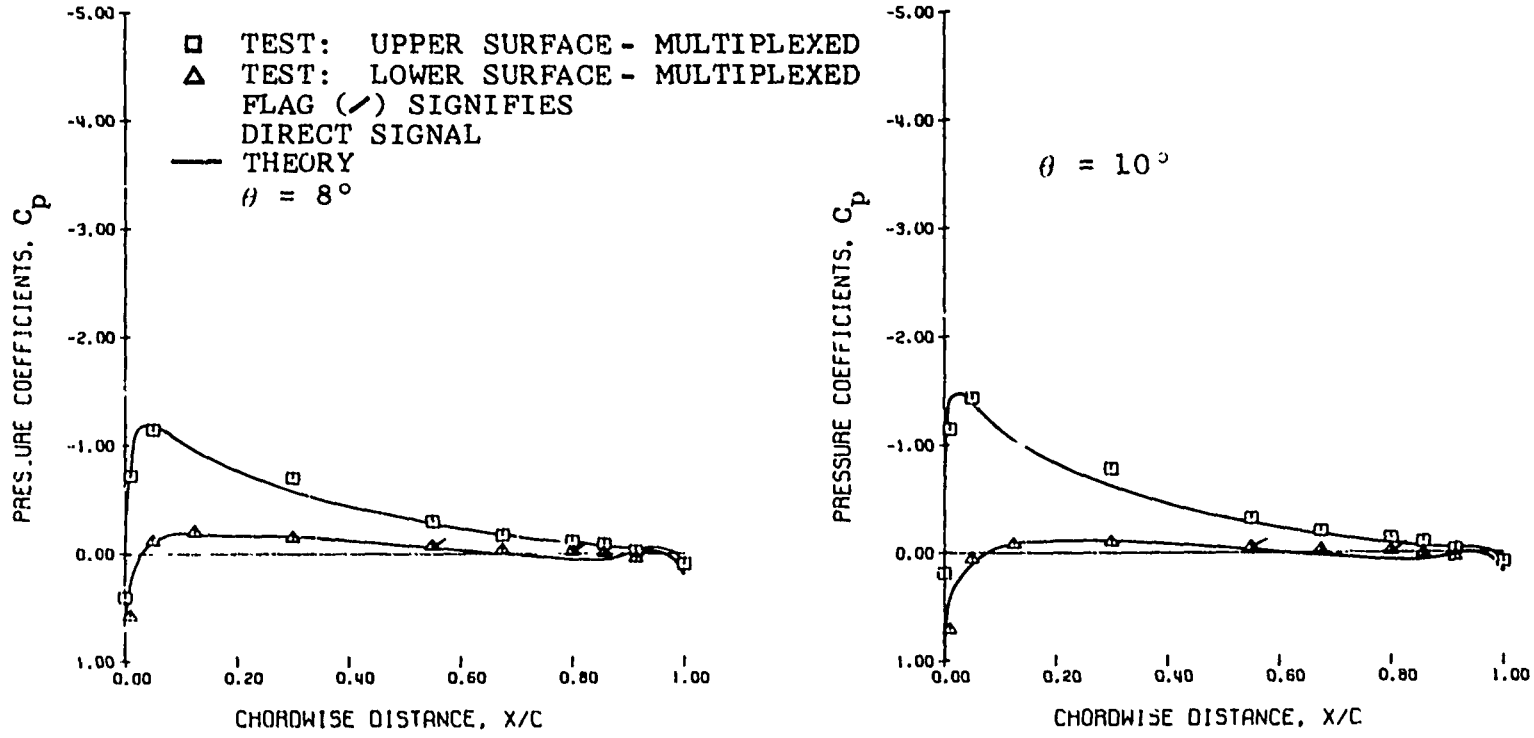

Figure 20. Continued.

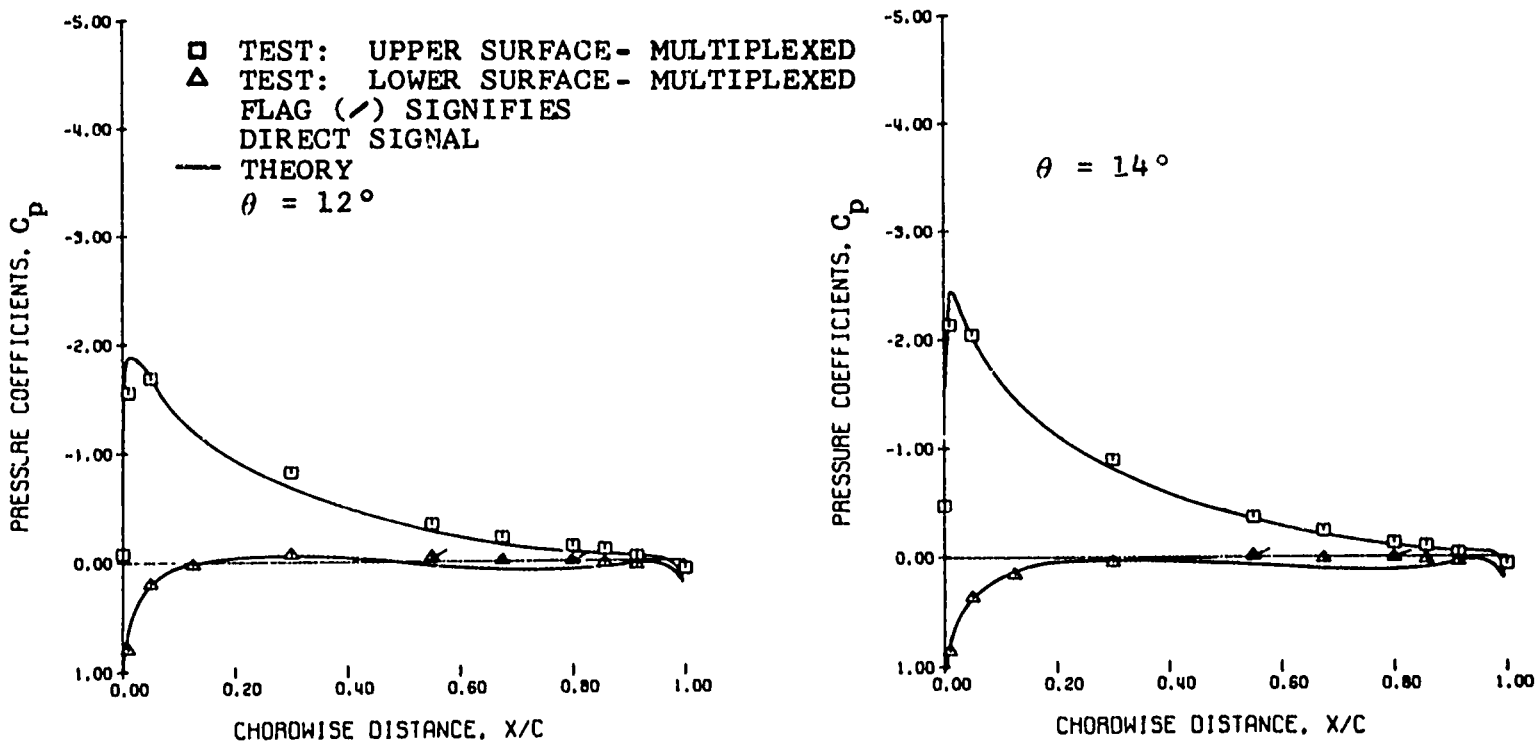

Figure 20. Continued.

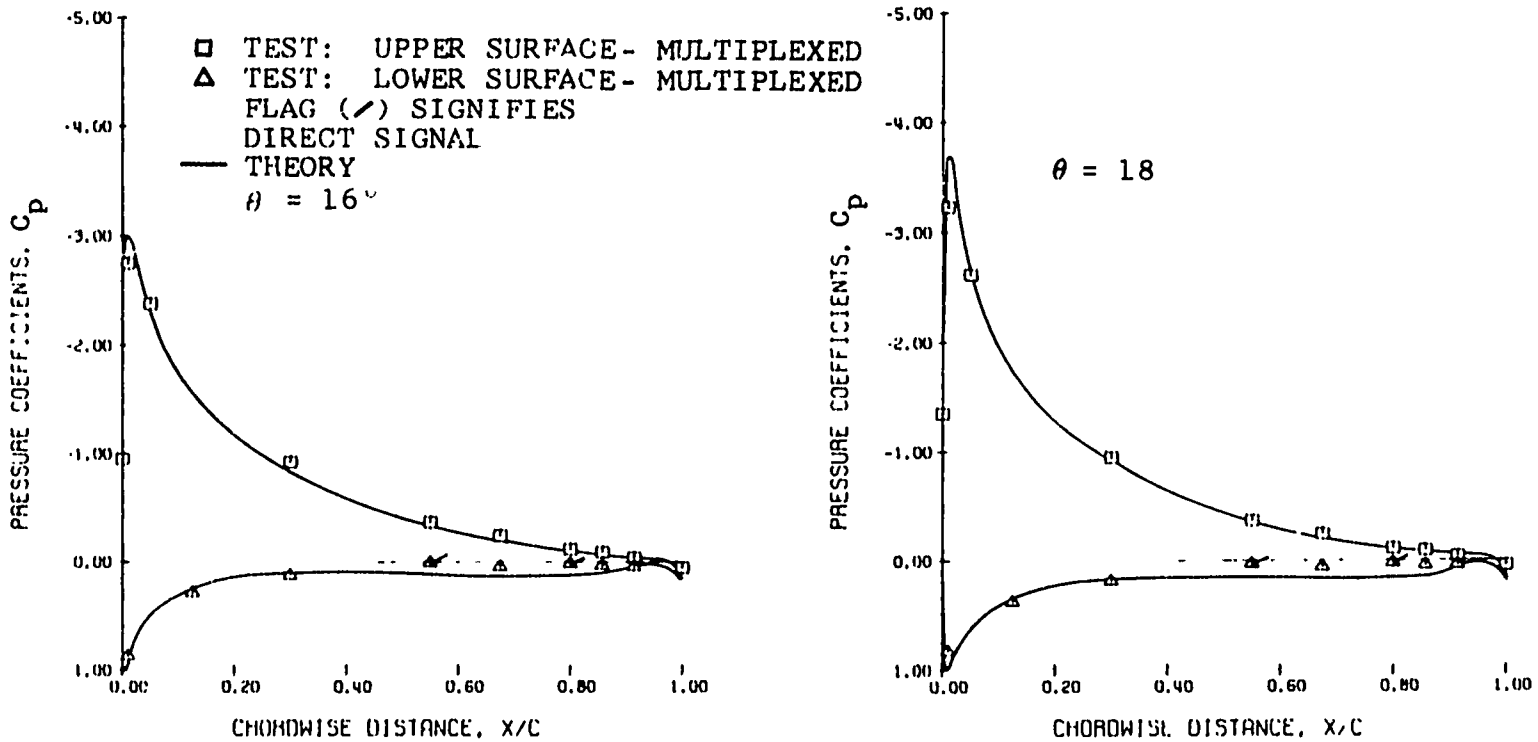

Figure 20. Continued.

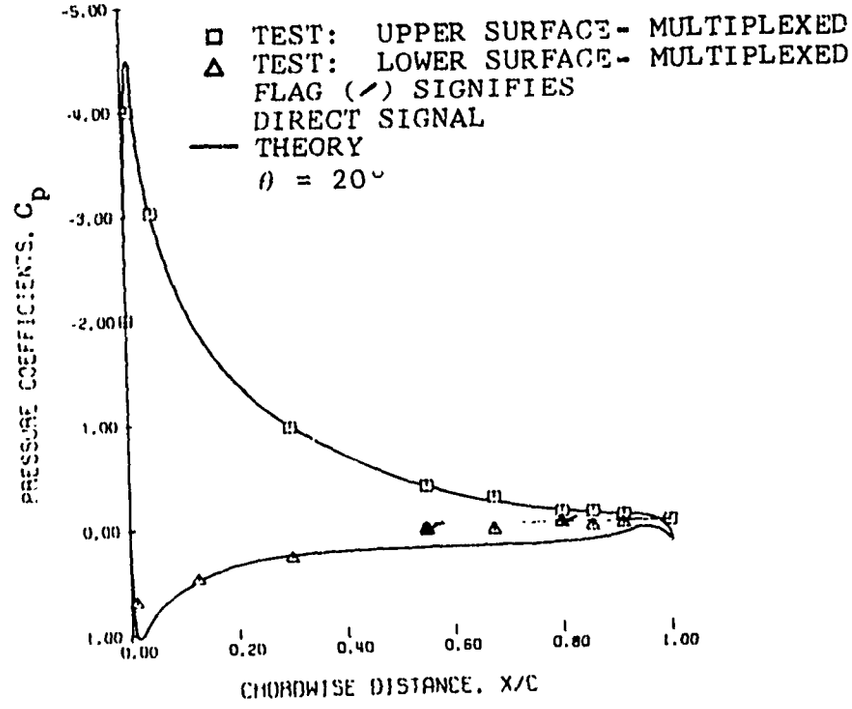

Figure 20. Concluded.

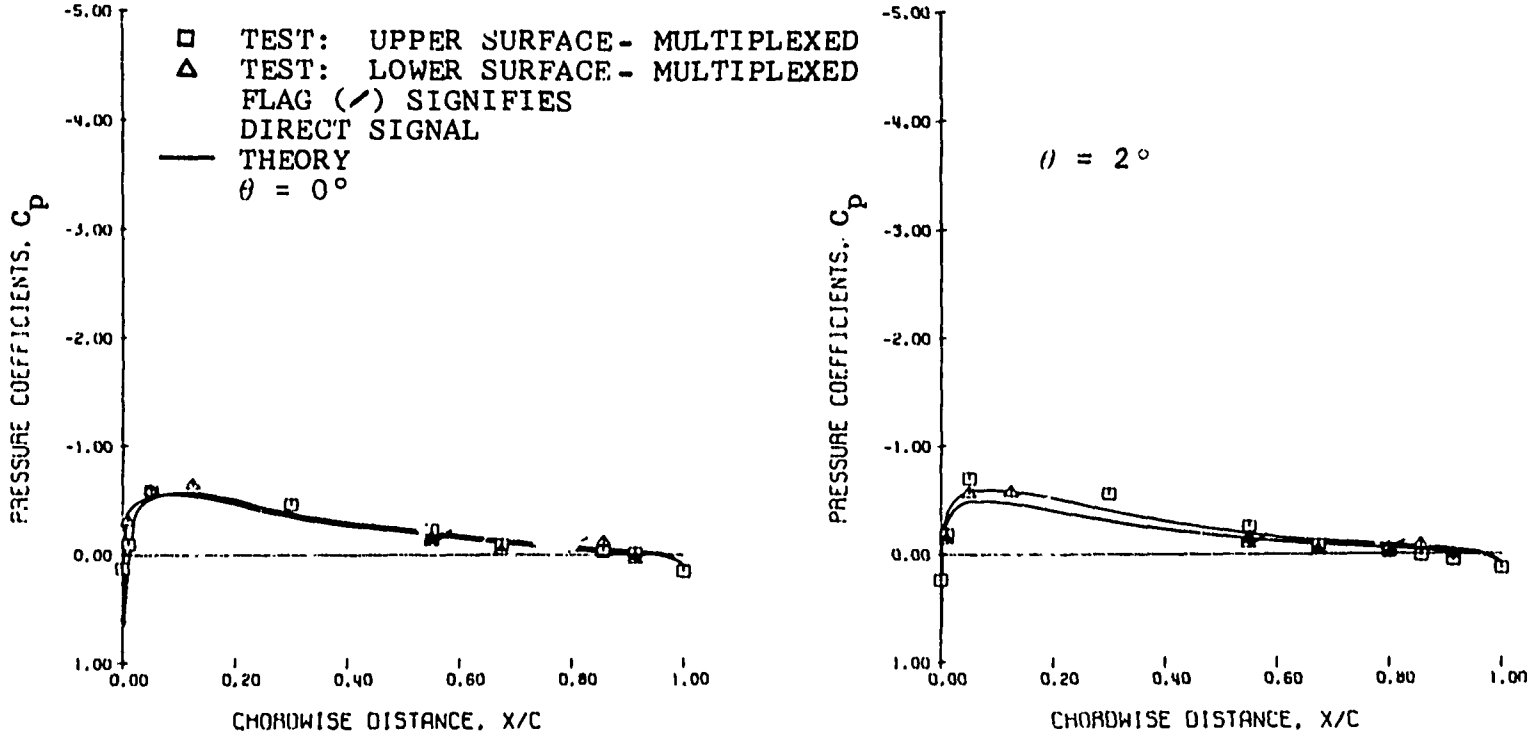

Figure 21. Average Chordwise Pressure Distributions Taken at 324 RPM for Various Blade Pitch Angles.

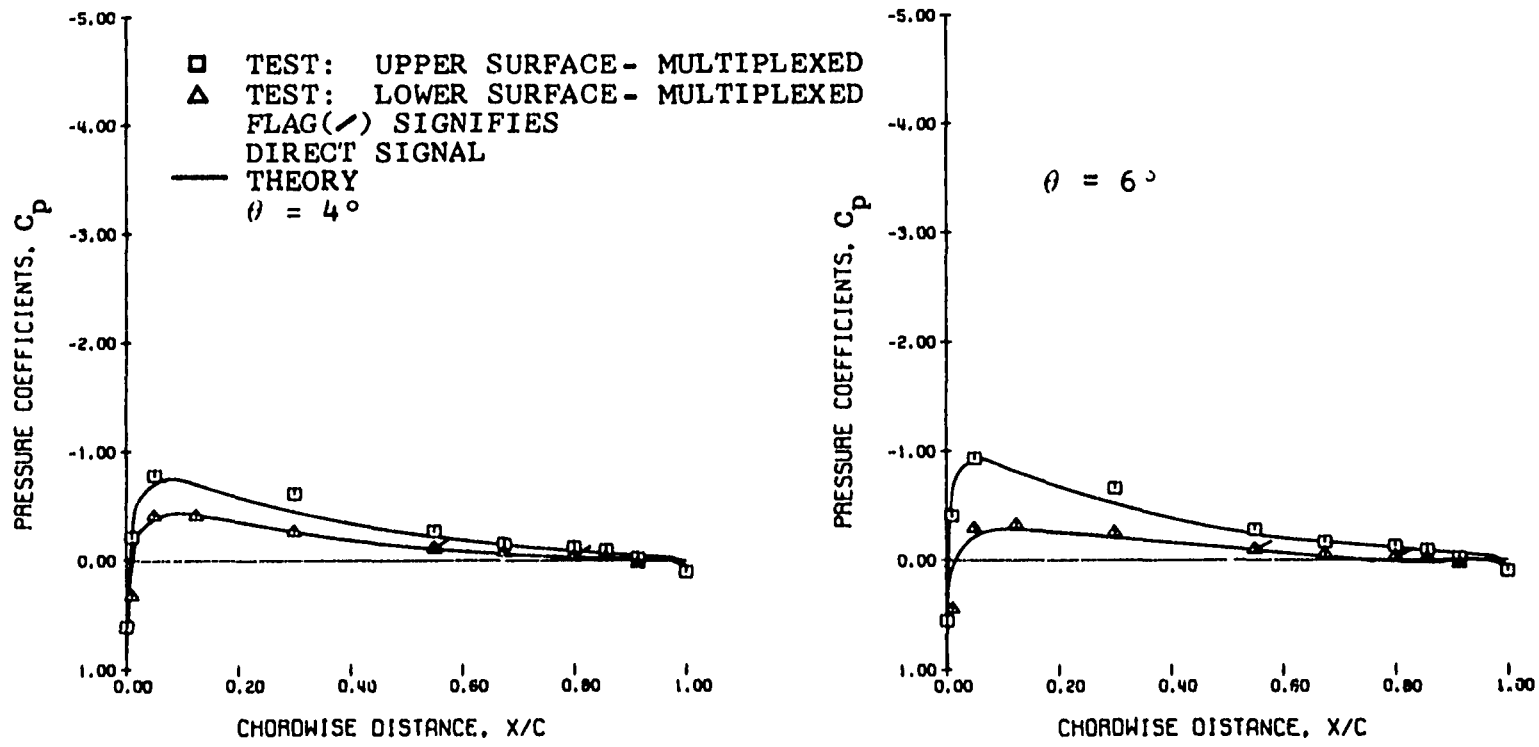

Figure 21. Continued.

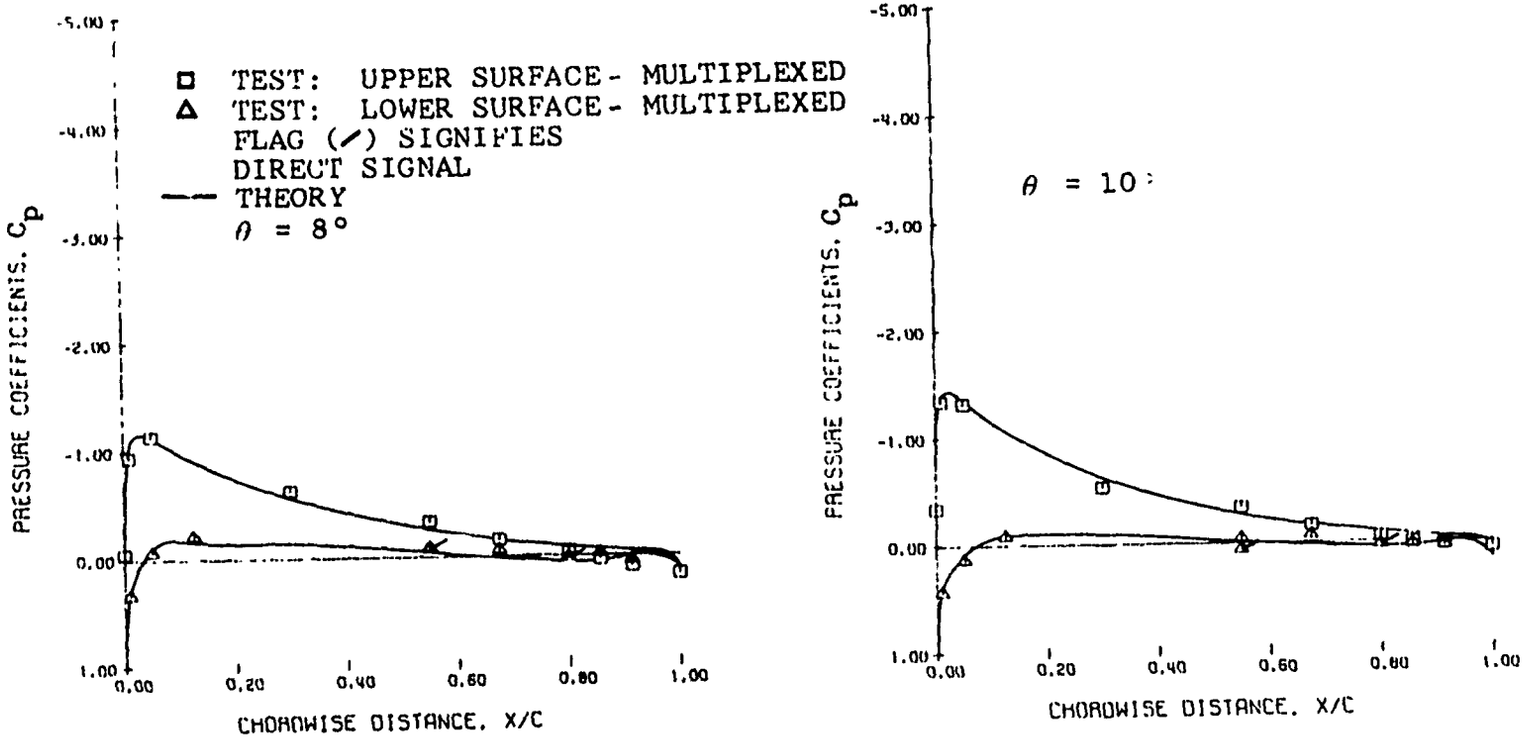

Figure 21. Continued.

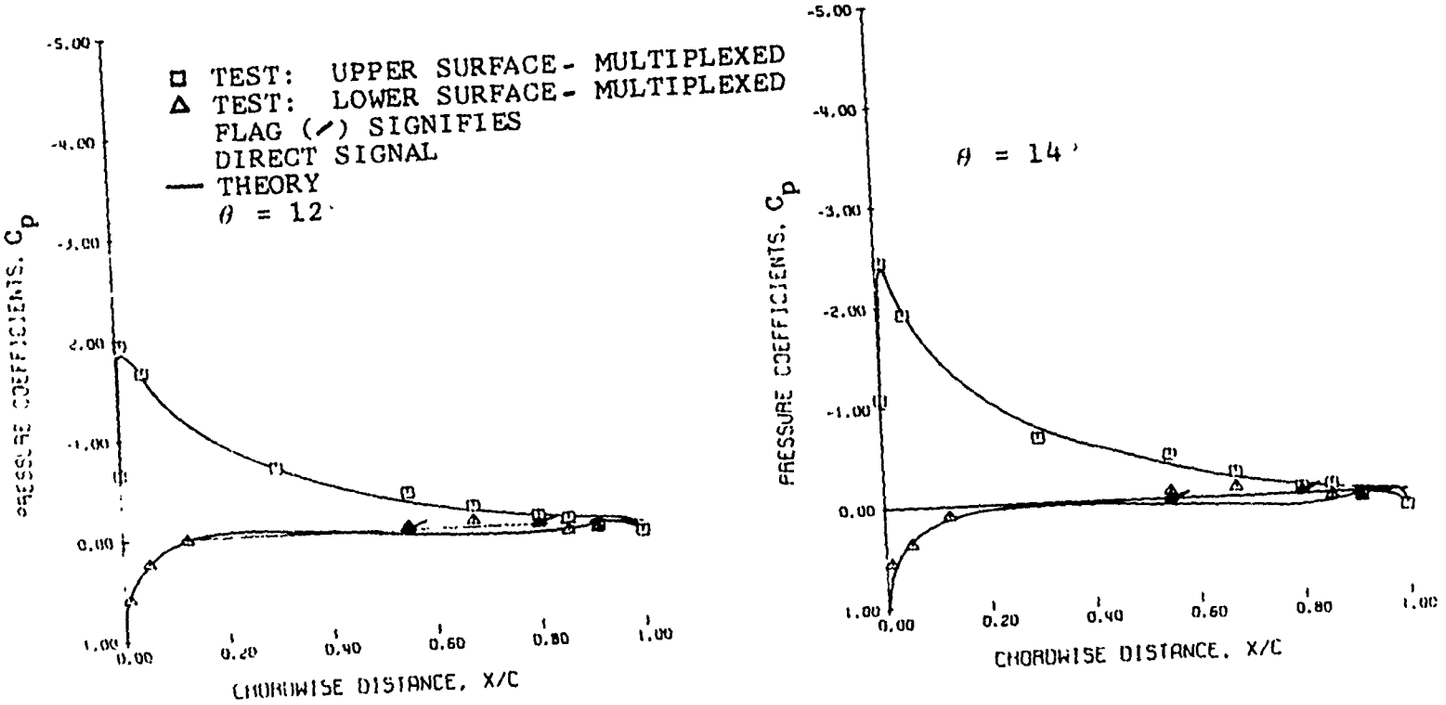

Figure 21. ontinued.

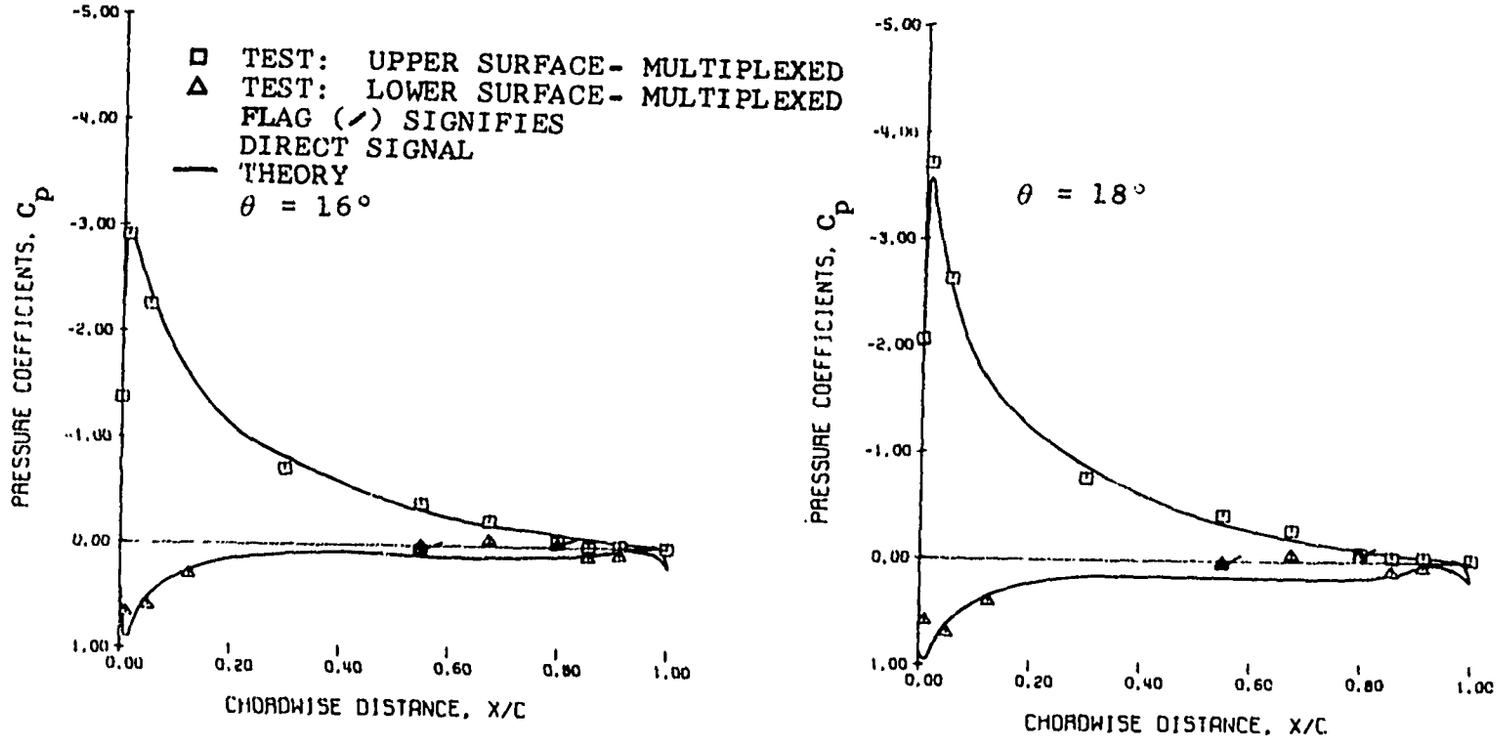

Figure 21. Continued.

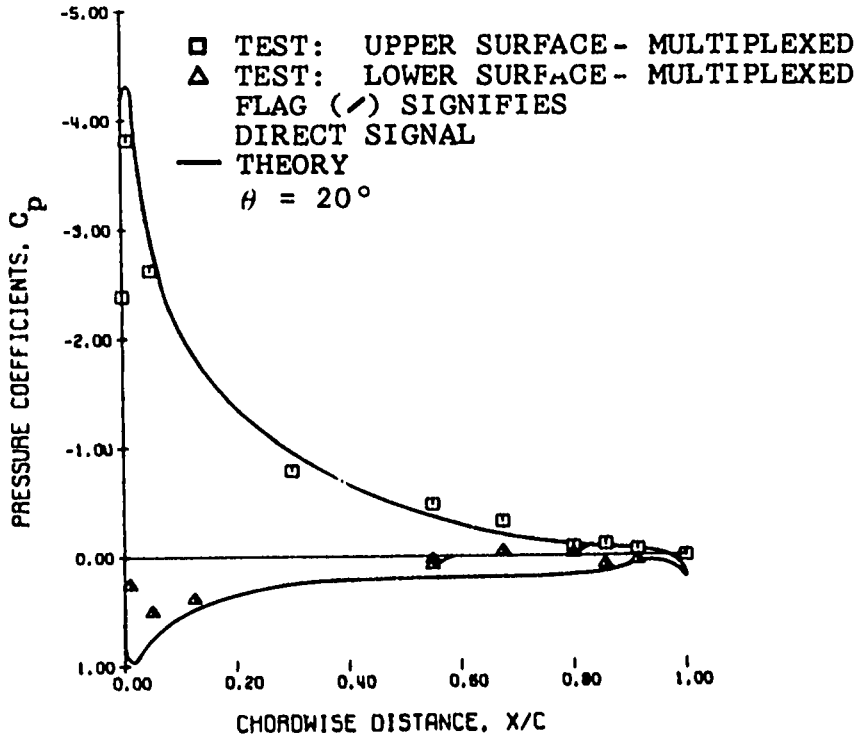

Figure 21. Concluded.

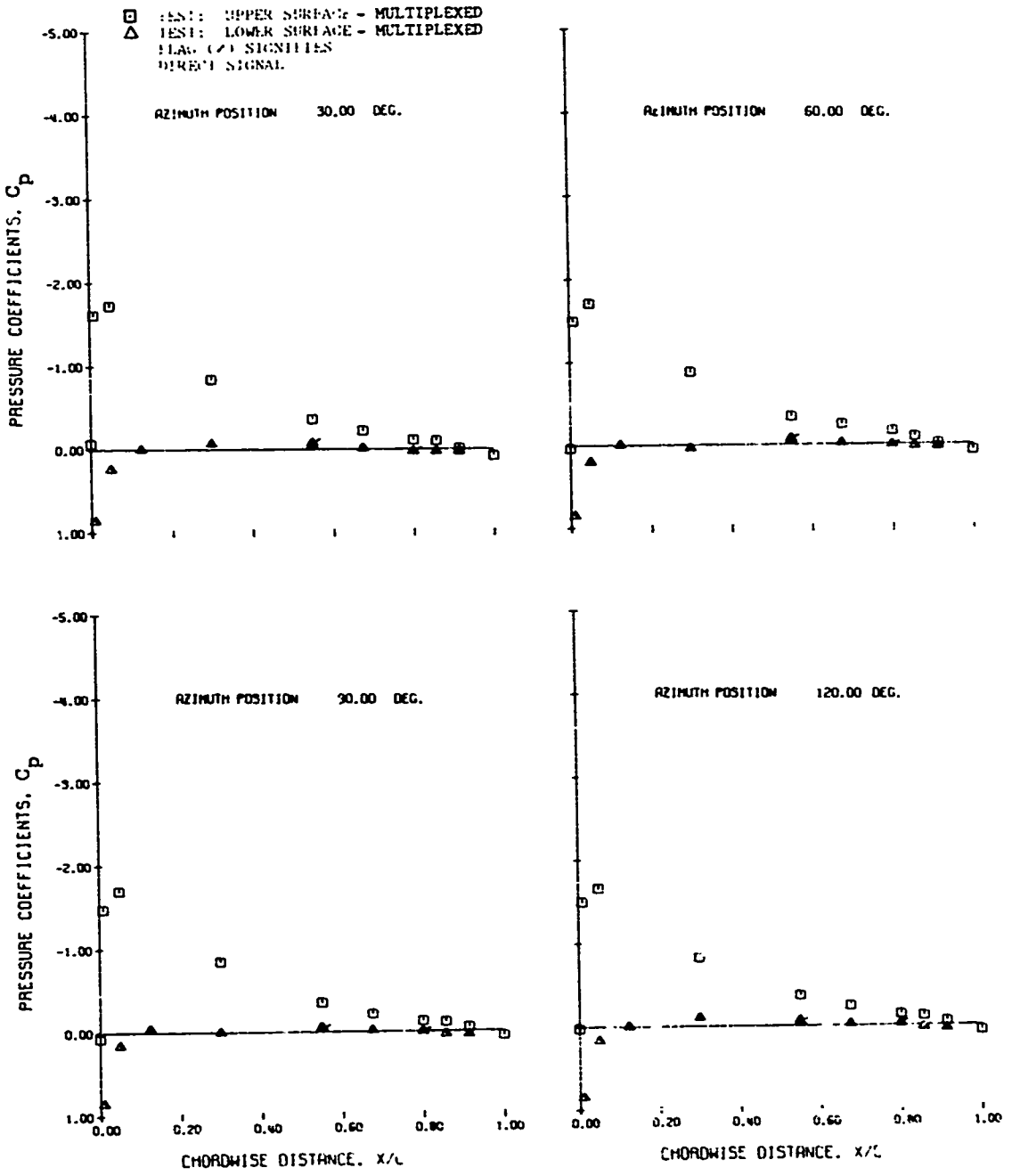

Figure 22. Chordwise Pressure Distributions at 866 RPM and 12 Degrees Blade Pitch.

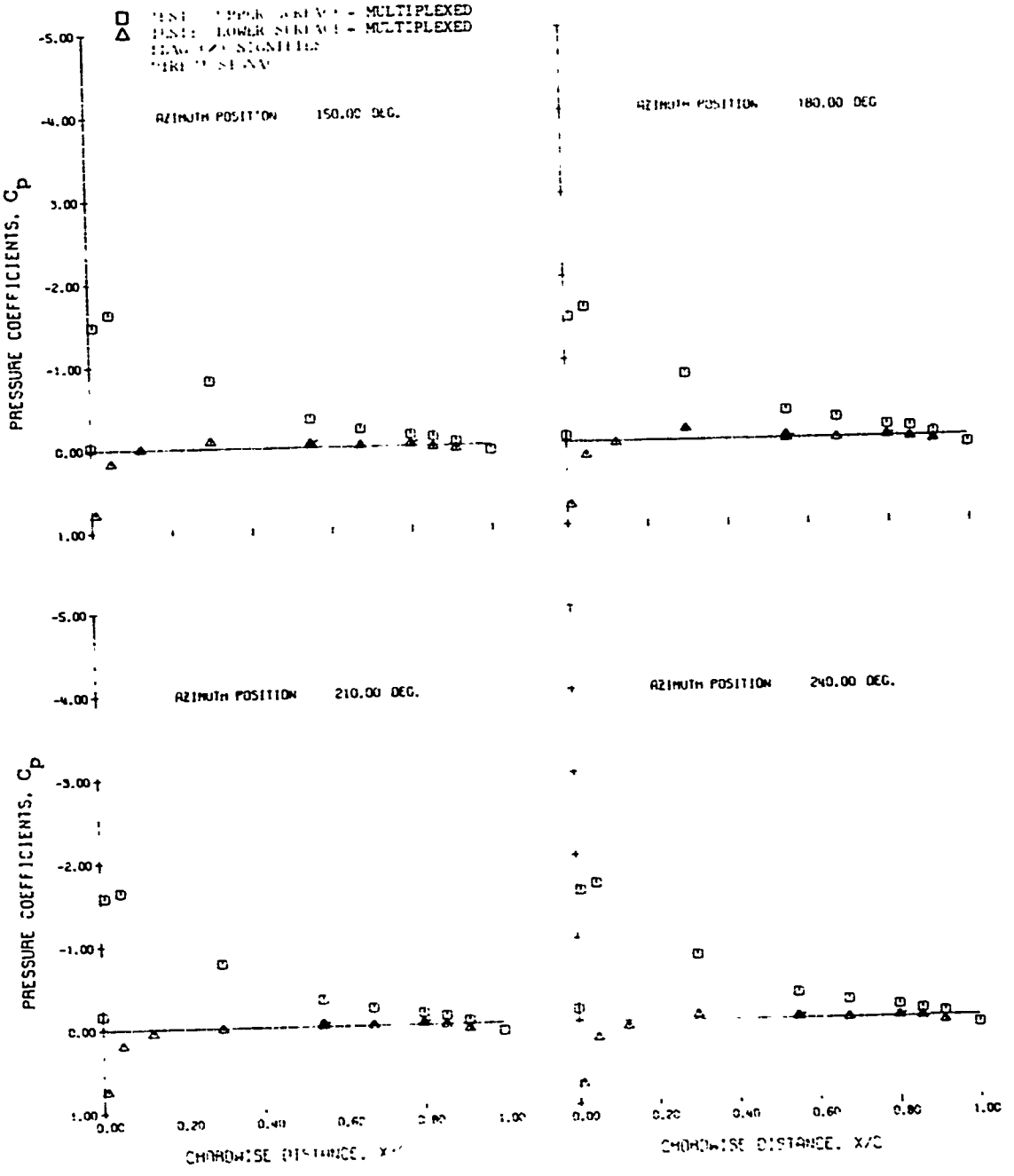

Figure 22. Continued.

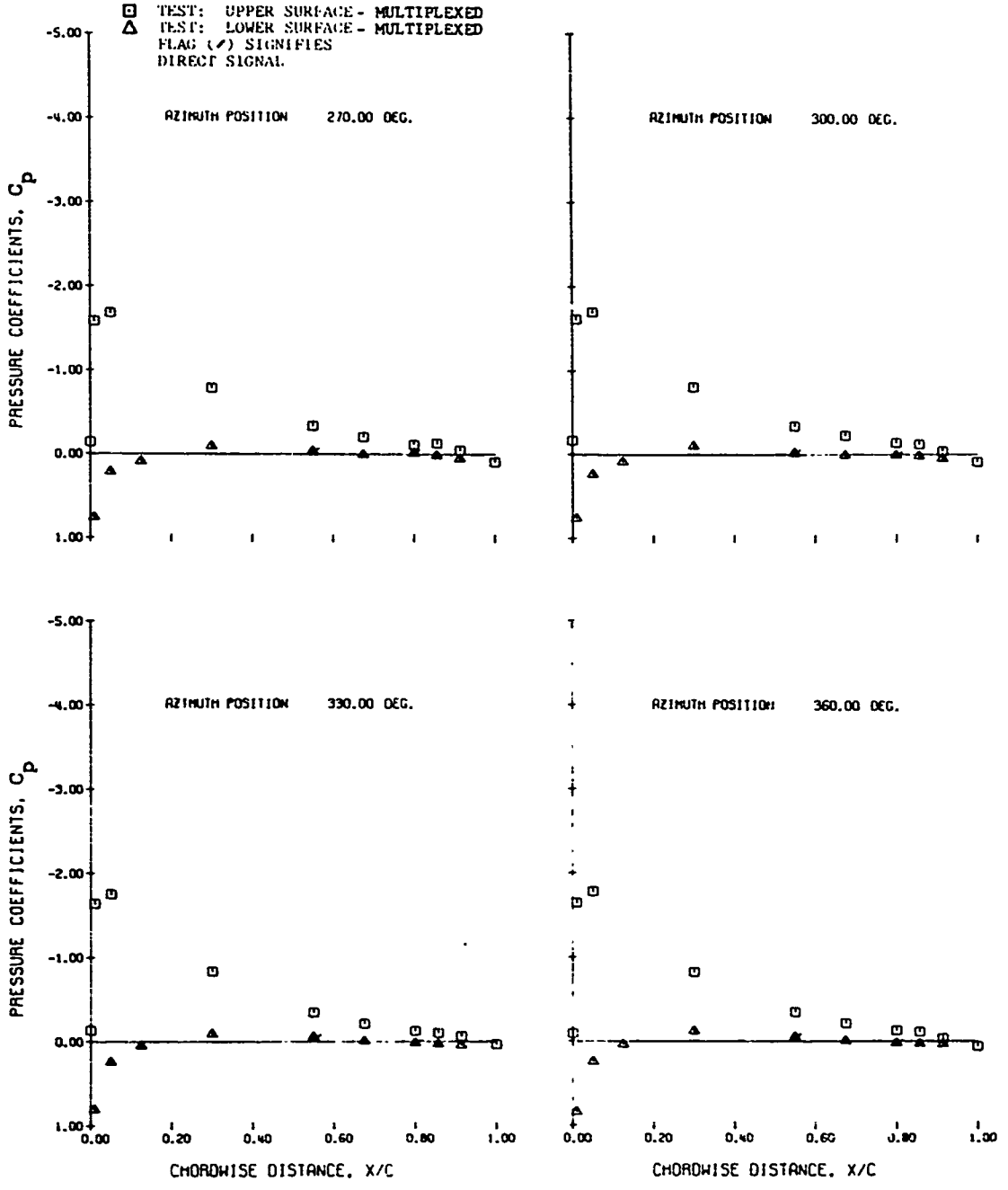

Figure 22. Concluded.

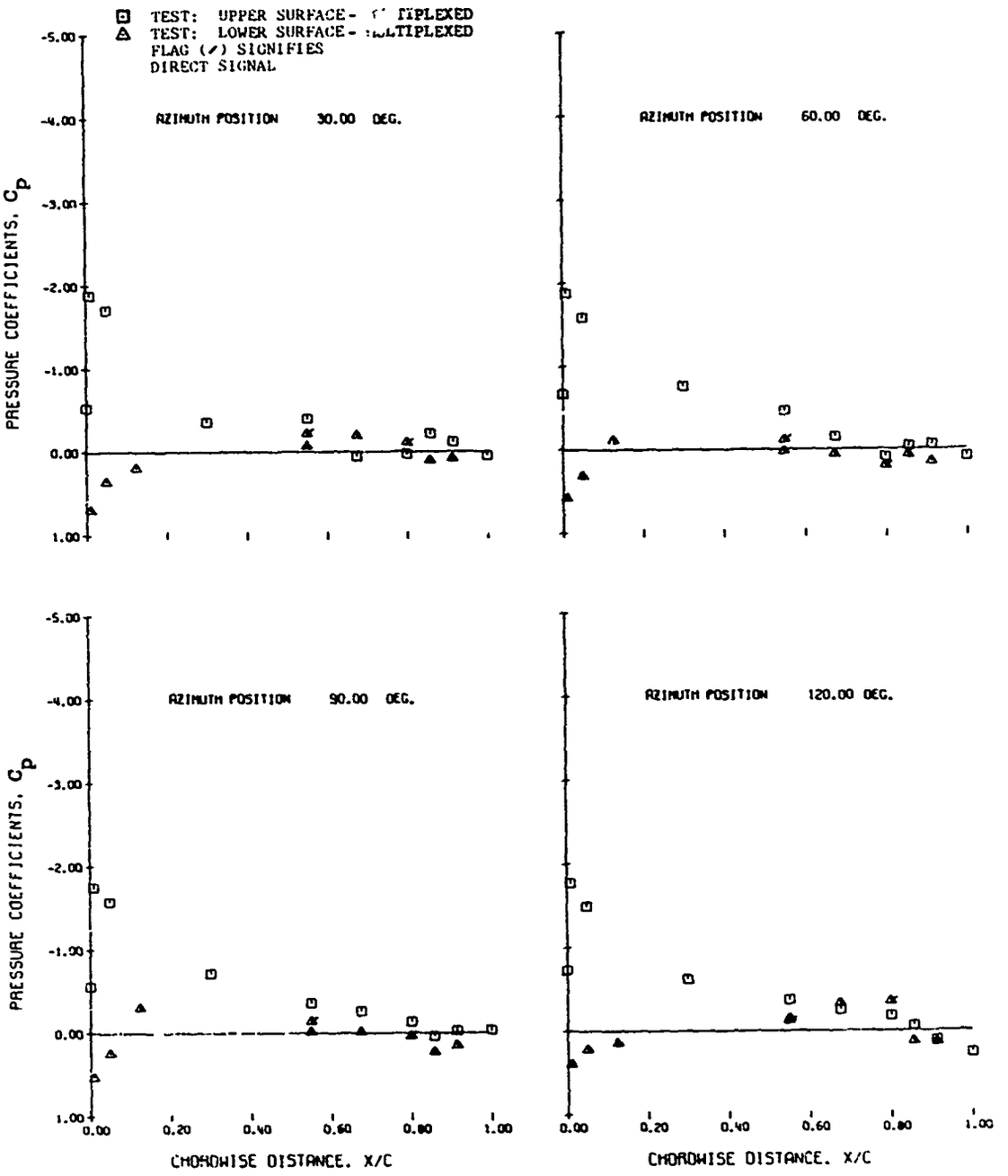

Figure 23. Chordwise Pressure Distributions at 324 RPM and 12 Degrees Blade Pitch.

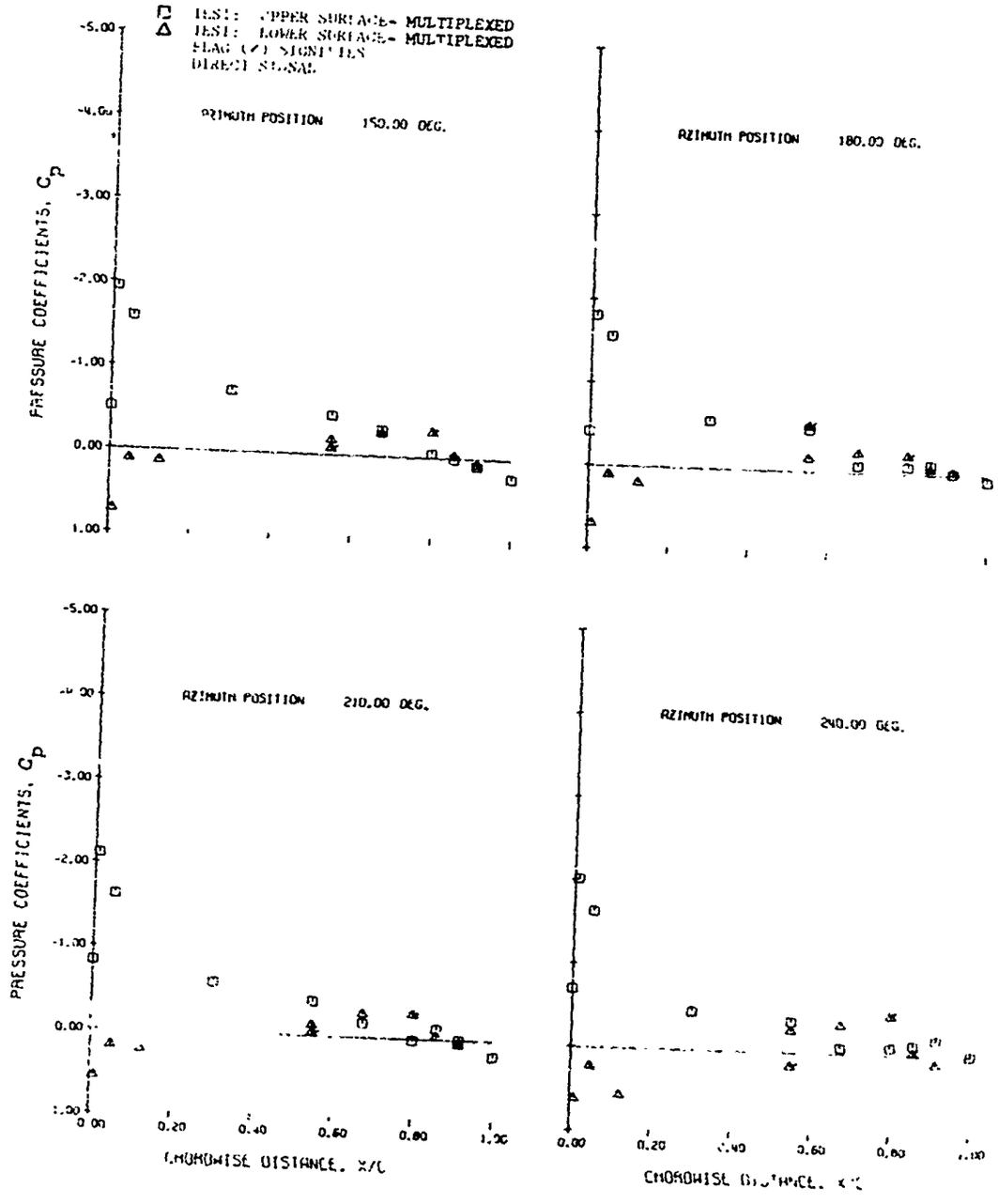

Figure 23. Continued.

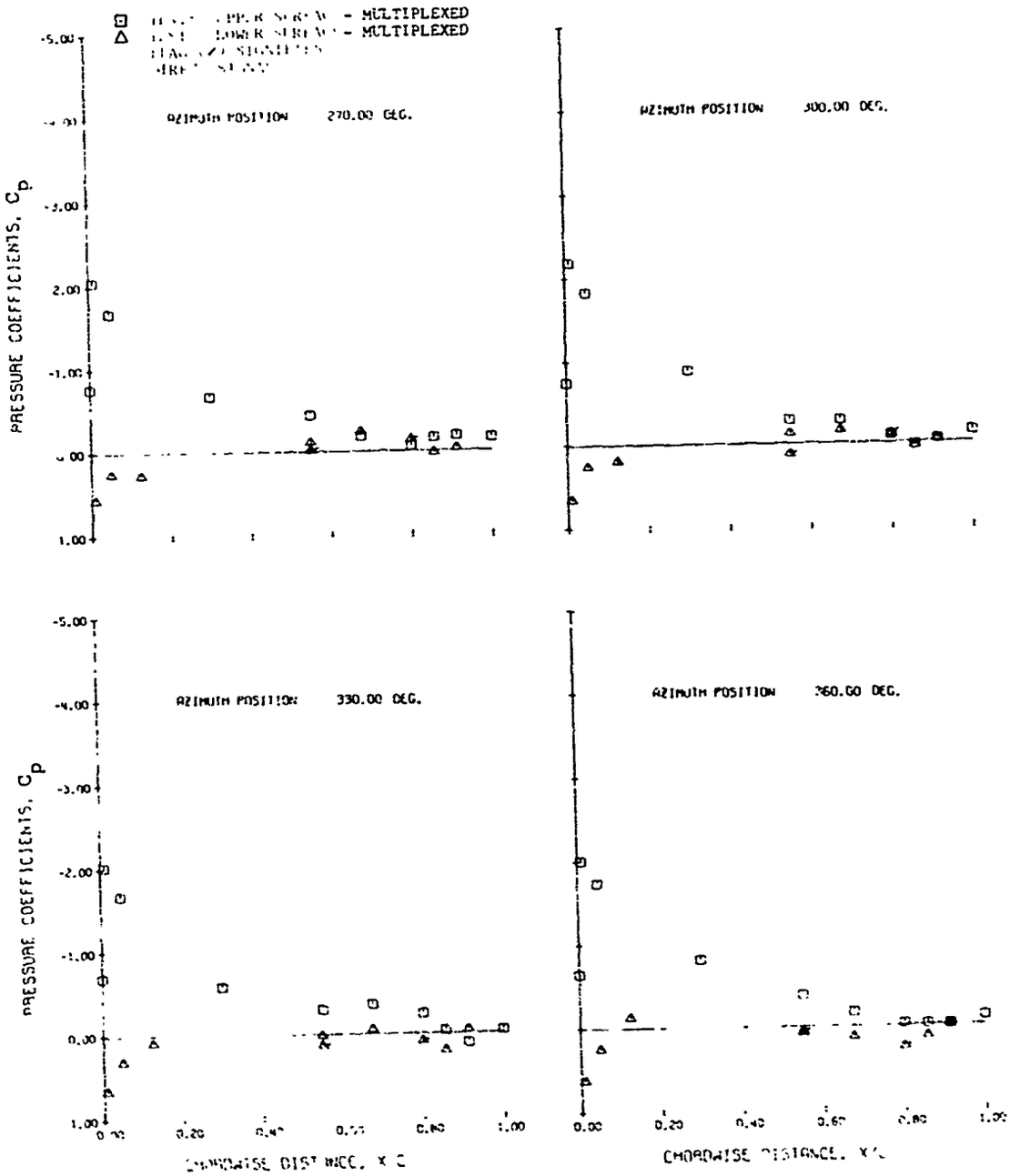

Figure 23. Concluded.

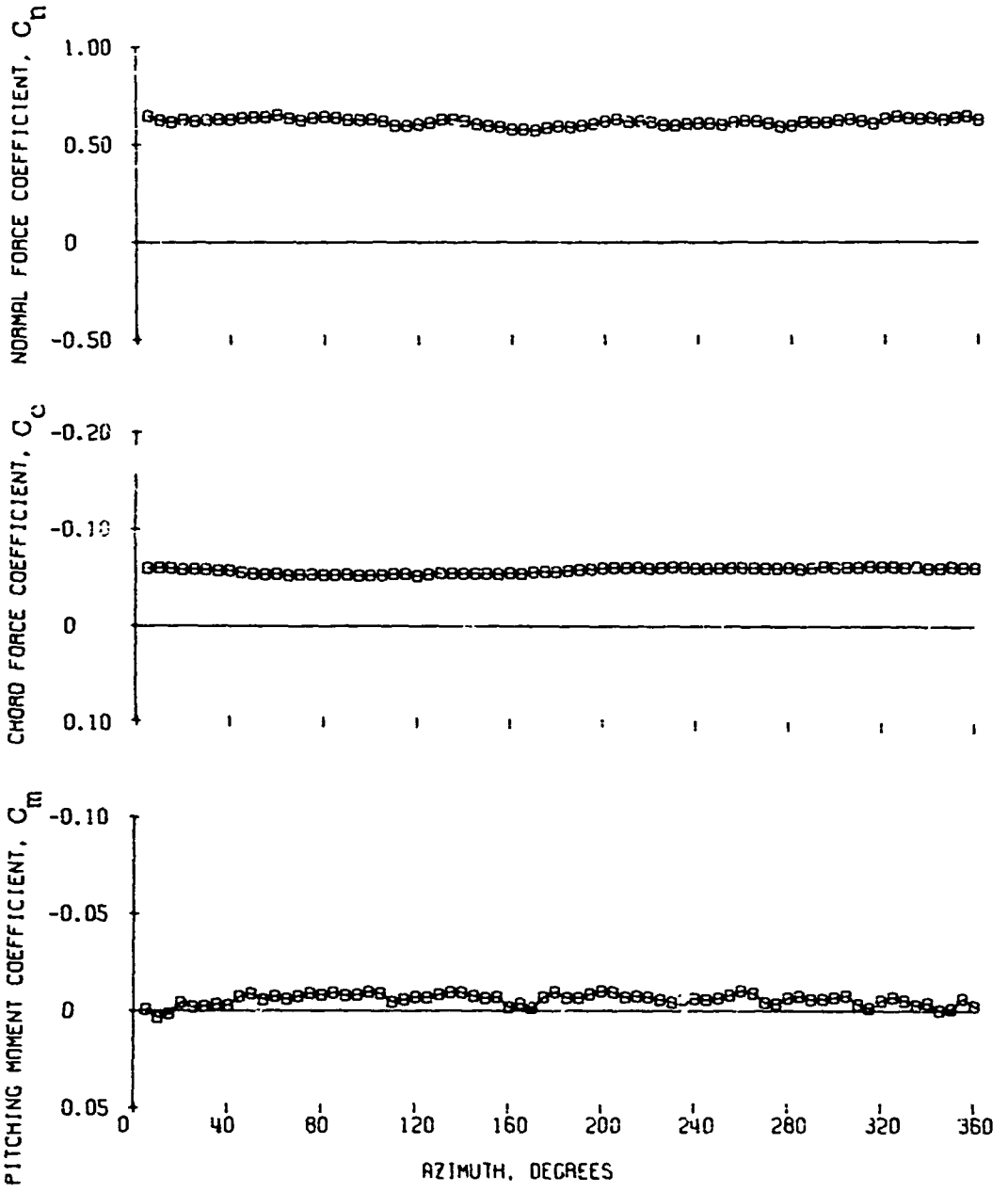

Figure 24. Integrated Force Coefficients Versus Azimuth at 866 RPM and 12 Degrees Pitch.

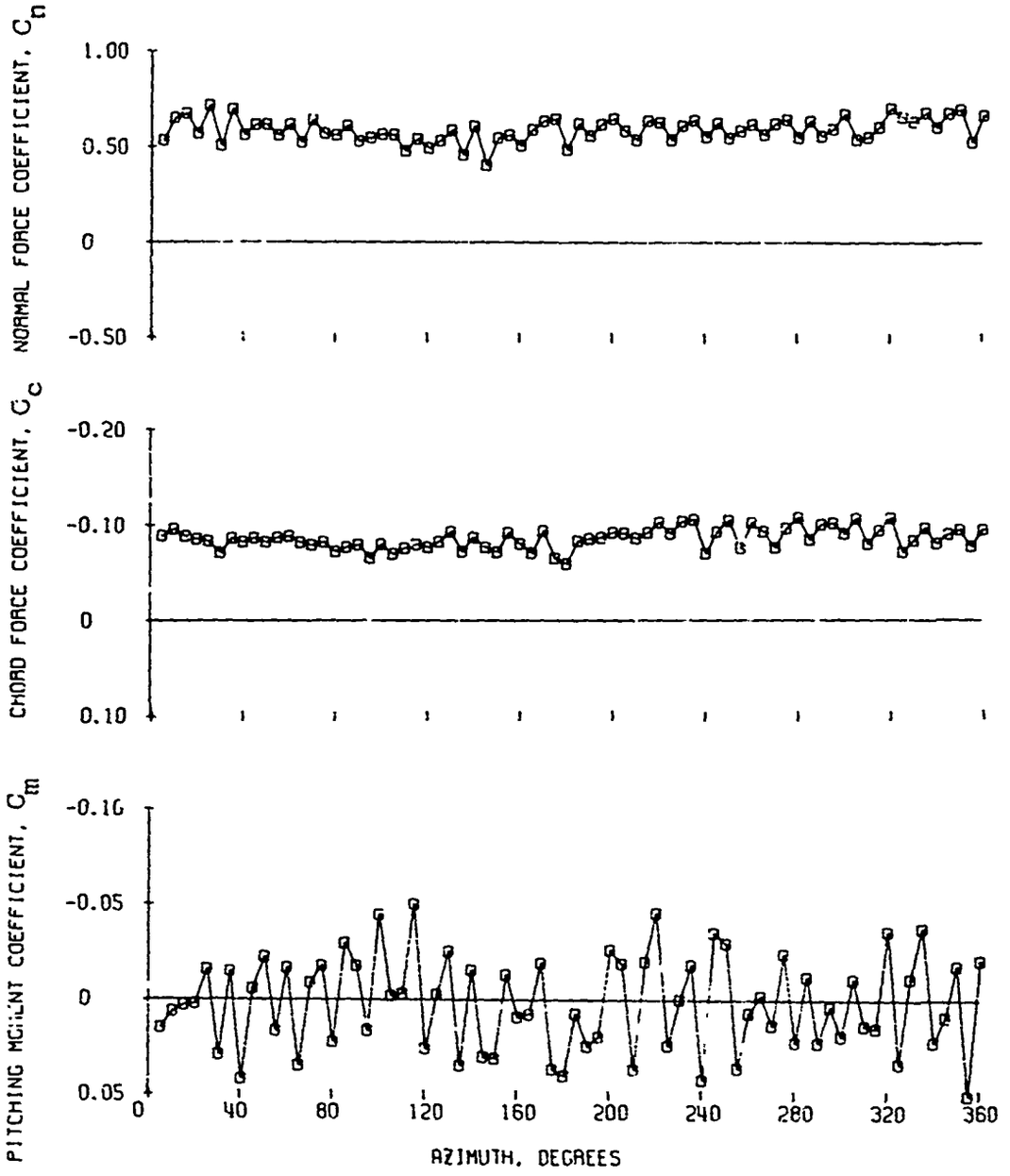

Figure 25. Integrated Force Coefficients Versus Azimuth at 324 RPM and 12 Degrees Pitch.

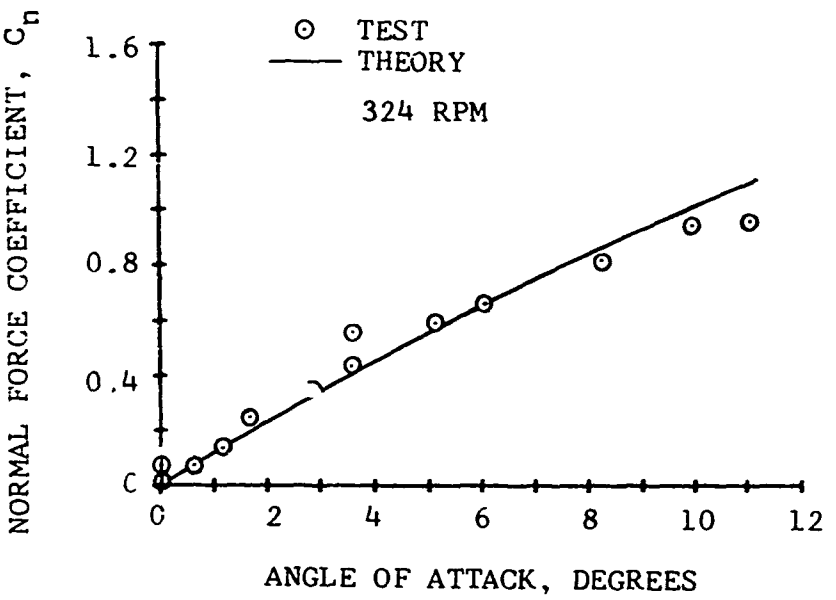

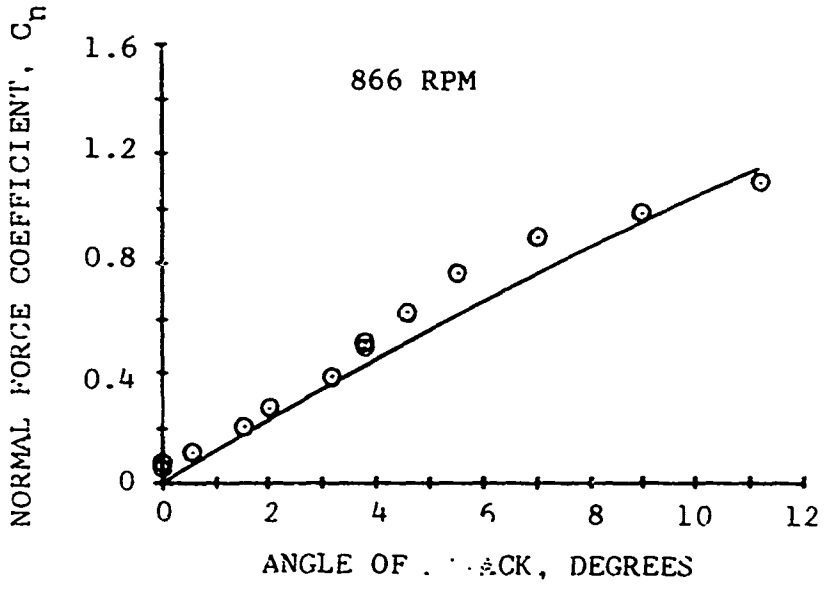

Figure 26. Average Force Coefficients Versus Section Angle of Attack.

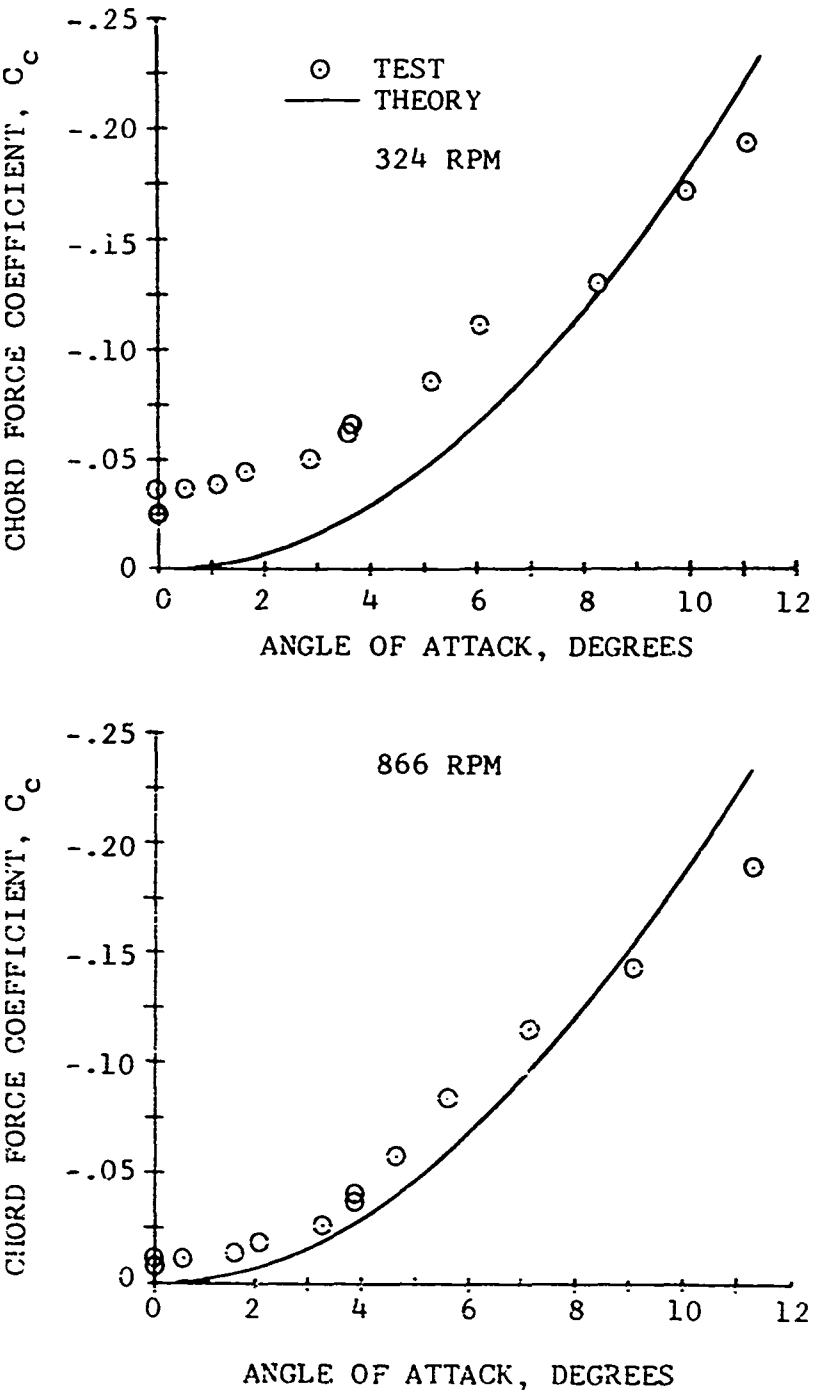

Figure 26. Continued.

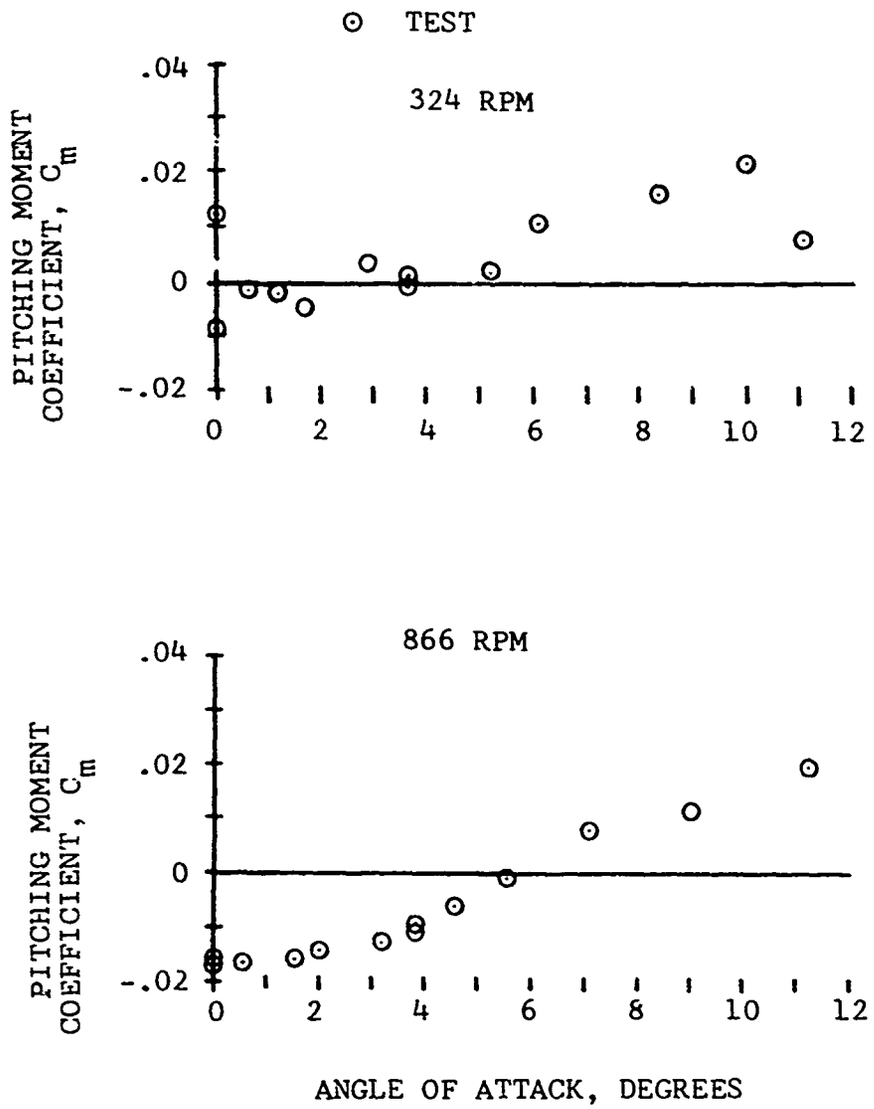

Figure 26. Concluded.

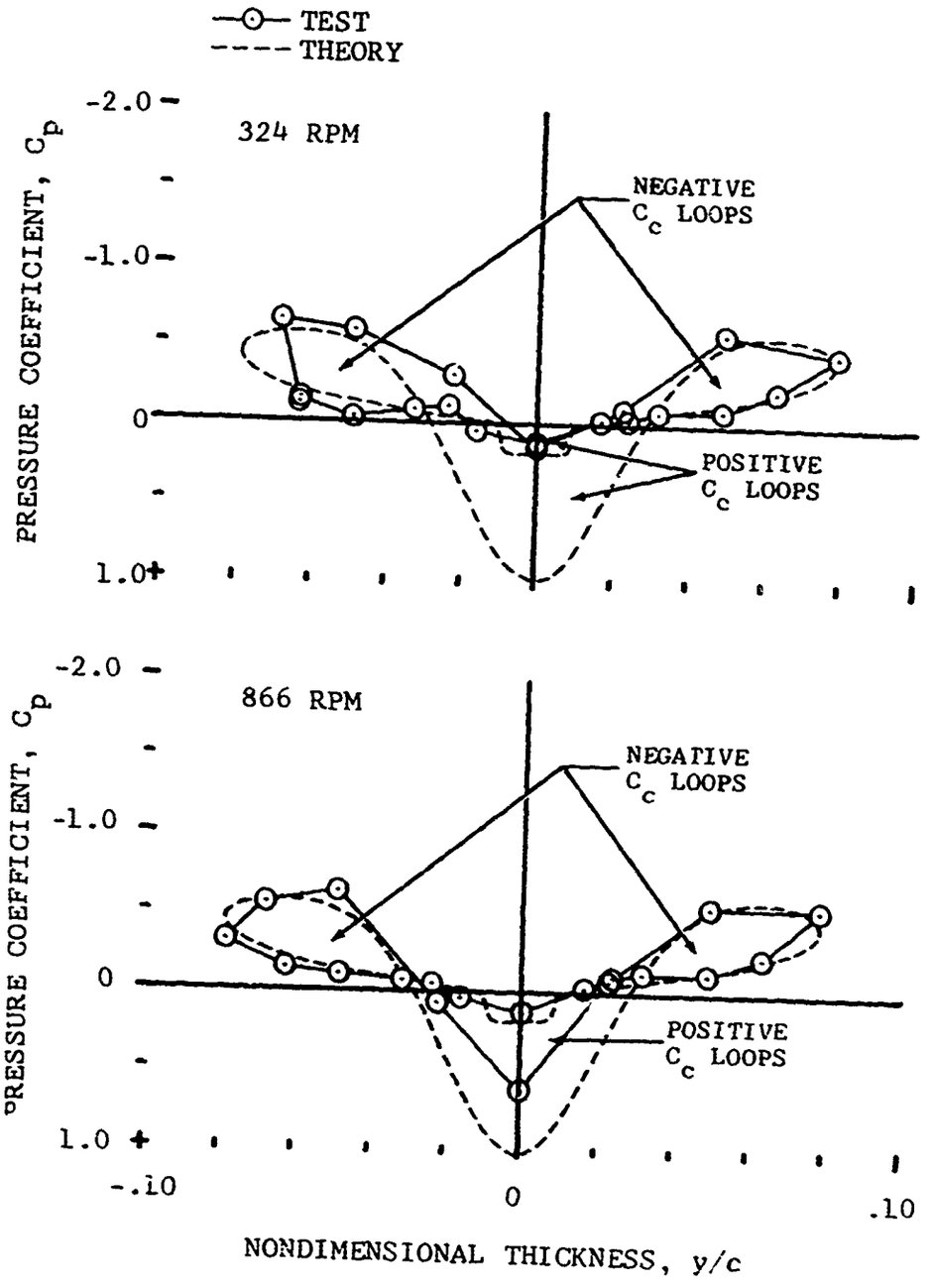

Figure 27. Chord Force Pressure Distributions At Zero Degrees Blade Pitch.

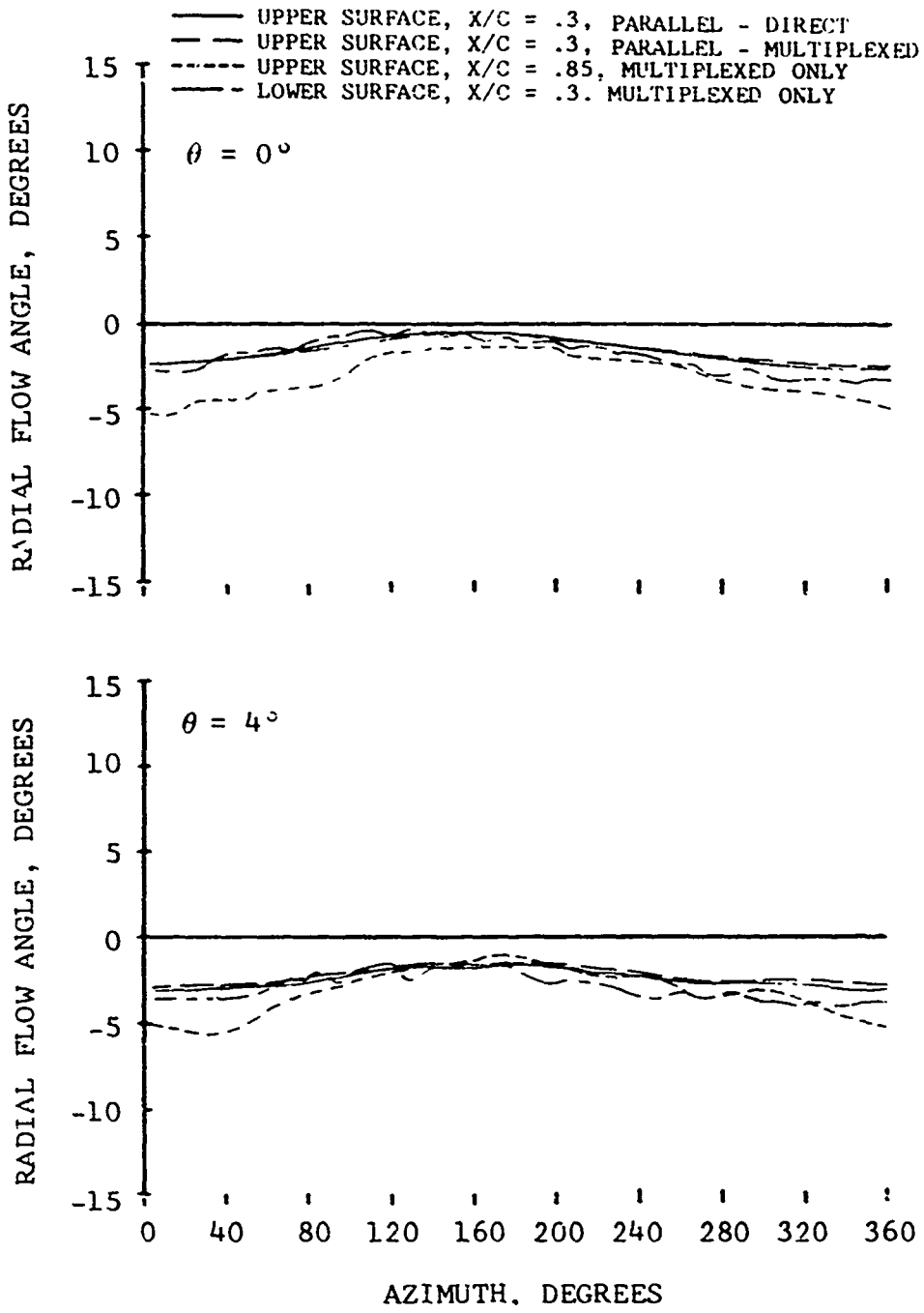

Figure 28. Local Radial Flow Angles Versus Azimuth at 866 RPM for Various Blade Pitch Angles.

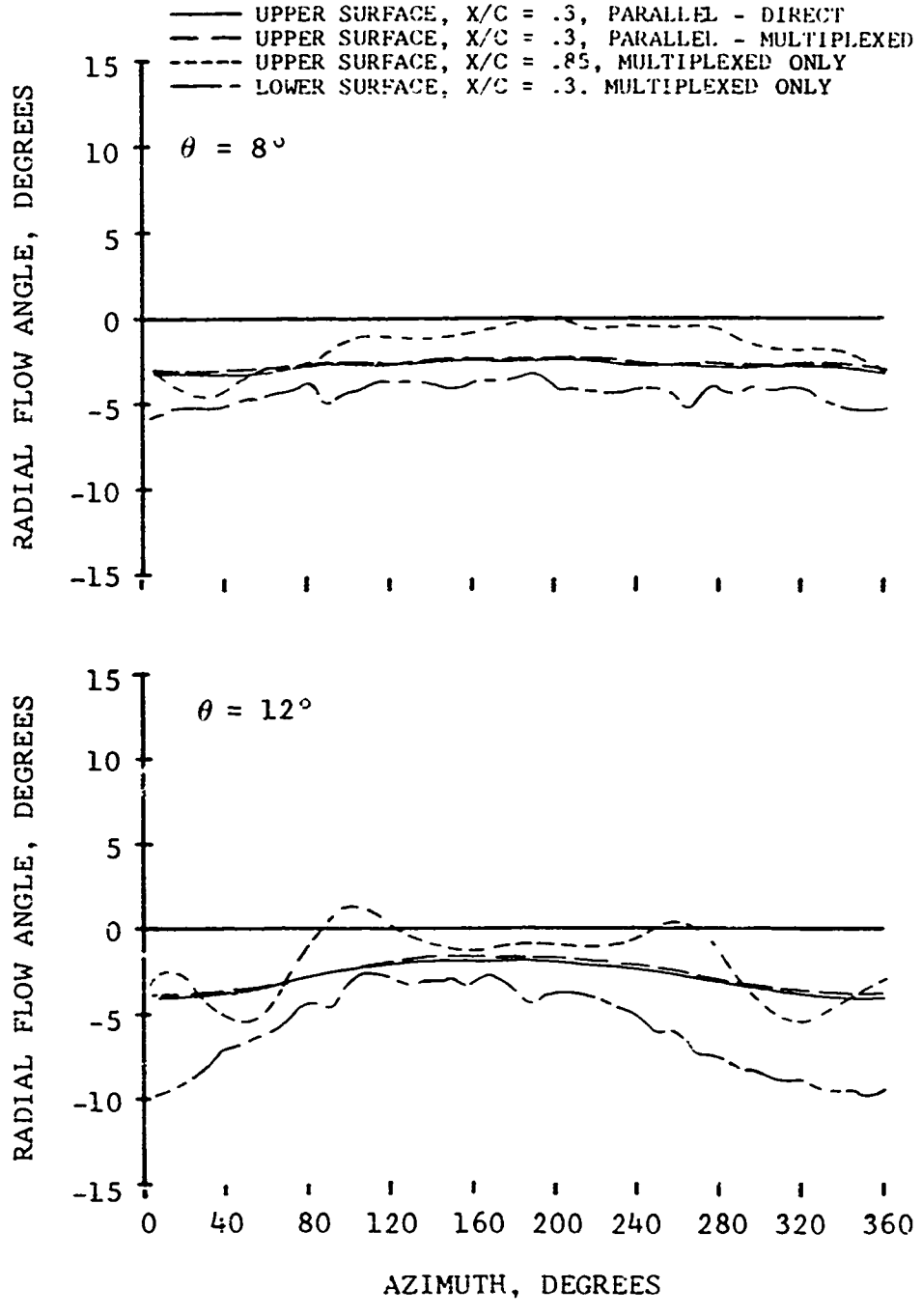

Figure 28. Continued.

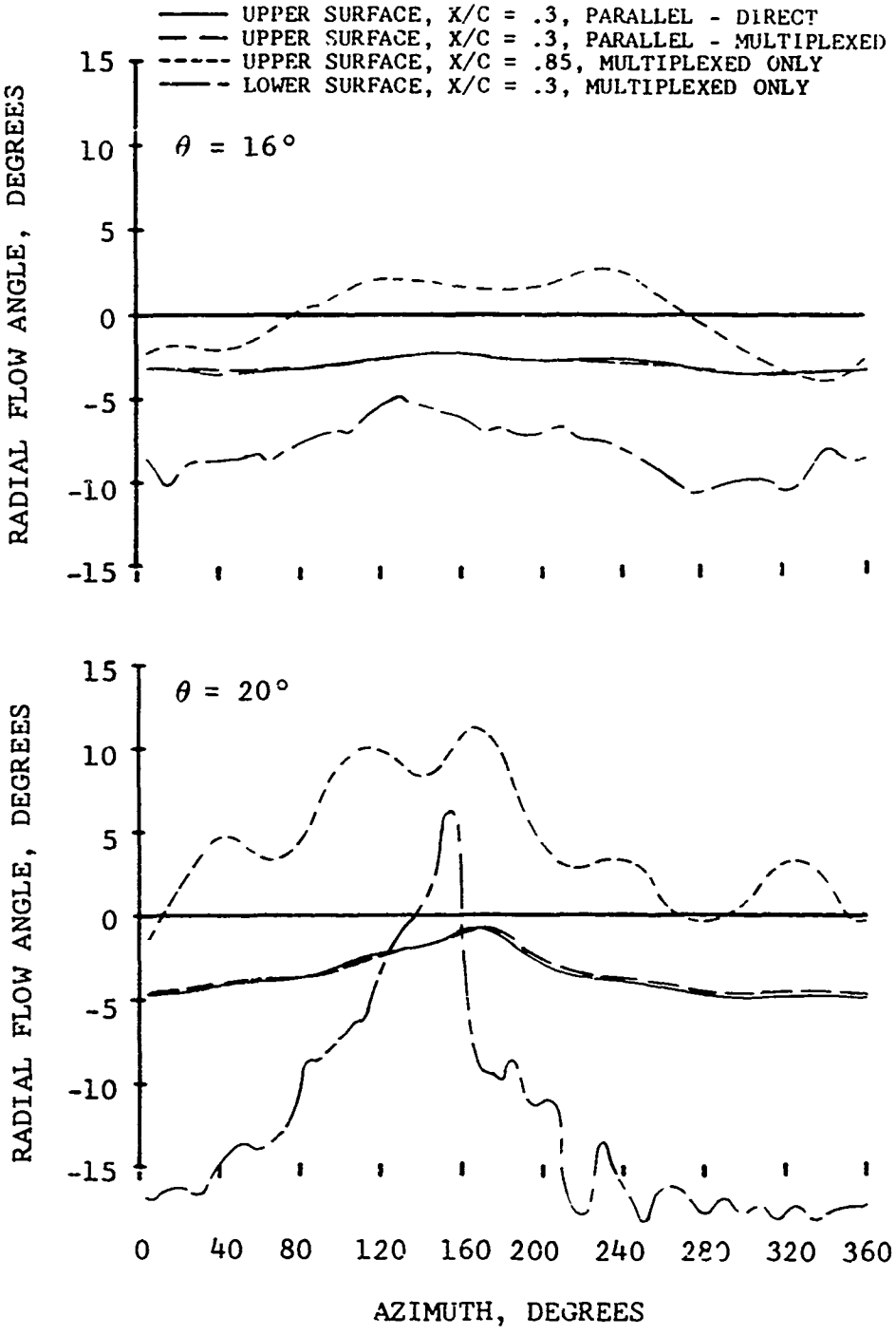

Figure 28. Concluded.

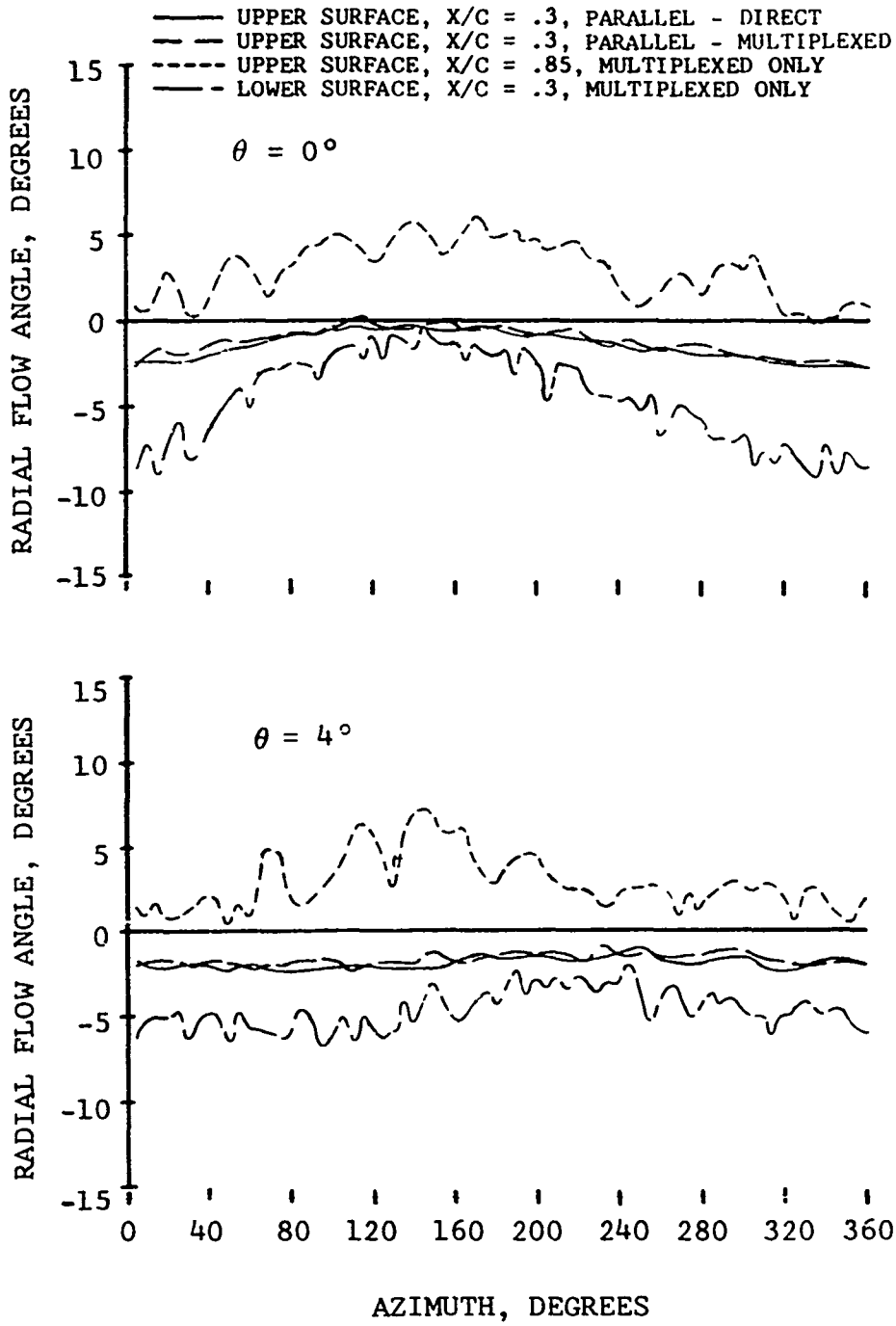

Figure 29. Local Radial Flow Angles Versus Azimuth at 324 RPM for Various Blade Pitch Angles.

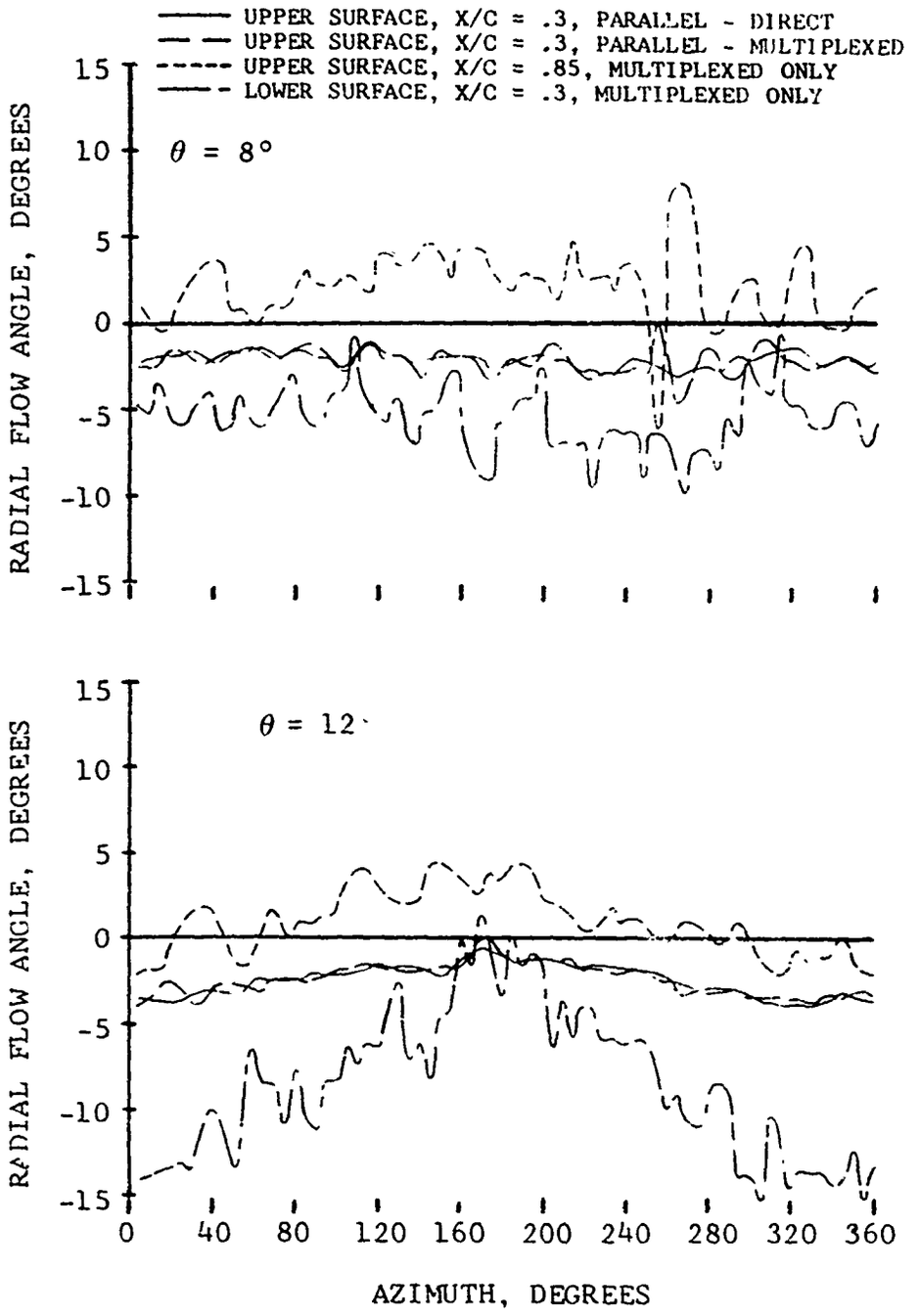

Figure 29. Continued.

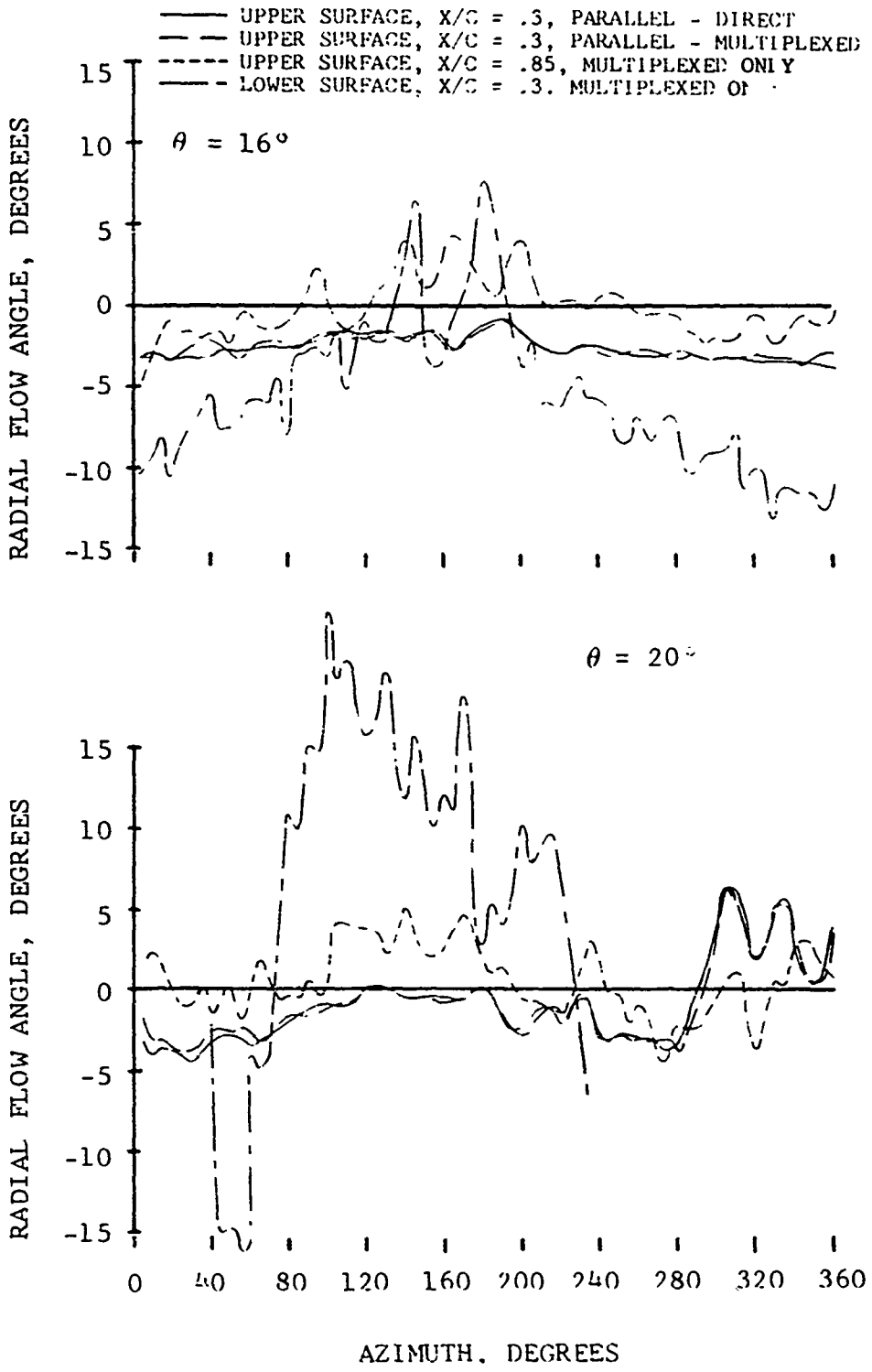

Figure 29. Concluded.

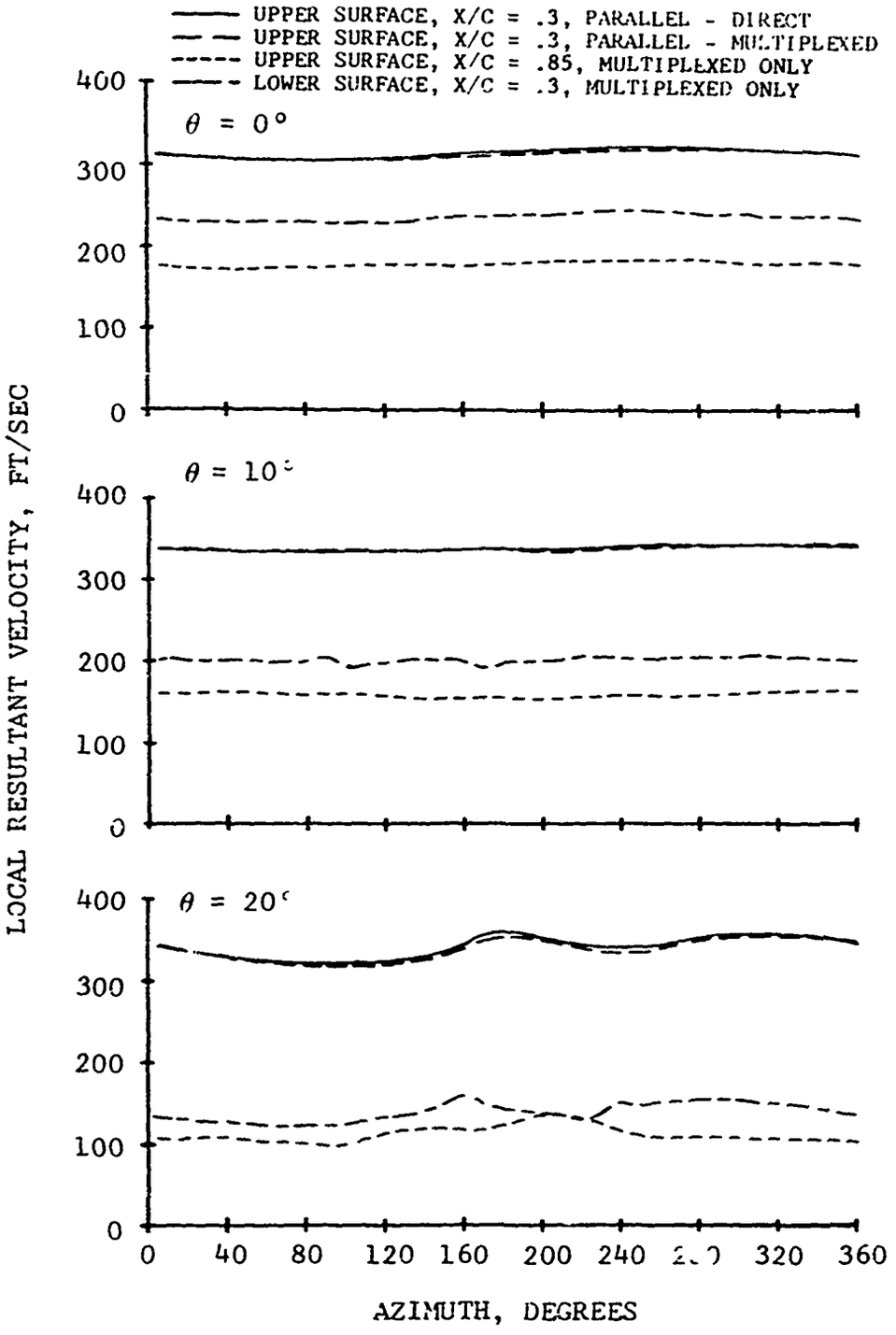

Figure 30. Local Resultant Velocity at .0625 Inch From the Airfoil Surface Versus Azimuth at 866 RPM for Various Blade Pitch Angles.

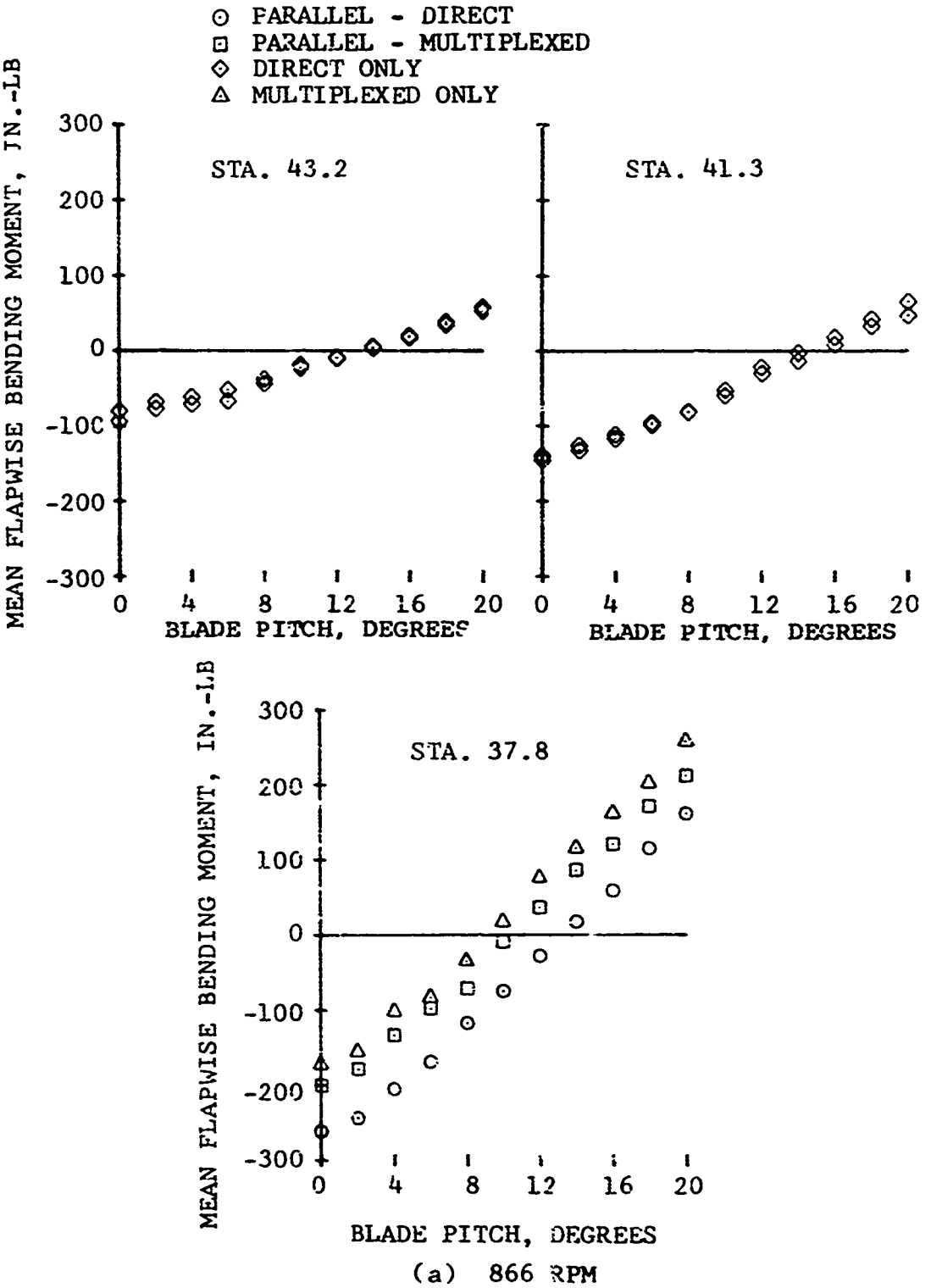

(a) 866 RPM

Figure 31. Mean Flapwise Bending at Radial Stations 43.2, 41.3, and 37.8 Versus Blade Pitch.

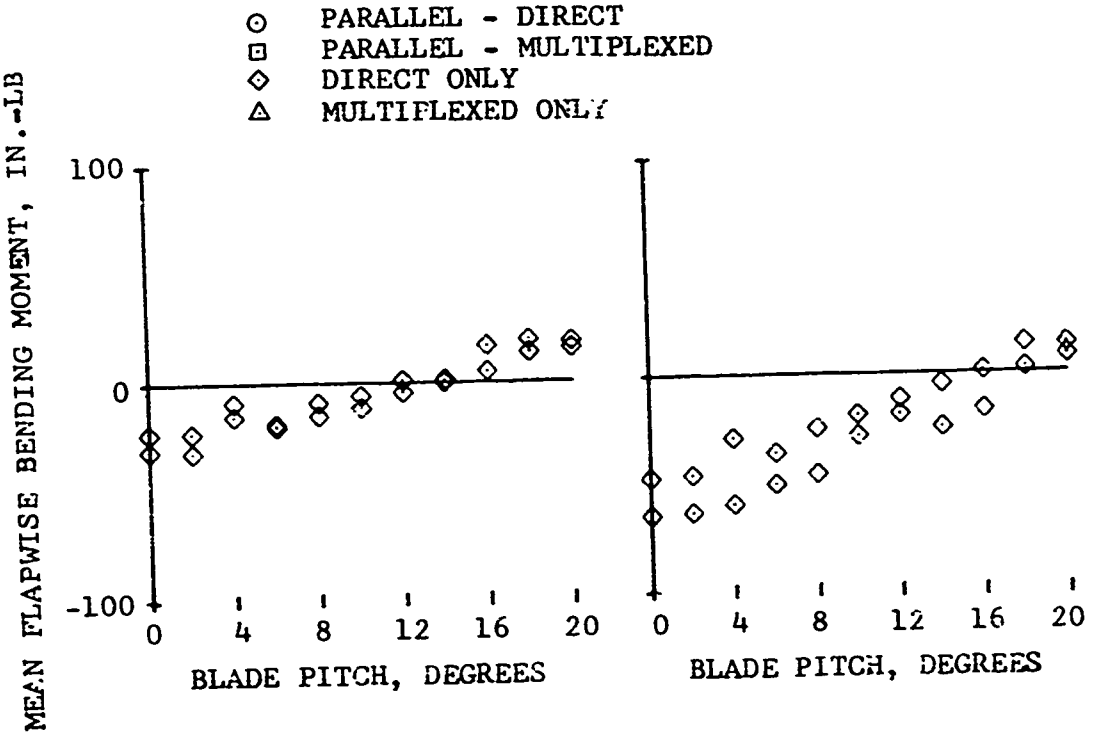

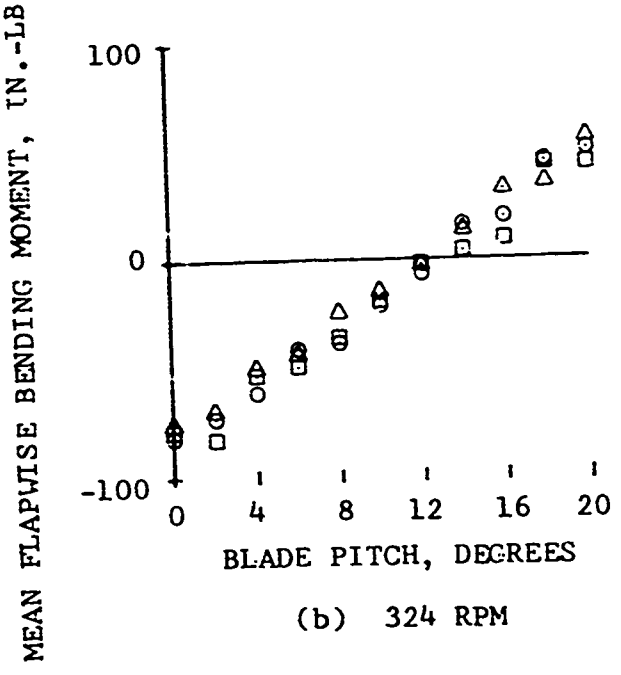

(b) 324 RPM

Figure 31. Concluded.

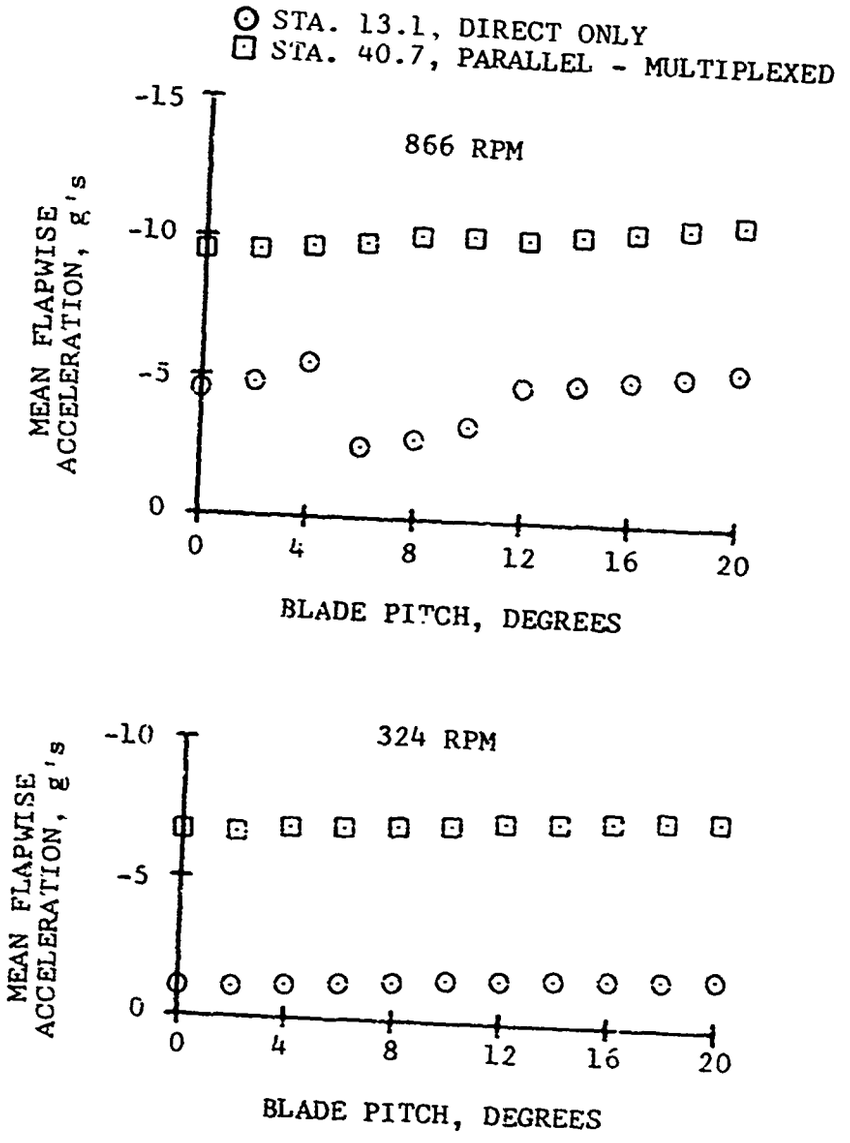

Figure 32. Mean Flapwise Accelerations At Radial Stations 13.1 and 40.7 Versus Blade Pitch.